ABSTRACT

A STUDY OF THE RELATIONSHIP BETWEEN
THE YIELD POINT, DELAY TIME, AND THE
BRITTLE TO DUCTILE TRANSITION IN A LOW
CARBON ALLOY

by

John Hrinevich, Jr.

In this investigation ingot iron samples were thermally treated in three different ways to vary the precipitate morphology. Samples were annealed by heating to 1350° F for one and one half hours followed by furnace cooling. Samples were solution treated by heating to 1350° F for one and one half hours followed by quenching in iced brine. Samples were solution treated-aged by heating to 1350° F for one and one half hours, quenched in iced brine, and then heated for six hours at 158° F. Modified Izod impact samples, 0.505 inch diameter cylindrical compression samples, and delay time specimens were made from the ingot iron in the three conditions and tested at temperatures between 14 and 305° F to determine the relationship between the behavior of the yield point, delay time, and the transition temperature.

The annealed samples showed a brittle to ductile transition at approximately 160° F. All annealed samples tested in compression below 160° F showed a yield point. Samples tested above 160° F showed no yield point. The annealed samples also showed a delay time when tested below 160° F. Above 160° F, these samples showed no delay time. The yield point and delay time disappeared above the brittle to ductile transition. The solution treated and solution treated aged samples showed no brittle to ductile transition. The solution treated and solution treated aged samples showed no brittle to ductile transition, yield point, or delay time in these tests.

Careful examination of all three types of samples under the optical and electron microscopes revealed that there were definite differences between the samples. The annealed samples showed wide grain boundaries with definite precipitates present. The as-quenched samples showed very little grain boundary precipitates and narrow well define grain boundaries. The solution treated aged samples like the as-quenched samples did not show much grain boundary precipitate. However, the low aging temperature of 158° F did cause a fine general precipitate which was reflected in the higher yield and tensile strengths of the solution treated-aged samples. Carbides, nitrides, and oxides made up the precipitates observed.

The yield point arises when dislocations from the

interior of the grain move outward until they meet the grain boundary. At the grain boundary, the dislocations pile-up causing a stress concentration until dislocations in the neighboring grain break away, fresh dislocations are generated in the neighboring grain, the dislocations penetrate the grain boundary and move through the neighboring grain, or fresh dislocations are generated from grain boundary sources. The important point is that the grain boundary can be a major obstacle. The delay time likewise arises because the dislocations are not able to move as soon as the stress is applied.

The annealed samples were the only samples to show a brittle to ductile transition, yield point, delay time, and grain boundary precipitates. Below the brittle to ductile transition, the dislocations can move relatively easily in the interior of the grains. When the dislocations reach the grain boundary, a pile-up occurs at the precipitates which causes a stress concentration. At low temperatures with oxides, nitrides, and carbides in the grain boundaries, the dislocations cannot propagate the slip into the next grain before the grain boundary actually fractures. Above the transition temperature, the dislocations have enough mobility to move around the precipitates and thus reduce the stress concentration.

In ingot iron the brittle to ductile behavior is related to the precipitates in the grain boundary and thus to the yield point and delay time.

A STUDY OF THE RELATIONSHIP BETWEEN THE YIELD POINT, DELAY TIME AND THE BRITTLE TO DUCTILE TRANSITION IN A LOW CARBON ALLOY

by

John Hrinevich, Jr.

A THESIS

Submitted to
Michigan State University
in partial fulfillment of the requirements
for the degree of

DOCTOR OF PHILOSOPHY

in

Metallurgy

Department of
Metallurgy, Mechanics, and Materials Science

1966

ACKNOWLEDGMENTS

I wish to express my sincere appreciation to Professors Austen J. Smith and Lawrence E. Malvern. Their guidance and counsel throughout this research were invaluable.

Thanks are also given to Dr. William E. Taylor who suggested the problem and to Dr. Howard Womachel who gave many helpful suggestions during the project.

Appreciation is also expressed to Dr. Robert Engle who helped with the instrumentation, to Dr. C. T. Wei for many helpful discussions, to Mr. Donald Childs and his staff for their excellent job of preparing samples, and to my fellow graduate students.

This project was supported in part by the National Science Foundation under Grant No. G-24898.

To my dear wife Mary Alice, who spent many hours in typing the rough drafts and the final draft, I will always be thankful for her understanding, encouragement, and confidence.

I also wish to thank my parents, for their encouragement all through college and this project.

TABLE OF CONTENTS

LIST OF TABLES

LIST OF FIGURES

LIST OF FIGURES (continued)

LIST OF FIGURES (continued)

LIST OF FIGURES (continued)

CHAPTER I

INTRODUCTION

Low-carbon steels at room temperature are normally considered impact resistant and ductile. Impact strengths as high as forty-five foot-pounds in a standard Izod test with considerable plastic deformation are commonly recorded. At very low temperatures, however, low-carbon steels often behave quite differently. Their impact strength in the standard Izod test may drop as low as two foot-pounds and the fracture shows practically no plastic deformation. This change from ductile behavior to brittle behavior occurs abruptly over a small temperature region. The average temperature of the transition zone is referred to as the Transition Temperature.

Some structures made of low carbon steel are used at temperatures below the transition temperature of the material and may fail in a brittle manner. The failures, while not an everyday event, have happened frequently enough to be both a very costly and aggravating problem for nearly the last eighty years.

One of the most famous and catastrophic brittle failures of a low carbon structure was the Boston molasses tank.[1] One January day in 1919, when the tank contained 2,300,000 gallons of molasses, it burst open. Twelve persons were drowned in molasses or died of injuries, forty

others were injured, and horses were drowned. Houses were damaged and a portion of the Boston Elevated Railway structure was knocked over.

Bridges also have suffered from brittle failure.[2] Just prior to World War II, about 50 bridges of a type known as a Vierendeel truss were built across the Albert Canal in Belgium. Some of these bridges were built of welded or rolled I-beam and plate, others entirely of plate. In March, 1938, when the weather was quite cold, the bridge at Hasselt, with a span of 245 feet, collapsed into the canal. Eyewitnesses heard a sound like a shot and saw a crack open in the lower chord. Six minutes later the bridge broke into three pieces, and fell into the canal. All the fractures were brittle, some through welds, others in solid plate away from the welds. The bridge was lightly loaded at the time. Within two years, two similar bridges failed in the same way.

Brittle failure has claimed a number of ships.[3] Between 1942 and 1952 about 250 welded ships suffered one or more brittle fractures of such severity that the vessels were lost or were in a dangerous condition. Nineteen of these 250 ships broke completely in two or were abandoned after their backs were broken. In the same ten-year period, 1200 welded ships suffered brittle cracks, generally less than 10 feet in length, which did not disable the ships but were potentially dangerous.

For brittle fracture to occur, three conditions seem to be necessary.[4]

1) Low temperature, such as exists in the winter months.
2) The presence of a notch, introducing triaxial stress.
3) High strain rate, or impact loading. This factor is not wholly necessary for the initiation of brittle failure.

The temperature at which the fracture changes from brittle to ductile, the transition temperature, is affected by various metallurgical factors.[5] It has been found that a fully-killed steel will have a lower transition temperature than a semikilled or rimmed steel. Small ferritic grain size, the use of a lower finishing temperature in hot rolling, increasing manganese content, nickel in amounts up to 1.80% and silicon in amounts up to 0.25% lower the transition temperature. Cold working and increasing contents of carbon, phosphorous, molybdenum, and boron increase the transition temperature. The first small amounts of aluminum lowers the transition temperature, but increasing amounts cause no change. Chromium appears to have little effect.

In this work, the beginnings of a more fundamental understanding of the brittle to ductile transition in low carbon alloys will be sought.

CHAPTER II

HISTORY AND BACKGROUND

2.1 Crystallographic and Metallographic Features of Brittle and Ductile Fractures

Brittle fracture may occur in ferritic steel and some other body-centered cubic materials and certain hexagonal close-packed metals. Face centered cubic metals like pure aluminum, copper, silver, and gold, even at temperatures near absolute zero and with sharp notches, do not fail in a brittle fashion or cleave.

During ductile fracture, slip in iron occurs in a pencil fashion[6] on planes containing the $\langle 111 \rangle$ family of directions. The $\{110\}$, $\{112\}$, $\{123\}$, or combinations of these families are the active slip planes. The resulting fracture surface is wavy and irregular. A brittle or cleavage failure occurs by separation without macroplastic deformation on the $\{100\}$ or cube faces.[7] The resulting fracture surface is relatively smooth and well defined.

The high-speed cracks occurring in a cleavage failure are not smooth but run in a discontinuous fashion.[8] Since each crystal cleaves on a (100) face, the crack must change direction as it goes from one crystal to another. Cleavage probably starts independently in neighboring grains. The resulting crack segments are then connected by plastic deformation at the grain boundaries.[9] One

should be able to observe the crack segments adjacent to or ahead of the main fracture in steel that has failed in a brittle manner. Jaffe[10] has observed such unconnected crack segments.

The surface of a brittle fracture shows little plastic deformation.[6] X-ray diffraction studies indicate that some plastic deformation does occur. The depth of the cold worked layer as revealed by etching the surface away and re-examining with x-ray techniques was approximately 0.05 mm.

2.2 Brittle to Ductile Transition Theory

One of the earliest attempts to explain the transition from brittle to ductile behavior was carried out by Mesnager,[12] who noted that to produce a brittle fracture, high speed loading was not necessary. Slow bending or slow tension can introduce brittle fracture if the specimen contains a sharp deep notch. His theory of triaxial tension in notch brittleness described how brittle fracture could occur under very low speed loading when a notch or crack was present.

When a uniform stress below the elastic limit is imposed on a plate in a direction perpendicular to a crack, a comparatively high stress in the same direction will exist just behind the root of the crack. The stress at the crack root is biaxial. If plastic flow is to occur at the crack root, there must be lateral contraction of

the material at that place in order to preserve constant volume of material. This lateral contraction is opposed by the large amount of material, stressed to a lower value behind the root of the crack. This will induce a state of triaxial stress, the third stress being perpendicular to the plane of the plate and tending to contract the material laterally at the root of the notch. As a result the axial stress at the root of the crack will build up beyond the uniaxial yield stress, Y, of the material to some value, Y_n, before flow can occur. The ratio of Y_n to Y is known as the "plastic constraint factor." Ludwik[13] in 1923 developed a similar theory.

Until 1945, it had been believed that if the notch was of correct depth and sharp-ended, the stress at the root and the plastic constraint factor would rise to infinity. Orowan, Nye, and Cairns[14] in 1945 showed that the maximum constraint factor is approximately three. As a result if a sharp crack is present in a stressed plate, the stress at the crack root must rise to about three times the normal uniaxial yield stress of the material before plastic flow will occur.

Davidinkov and Wittman further explained the phenomenon of transition in 1937. They drew a logical qualitative picture using the concept of "brittle strength." The resulting picture is shown in Figure 1.[15] The brittle strength B, yield strength, Y, and three times the yield

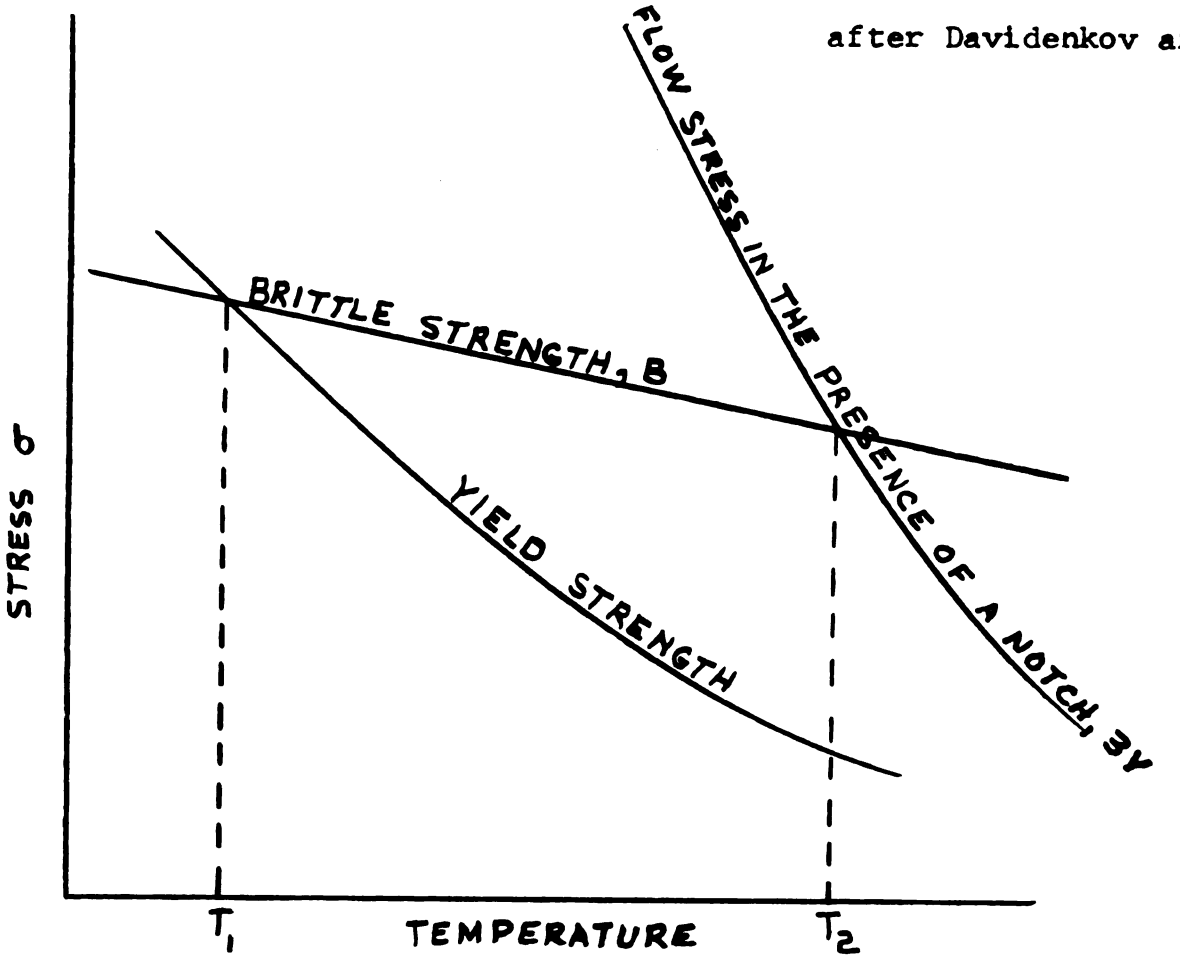

FIGURE 1

STRESS VERSUS TEMPERATURE FOR BRITTLE STRENGTH,

YIELD STRENGTH AND THREE TIMES THE YIELD STRENGTH

strength, 3Y, are sketched as a function of temperature. Experimentally, it is known that the yield strength rises with decreasing temperature. It was assumed that the brittle strength rose with decreasing temperature but not at so steep a gradient. Above temperature T_2 where the curves of brittle strength and of 3Y intersect, the material will be fully ductile, with or without the presence of a notch. Below temperature T_1, where the brittle strength intersects the yield strength, the material will always fracture in a brittle manner. The region between these two temperatures is the "notch brittle zone," wherein the material will behave in a ductile fashion in the presence of uni-axial stress, but if a notch is present, it will fail in a brittle fashion before the stress of 3Y with attendent plastic flow can be reached. In practice the transition from full ductile to full brittleness occurs in a narrow temperature zone rather than at a particular temperature.

In 1951, Eldin and Collins[16] determined the fracture and yield stress of A.I.S.I. 1020 steel at temperatures from 12°K to 185°K. From 12 to 61.5°K, all specimens exhibited typically brittle fracture, with no reduction in area, and the strength dropped steadily and linearly as the temperature was increased. At 61.5°K a sharp transition occurred. Above 61.5°K the reduction of area increased rapidly as the testing temperature was increased, and a yield stress, as well as a fracture stress could be measured.

A reproduction of some of their data is shown in Figure 2.

High strain rates favor brittle failure. This effect may very well be related to the strain-rate dependence of the yield strength. The yield strength of most metals is not particularly sensitive to strain rate.[17] In typical nonferrous metals, for instance, increasing the strain rate by several orders of magnitude will increase the yield strength by less than 20 percent. In low-carbon steels, however, a corresponding increase in strain rate will increase the yield stress by one hundred to two hundred percent. The brittle strength, on the other hand, shows a relatively small dependence on strain rate. The net result at higher strain rates is to displace the yield stress curve upward while the brittle strength curve remains nearly fixed. Brittle failure is thus more likely to occur.

Robertson[18,19] furthered our understanding of the transition temperature with studies carried out on flat plates. In effect, a saw cut was placed at the edge of the plate and a brittle crack was initiated by a wedging impact force. The specimen had a temperature gradient across it, the notch end being cold, and the opposite end being warm. All the while the specimen was in tension in a direction perpendicular to the notch. The crack traveled across the plate, and was arrested at some particular point. Beyond this point and above the

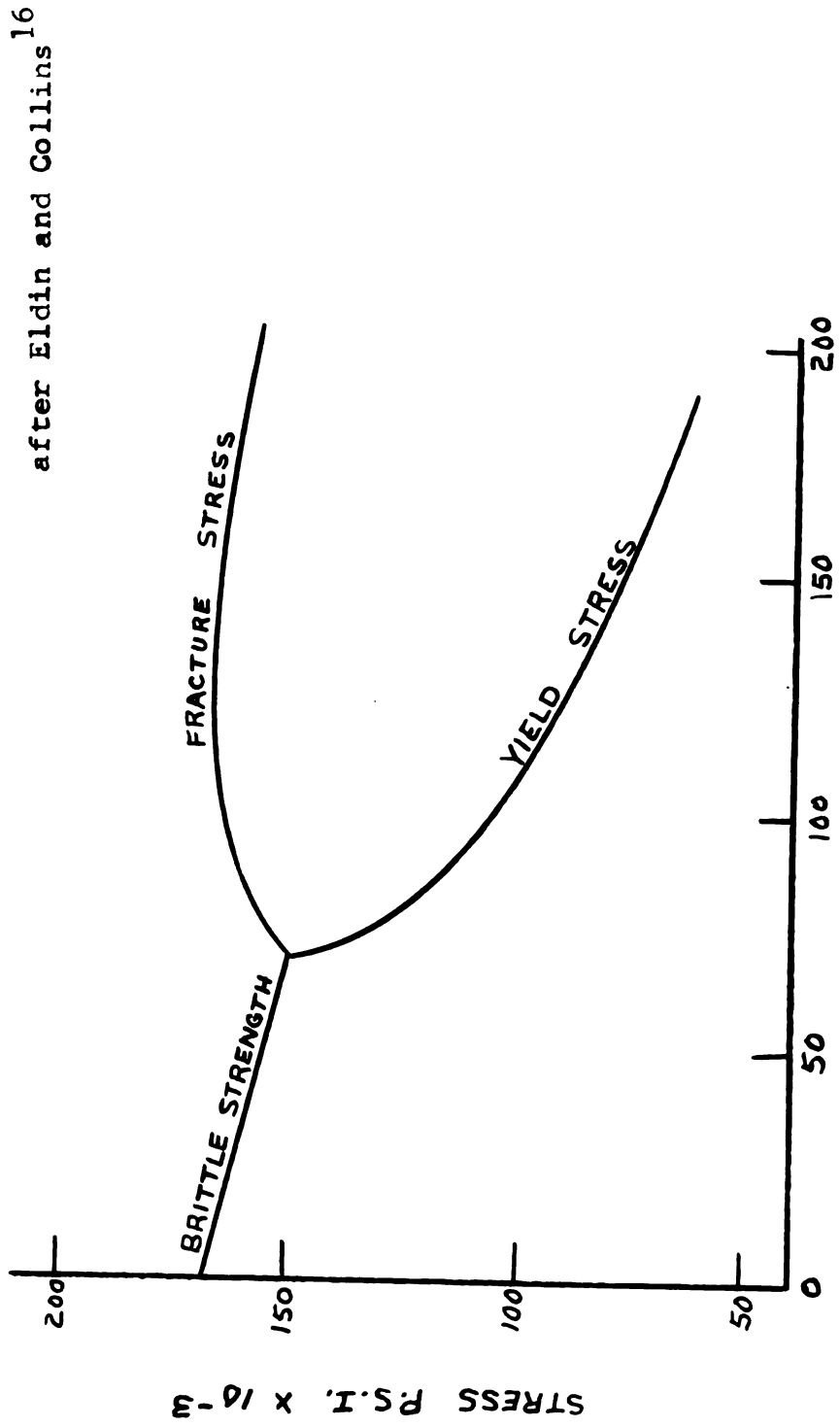

FIGURE 2

BRITTLE STRENGTH, FRACTURE STRESS,

AND YIELD STRESS VERSUS TEMPERATURE

particular temperature at this point, only ductile failure could take place. These experiments with different values of the tensile stress in the plate, but with a similar temperature gradient were repeated. The stress versus arresting temperature was then plotted. Typical results are shown in Figure 3. It will be noted that there appears to be a sharply defined temperature limit above which a brittle crack cannot propagate. This temperature agrees roughly with measurements of the transition temperature.

Wessel[20] has examined the relationship between brittle fracture and early stages of plastic deformation. Prior to an abrupt yield or brittle fracture, many dislocations move through the lattice but are subsequently piled up at barriers. An appreciable amount of plastic strain is associated with the piling up of these dislocation groups. The magnitude of the plastic strain increases with decreasing temperature, reaching a maximum at the transition temperature, below which the plastic strain decreases with decreasing test temperature. At temperatures above the transition temperature, abrupt yielding occurs when the stress concentrations that are present in the vicinity of piled-up dislocation groups become sufficiently high to overcome the resistance to deformation and activate other sources in the adjoining material, triggering a general catastrophic yielding. At temperatures below the transition temperature, the

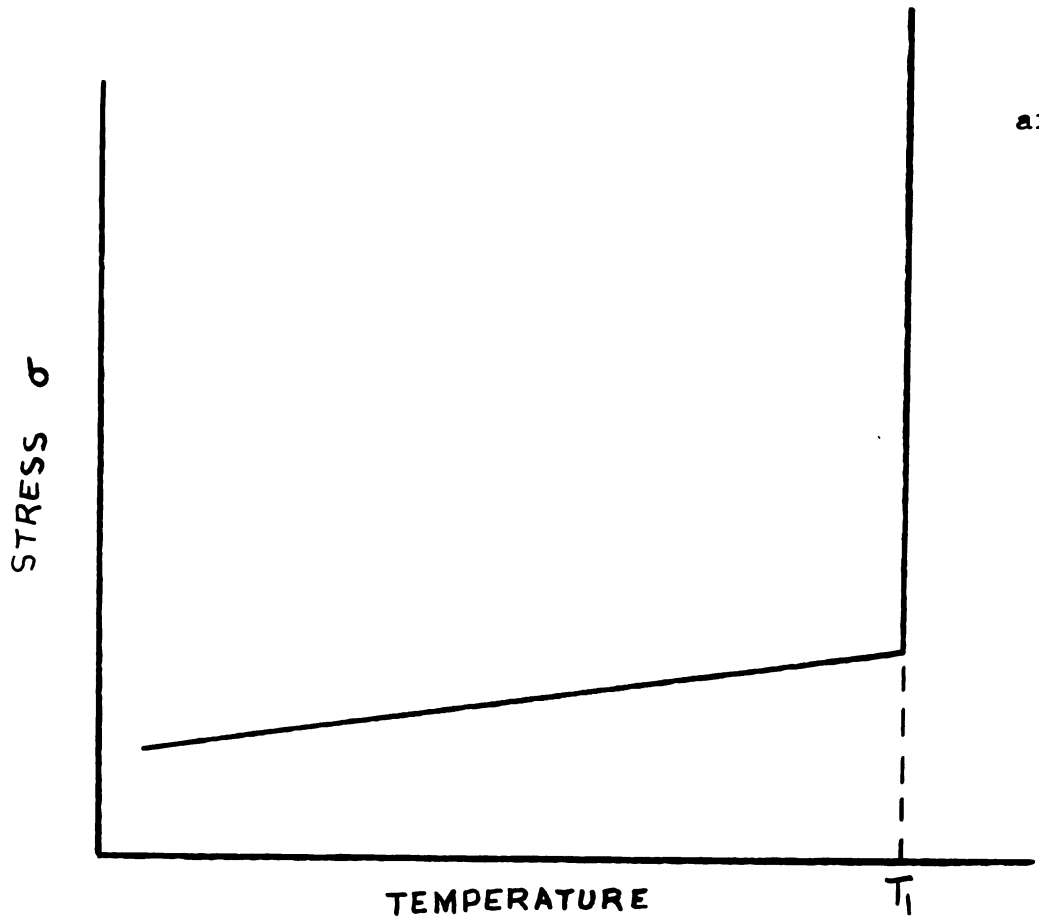

after Robertson[18, 19]

FIGURE 3

STRESS VERSUS TEMPERATURE FOR BRITTLE FRACTURE

Above T_1 a brittle failure cannot occur.

resistance to plastic deformation is so great that the stress concentration in some of the regions of piled-up dislocation groups becomes sufficiently high to initiate microcracks in these areas. The achievement of these high localized stresses and the resulting formation of some microcracks together with some plastic deformation triggers a combined general catastropic yielding and crack formation, terminating in complete brittle fracture.

Recently, attempts have been made to explain the brittle to ductile transition from a more fundamental view point. Zener,[21] Mott,[22] Koehler,[23] and others have suggested that the stress concentration at the tip of a slip band by piled up dislocations causes a small crack to form. Cottrell[24] by considering the surface energy of the crack, the stress field of the dislocations, the elastic energy of the crack, and the work done in opening up the crack has described the conditions for the crack to blunt out or to propagate and cause a brittle failure in an unnotched specimen. The final form of the equation is

$$\sigma_y \quad K_y \quad d^{\frac{1}{2}} = \beta 4 \gamma \qquad (1)$$

where

σ_y = shear yield stress

$K_y = \sigma_d L^{\frac{1}{2}}$

σ_d = unpinning stress for the temperature and time considered.

L = the distance from the piled-up avalanche to the nearest sources

d = grain radius

$\beta \cong 1$

μ = rigidity modulus or shear modulus

γ = surface energy per unit area

When the left hand side is smaller than the right hand side, a crack may form but is unable to grow beyond a certain length. In such cases the crack will blunt out. Low[25] and Owen, Averbach, and Cohen[26] have observed microcracks of the type expected. When the left hand side exceeds the right hand side, the yield stress is more than sufficient to make the crack grow into a full fracture. A transition is thus predicted.

Petch[27] considers that within the transition temperature range for a notch test the fracture is first ductile near the notch but changes to cleavage as it advances. The essential condition for this to happen is that the crack as it gathers speed moves into a region of greater triaxiality of stress. The fracture stress in front of the crack eventually becomes sufficient for Griffith propagation of the dislocation crack.[28]

The ductile fracture will change to cleavage failure when

$$\sigma \simeq 4\mu\gamma' / k^* L^{\frac{1}{2}} \qquad (2)$$

where

σ = fracture stress

μ = rigidity modulus

γ' = the effective surface energy associated with the growth of crack.

k^* = constant

L = length of the slip planes

Large grain size favors cleavage, and an increase in γ' favors ductile fracture.

The transition temperature arises from the temperature dependence of γ' and σ.[27] An increase in temperature weakens the dislocation locking which increases the number of active dislocation sources and thus raises γ' favoring ductile fracture. σ is given by the expression

$$\sigma = \sigma_o + k^* L^{-\frac{1}{2}} \qquad (3)$$

where σ_o = friction on an unlocked dislocation

With increasing temperature, σ_o decreases. This favors ductile fracture. The temperature-dependent changes in σ_o appear to be more important than the changes in γ'.

The lower yield point, σ_{lyp}, depends on the grain size[29] in the following way:

$$\sigma_{yp} = \sigma_o + k L^{-\frac{1}{2}} \qquad (4)$$

where σ_o = friction on an unlocked dislocation

L = grain diameter

k = constant

The constant k appears to be a measure of the stress required to unlock a dislocation to permit a slip band held up by a grain boundary to transmit yielding to the next grain as a Luders band. k is thus dependent on the temperature variation of the locking strength. Plots of σ_{lyp} versus grain size $^{-\frac{1}{2}}$ at a given temperature are

straight lines with constant slope. This suggests that the temperature dependence of the transition temperature of notched specimens arises mainly from σ_o.

σ_o is made up of a temperature independent friction σ_o^* and a temperature dependent σ_o^+. σ_o^* is caused by the resistance of random solute atoms, fine precipitates and lattice defects that resist dislocation motion. It amounts to approximately 4,000 pounds per square inch at the lower yield point[30] for an annealed mild steel. σ_o^+ is a Peierls-Nabarro stress. Its magnitude varies from 4,000 pounds per square inch at room temperature to 48,000 pounds per square inch at -196 C.[31]

Considering that σ_o^* is not too large, that σ_o obeys the relationship $\ln \sigma_o = \ln B - \beta T$ where B and β are constants, γ' is a constant, and that σ_o^+ varies linearly with temperature over small temperature ranges, the transition temperature, T_c, may be expressed as

$$\epsilon T_c = \sigma_o^* + C - \left(\frac{4q\gamma'}{k^*} - k^* \right) L^{-\frac{1}{2}} \qquad (5)$$

where ϵ, C, k^* = constants

q = the triaxiality $\cong$ 1/3

Thus the transition temperature is dependent on the grain size, friction of unlocked dislocations, the strength of dislocation locking, and the degree of triaxiality of the applied stress.

2.3 The Sharp Yield Point

Cottrell's[32] theory for the sharp yield point in body-centered cubic materials is based on the strong affinity of dislocations for carbon, nitrogen, and other atoms. In the unyielded or strain-aged condition, the dislocations are anchored by their atmospheres. In the yielded state, the dislocations are free of any atmosphere. Considerably higher stress is required to move a dislocation pinned by an atmosphere than to move one that is free of any atmosphere. To cause yielding, a stress high enough to move the dislocations with their atmospheres is required. However, as soon as the movement has begun, the dislocations are freed from their atmospheres and can move with a reduced stress. Since the change from the pinned to the unpinned state happens relatively fast at the beginning of plastic deformation, the material suddenly becomes softer and yields markedly. One of the best examples of sharp yield behavior is soft steel with 10^{-3} to 10^{-1} weight percent of carbon. Sharp yield points have been observed in a number of other materials.[33] Cadmium, zinc, brass, and molybdenum are a few examples.

Cottrell and Bilby[34] have described the atmosphere in greater detail. An important feature of the theory is that the atmosphere condenses into a line of solute atoms lying parallel and close to the dislocation at the position of strongest bonding. Under stress small segments of the dislocation are bowed out. Thermal fluctuations help the

loops grow to a stable size and then pull the rest of the dislocation away from its atmosphere. The authors calculated the ratio of the theoretical break-away stress at temperature T to the break-away stress at zero degrees Kelvin. The variation of the ratio with temperature agreed well with the variation of the yield strength with temperature.

Face centered cubic materials do not in general show a strong yield point.[35] Small atoms like carbon and nitrogen dissolved in a body-centered cubic metal distorts the lattice locally into a body-centered tetragonal structure. Because this distortion is not spherically symmetrical, these atoms interact with shear stresses, as well as with hydrostatic stresses, and so interact with both the screw and edge components of dislocations. A solute atom with a spherically-symmetrical elastic field, on the other hand, can interact only with an edge dislocation, since to a first approximation, a screw has no hydrostatic component in its field.

In the face-centered cubic lattice the arrangements of lattice positions around a substitutional site or the mainly used interstitial site at the center of the cube is too symmetrical to allow a solute atom in either site to produce a non-spherical distortion. Although there should be no direct elastic interaction between a pure screw dislocation and such solute atoms, it may still be possible to anchor the screws indirectly. In the face-

centered-cubic lattice ordinary unit dislocations in closepacked planes dissociate into pairs of half-dislocations, the lines of which run parallel to each other and are spaced a few atoms apart. The two dislocations in such a pair are joined to each other by a stacking fault and must glide together as a unit in the slip plane. Their Burgers vectors intersect at 60° so that there is no orientation of the line of the pair for which its members can both be pure screws; always, at least one of them must have a substantial edge component and therefore be able to be locked by solute atoms. If just one dislocation is locked, the other one cannot move either since they are coupled together by the stacking fault. While this locking is no doubt weaker, in general, than that in the body centered cubic lattice, nevertheless the possibility of producing yield points in face centered cubic crystals cannot be ruled out.

Adair, Hook, and McGaughey[36] have shown that the initial yield characteristics of iron with 20 parts per million carbon, 50 parts per million nitrogen, and 80 parts per million oxygen are strongly influenced by the extent of the segregation of interstitials to grain boundaries. Specimens cooled from 1292° F showed grain boundary precipitates in thin film specimens at 12,000 X. Samples quenched from 1292° F showed no precipitates in the grain boundaries. Slowly cooled samples showed a marked yield point and the quenched samples showed no

yield point. It is inferred that strong locking occurs when the grain boundaries have considerable segregation. This causes the marked yield drop.

Stein, Low, and Seybolt[37] developed a technique to lower the carbon content to as low as 5×10^{-3} parts per million in single crystals of iron using a hydrogen atmosphere continuously purified with ziroconium hydride. Samples with carbon contents from 5×10^{-3} parts per million to 0.02 percent were pulled in tension. The yield strength of samples with more than one part per million of carbon showed a strong dependence on temperature. The yield strength of samples with less than one part per million of carbon showed a marked reduction in temperature dependence. A reasonable explanation for these observations is that the temperature dependence of the yield strength in alpha iron of usual purity is due primarily to the interaction of mobile dislocations with interstitial impurities in solid solution.

Cottrell's theory of dislocation locking in the case of iron and related body-centered-cubic metals is well excepted. The dependence of the yield drop on interstitial impurities, the kinetics of strain aging, and direct observation by transmission electron microscopy of particles formed on dislocations provide a body of strong supporting evidence. However, the theory that unlocking dominates the yield drop is not entirely

satisfactory because the temperature, strain-rate, and grain-size dependence of the upper yield stress, lower yield stress, and of subsequent flow stress values are very similar. Yet the flow stress cannot be governed by an unlocking mechanism at low temperatures where the pinning points are essentially stationary.

Gilman and Johnston[38] accounted for the yield drop in lithium fluoride crystals quantitatively in terms of the rapid multiplication of dislocations and the stress-dependence of dislocation velocity. In lithium fluoride no evidence of unlocking has been found and grown-in dislocations remain locked. Dislocations responsible for the slip are heterogeneously nucleated and multiply rapidly.

Hahn[39] carried out the same type of analysis for alpha iron. According to him the abrupt yield is due to the presence of a small number of mobile dislocations initially present, a rapid dislocation multiplication and the stress dependence of the dislocation velocity. Considering the plastic strain rate, multiplication rate, and the dislocation velocity, the plastic strain is expressed as follows:

$$\dot{\epsilon}_p = 0.5\ bf\ (\rho_o + C\epsilon_p^a)\ (2\tau_o)^{-n}(\sigma - q\epsilon_p)^n \qquad (6)$$

where $\dot{\epsilon}_p$ = plastic strain rate

b = Burgers vector

$f \cong 10^{-1}$

C = experimental parameter related to the multiplication of dislocations.

a = experimental parameter related to the multiplication of dislocations.

τ_o = the resolved shear stress corresponding to the unit velocity.

n = experimental parameter related to the dislocation velocity.

q = proportionality factor relating the change in stress to the plastic strain.

The stress-strain curve calculated from this equation at constant strain-rate shows a pronounced yield drop as experienced with real metals. This suggests that unpinning may not be the only cause of the sharp yield point.

2.4 Delay-Time Phenomenia

Liu, Kramer, and Steinberg[40] observed that close-packed hexagonal zinc and body-centered cubic beta-brass showed a definite increase in critical resolved shear stress at temperatures below room temperature when the strain duration was decreased to about 10^{-3} seconds. However, in face-centered cubic copper crystals no delay time was apparent. Clark and Wood[41] found that rapid-load tests on type 302 stainless steel, SAE 4130 normalized steel, SAE 4130 quenched and tempered steel, 24S-T

aluminum alloy, and 75S-T aluminum alloy showed that no delay occurs for the initiation of plastic deformation and none of these materials exhibit a definite yield point in their static stress strain curve. Annealed low carbon steel showed a delay time and its static stress strain curve does have a definite yield point.

Kramer and Maddin;[42] and Lui, Kramer and Steinberg[40] imply that the type of crystal structure determines whether the delay time phenomenon will occur whereas Clark and Wood[41] feel that the appearance of a yield point on the static stress strain curve is the important criterion. This is almost the same criterion because usually body-centered cubic materials show a strong yield point.

Clark and Wood[43] compared the delay times for the initiation of yielding in a steel treated in four different ways: a) annealed; b) annealed and wet-hydrogen-treated to eliminate the static upper yield point; c) annealed, wet-hydrogen-treated and recarburized; d) annealed, wet-hydrogen-treated and renitrided. All four of the samples behaved in a qualitatively similar manner when subjected to rapidly applied constant stress, that is, a delay time for the initiation of plastic deformation exists for all four materials; the relations between this delay time and the stress are all quite similar in form; and the effect of temperature upon these relations is essentially the same in all cases. Furthermore, the behavior of these materials is similar to the behavior

of annealed low-carbon steels. However, definite quantitative differences in behavior are exhibited between the four materials. The test results showed that the principal effect of changing the carbon and nitrogen content of an annealed low carbon steel subjected to rapidly applied constant stress was to change the stress corresponding to a given value of the delay time. The magnitude of the stress for a given delay time was decreased by a reduction of the carbon and/or nitrogen concentration. This supports the theory that the delay time phenomenon is a result of the dislocations being unable to move as soon as the stress is applied. As the carbon and nitrogen content is decreased, there are interstitial atoms available for pinning, the dislocations can move more easily, and the delay time increases as a result.

Vreeland, Wood, and Clark[44] carried out some interesting repeated stress-pulse experiments which also supported the idea that the delay time is a result of the inability of the dislocations present to move as soon as an external stress is applied. The tests employed showed the effect of stress-pulses and aging on the delay time. Stress-pulses of essentially constant magnitude and duration on the specimen were used. The pulse was as follows:

a) Stress of 45,000 $\pm$ 800 psi applied in approximately 0.007 seconds.

b) Stress held essentially constant for 0.029 $\pm$ 0.001 seconds.

c) Stress removed in approximately 0.003 seconds.

The delay time for the material when subjected to a stress of 45,000 pounds per square inch is approximately 0.050 seconds, which is greater than the duration of stress-pulse and less than the duration of two stress pulses. Thus, the material might be expected to yield during the second stress-pulse if there were no recovery between pulses.

The specimens were aged for various intervals of time between stress-pulses at temperatures of 70, 150, and 200° F. The procedure for aging the specimens after a stress-pulse was as follows:

1) Specimen removed from rapid-load machine and placed in a bath at the desired temperature within five minutes after the stress pulse.
2) Specimen removed from the bath after the desired aging period and immediately cooled in powdered dry ice.
3) Specimen brought to approximately 70° F in an alcohol bath five minutes prior to the next stress-pulse.
4) Stress-pulse applied when the specimen reached 70° F.

The results of the repeated stress-pulse tests showed that a definite recovery from the effects of the previous stress-pulse takes place when the time and temperature

between stress-pulses is sufficient.

It was found that approximately fifty percent of the microstrain is recovered after removing the load. This indicates that some of the dislocations which were displaced by the applied stress return toward their original positions when the stress is removed, as might be expected.

The microstrain rate, prior to the initiation of yielding, decreases with time. This might be accounted for by a depletion of the reservoir of dislocations which may be moved by the applied stress. This may also account for the decreasing amount of microstrain induced by successive stress-pulses when recovery does not take place. When the aging treatment between stress-pulses induces recovery, a greater decrease in the microstrain in successive stress-pulses if found. The recovery mechanism may be explained by the diffusion of carbon and nitrogen to the dislocations which have been displaced. The resulting array of dislocations, anchored by atmospheres of carbon and nitrogen, may be expected to be more stable than the original array under the particular stress condition. Successive stress-pulses and aging cycles then produce less microstrain, and yielding does not take place. The more stable configuration of dislocations for the particular stress condition is also indicated by the results of the rapid load tensile tests on the

material which had previously been subjected to stress-pulses and aging cycles in which recovery took place. The delay times for the initiation of yielding are increased by a factor of approximately four over the delay times for the original material for corresponding stresses.

Fisher[45] derived an expression for the delay time. Taking into account the energy necessary to unpin the dislocation, the energy necessary to extend the dislocation line, the rate of thermal nucleation of loops, and the idea that the delay time is associated with the generation of a large number of dislocation loops; the expression for the delay time is as follows:

$$\text{Log (D.T.)} = A + BG^2/\tau T \qquad (7)$$

where

(D.T.) = delay time

G = the rigidity modulus

τ = resolved shear stress on the slip plane.

T = absolute temperature

The agreement with experimental data was good except at low temperatures. Thus the delay time for yielding under constant stress depends upon the single parameter $G^2/\tau T$ and not upon stress or temperature independently.

CHAPTER III

EXPERIMENTAL METHODS

3.1 Material

Armco magnetic ingot iron was used for all specimens. The ingot iron was purchased in cold-drawn three quarter inch diameter bars twelve feet long. The chemical composition was determined from a 0.400 inch by 0.400 inch by 2.0 inch sample machined from the middle of a twelve foot bar. Care was taken to remove equal amounts from all four sides to eliminate surface effects. The analysis was carried out by the United States Steel Research Laboratories. Table 1 shows the average chemical composition.

The iron in the as-received condition was essentially all ferrite with some oxides and manganese sulfide present. Figure 4 shows a typical cross-section microstructure of the as-received ingot iron. As expected, the as-received ingot iron showed considerable cold working. Figure 5, a longitudinal section, illustrates this point.

3.2 Atmosphere for Heat-Treating

High purity dried argon gas (99.995) was used as a protective atmosphere for all high temperature treatments. The argon was purchased from the National Cylinder Gas Company in cylinders containing 330 cubic feet of the compressed gas. Only one cylinder of gas was required for the entire test series.

TABLE 1

Average Chemical Composition of the Ingot Iron.

Element	Percent by Weight
Carbon	0.015
Manganese	0.063
Silicon	0.004
Phosphorous	0.004
Sulfur	0.021
Nitrogen	0.004
Oxygen	0.092

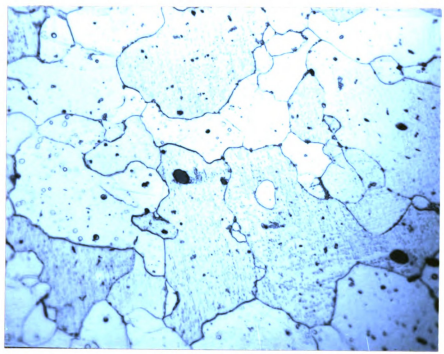

Etch: 4 percent Nitric Acid in Amyl Alcohol

500 X Mount # 65-129

FIGURE 4

Cross-section of As-received Ingot Iron.

The matrix is ferrite with some manganese sulfide and oxides present.

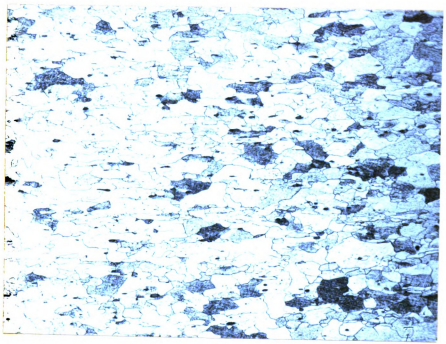

Etch: 4 percent Nitric Acid in Amyl Alcohol

100 X Mount # 65-131

FIGURE 5

Longitudinal Section of As-received Ingot Iron.

The elongated grains show that the material has been cold worked.

In use the gas was passed through a Linde Inert-Gas Double-Stage Regulator to reduce the tank pressure to a constant value of five pounds per square inch and then through a needle valve to regulate the flow before being passed into the drying train. From the drying train, it was piped into the heat-treating furnace in a 1.25 inch soft copper tube.

The drying train was assembled especially for these experiments. A one-inch-diameter 36 inch-long heavy-wall black iron steam pipe was threaded on both ends for standard pipe fittings. The tube was then pickled in an aqueous 30-percent nitric-acid solution to remove the oxides left from manufacturing. After rinsing in water and drying, a two-inch plug of fine clean copper turnings was pushed just past the center of the pipe. Next a tight-fitting 80 mesh austenitic stainless steel screen was placed over the copper turnings, and three inches of minus ten plus thirty mesh titanium powder were added. Over the titanium powder another tightly fitting 80-mesh austenitic stainless steel screen was placed followed by another two-inch plug of fine clean copper turnings. Figure 6 shows a cross section of the drying train.

The assembled drying train was placed in a Burrell-High Temperature Furnace, Type CTA1-9, and standard pipe-reducers were screwed onto both ends, using teflon tape as a sealant. Brass half unions were used to connect the incoming and outgoing copper tubes. A platinum platinum-

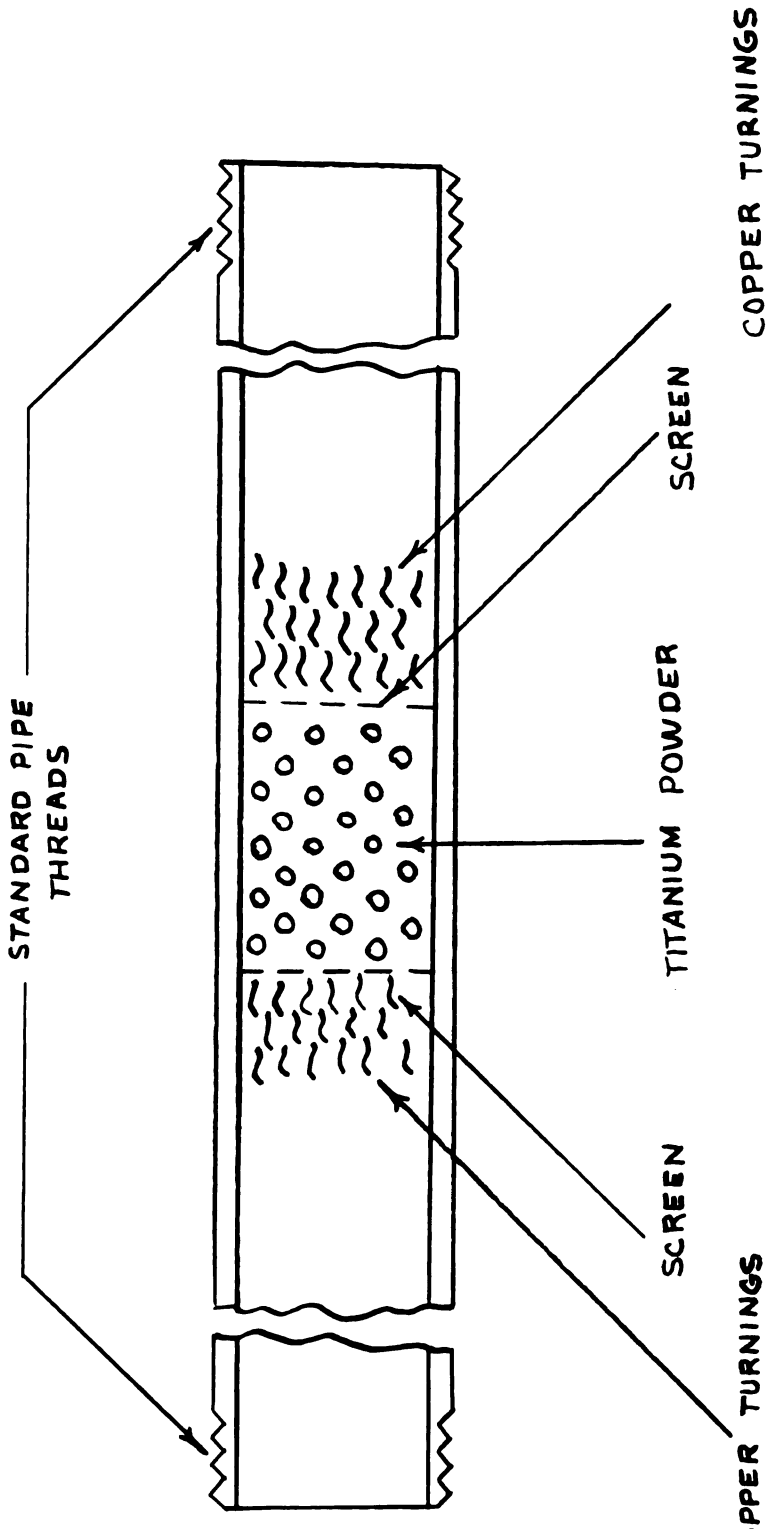

FIGURE 6

CROSS-SECTION OF DRYING TRAIN

rodium thermocouple was positioned near the drying train tube through the top of the furnace. The output of the thermocouple was connected to a Leeds and Northrup Micromax Recorder which controlled a set of mercury relays used to turn the furnace on and off. A variable transformer was placed in the incoming power line and adjusted to keep the over drift of the heating cycle to a minimum. The temperature of the drying train was kept at 1000° F. Figure 7 shows the assembled drying set- up.

3.3 Heat-Treating Equipment

A furnace to homogenize samples at 1350° F was built from a Hoskins type FD204C furnace. The furnace has a silicon carbide muffle around which nichrome heating elements are wound. To rebuild the furnace, the door and back wall were replaced with insulating bricks. The bricks were cemented in place to prevent gross air currents and to provide good mechanical strength. A 1.25 inch diameter hole was cut through the front and back bricks and a 1.25 inch diameter by thirty-inch-long fused silica tube was positioned in the middle of the furnace. The tube was located at equal distances from the sides, top, and bottom of the muffle. A chromel-alumel thermocouple was placed on the outside of the tube opposite where the samples were heated. The output from the thermocouple was connected to a Foxboro Model 5041-40 controller which controlled a relay.

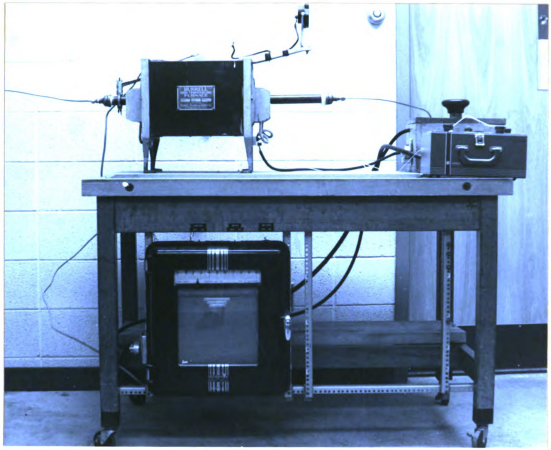

FIGURE 7

ASSEMBLED DRYING SET-UP

A large variable resistor was placed in the incoming power supply to prevent over-running during the heatup cycle. .25 inch diameter copper cubing cooling coils were wound around both ends of the silica tube to protect the rubber stoppers used to seal the incoming and outgoing tubes used to carry the protective atmosphere. A cross section of the furnace is shown in Figure 8. The completed furnace is shown in Figure 9.

3.4 Heat-Treating Procedure

The drying train and furnace were purged for thirty minutes with argon before turning on the drying train to 1000° F and the furnace to 1350° F. An hour and one half was allowed for them to come to temperature and stabilize. The sample to be heat-treated was washed in 1,1,1 trichlorethane and rinsed in ethyl alcohol before a fourteen inch eighteen gauge annealed wire was attached to serve as a handle. The sample was then placed inside the front rubber stopper with the wire running out the stopper through the atmosphere bleed off tube. After purging the system for thirty more minutes, the sample was pushed into the high heat zone with the aid of the attached wire. During the transfer from the cold zone to the hot zone, the furnace atmosphere was not disturbed and the position of the sample was determined by index marks on the wire. After one and one half hours in the high heat zone, the front stopper was removed and the sample was quickly withdrawn

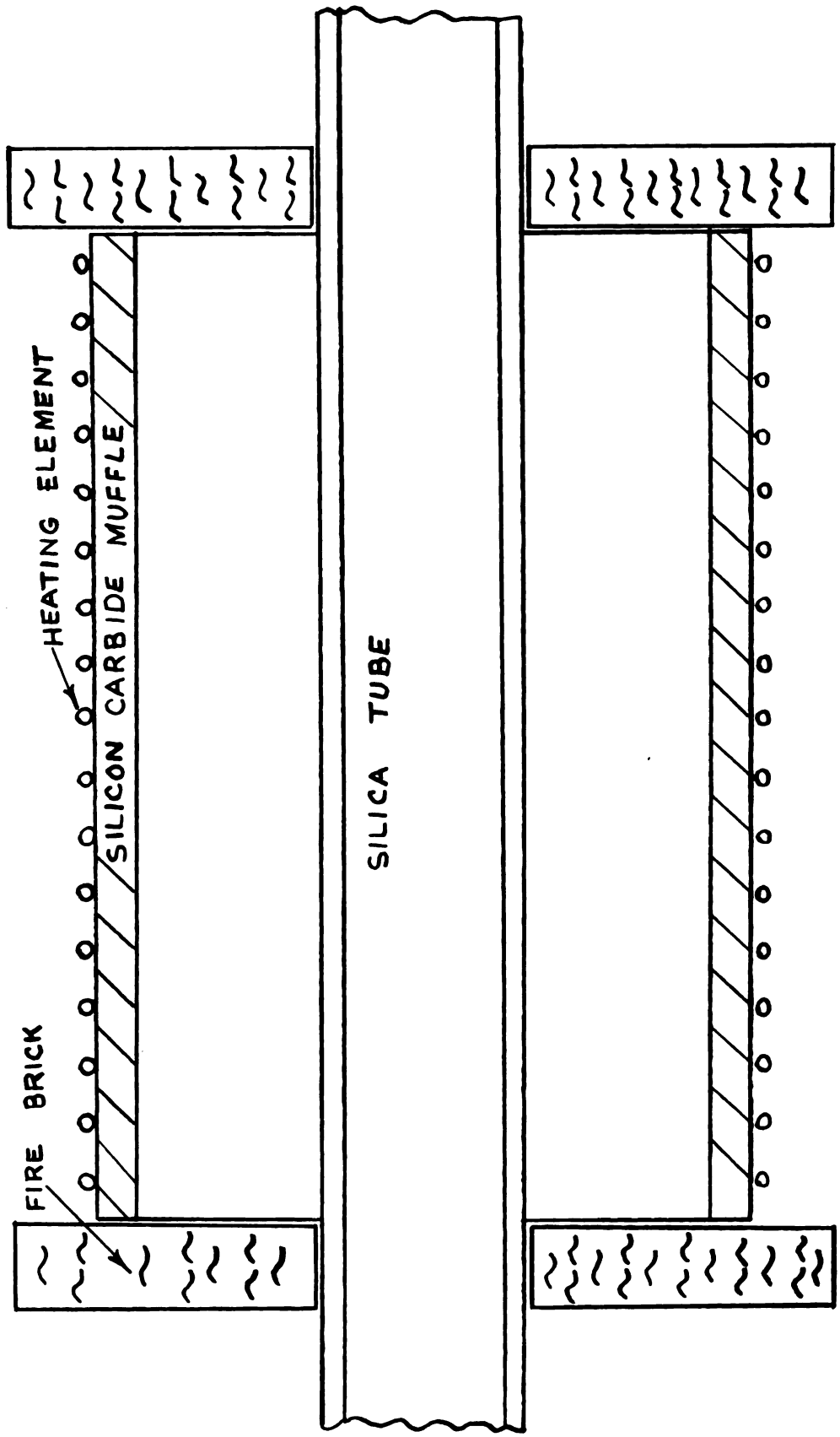

FIGURE 8

CROSS SECTION OF FURNACE

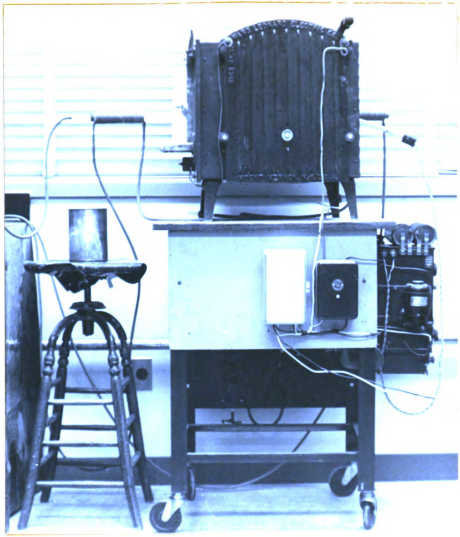

FIGURE 9

COMPLETE FURNACE

and quenched. A 10 percent solution by weight of sodium hydroxide in water was used as the quench. Before each run, the quenching bath was placed in the freezer of a standard home refrigerator and cooled to 14° F. Hereafter, this heat-treatment will simply be referred to as solution-treating.

The controller on the furnace and the recorder on the drying train were balanced before each run. About once a week, a twenty-eight gauge thermocouple was fastened to a sample and the sample was run through its heat-treatment. During the run, the temperature was checked using a Leeds and Northrup #8692 Temperature Potentiometer. Since there was a temperature drop from the outside to the inside of the silica tube, it was necessary to set the furnace slightly higher than 1350° F to insure that the sample reached 1350° F. The temperature of the drying train was periodically checked using the same Leeds and Northrup potentiometer and chromel-alumel thermocouple. In Figure 10, an overall view of the heatreat facility is shown.

3.5 Aging Experiments

Samples three eighths-inch thick by three-fourths-inch wide by three inches long were milled from the as-received ingot iron. The tool marks from the top and bottom surface were removed by polishing on 1, 2/0, 3/0, and 4/0 emery paper. Special care was taken to insure that both surfaces were flat.

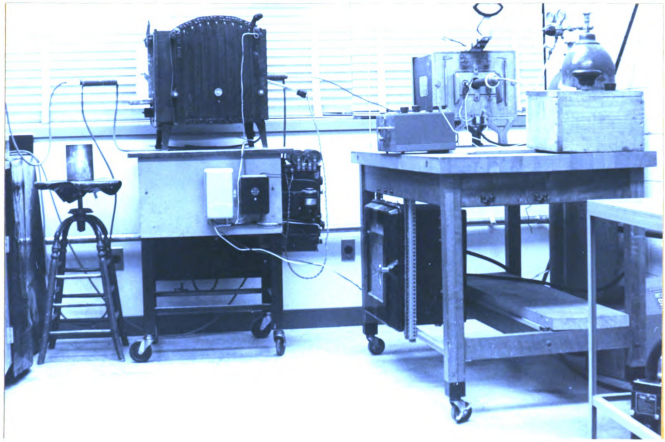

FIGURE 10

OVERALL HEAT-TREATING FACILITY

Samples were then solution treated as described in section 3.4 and then aged by heating to various temperatures from 32° F up to 300° F for up to four days.

The extent of aging was determined by checking the hardness at various time intervals up to four days. One Wilson Rockwell Hardness Tester (MT-755) was used for measuring the hardness. The Rockwell "K" scale (one eighth inch diameter ball with a one hundred and fifty kilogram major load) was found to give the best results. At each time interval, the sample was removed from the oven, and nine readings were taken on the upper surface and then averaged. Care was taken to insure that the readings were taken over the entire surface rather than in one localized area. Hardness readings were taken only on one side to insure the best accuracy.

Temperatures above room temperature, needed for aging the solution treated samples, were generated in a Thelco #31479 oven. The oven is heated by nichrome heating elements located on the bottom of the hearth and is equipped with a fan to circulate the air inside to insure uniform temperature. A bimetal strip turns the oven on and off, maintaining the desired temperature. A mercury thermometer was used to check the temperature during all runs. Temperatures below room temperature were obtained from a standard household refrigerator. No special atmosphere was used during aging.

3.6 Impact Tests

To insure reproducibility and to decrease the danger of distortion during heatreatment, a special impact sample was designed. Essentially, the sample was an Izod sample with a key-hole notch. This notch can be accurately reproduced more easily than a vee-notch and also makes heatreatment of the samples easier because it does not concentrate stress as much as other notches. The drawing used to produce the samples is shown in Figure 11.

The impact samples were produced by milling rough blanks from the three fourths inch diameter Armco ingot iron bars. The rough blanks were ground to size on a surface grinder. The ends of the samples were finished on a belt sander using a special jig which insured that the ends were perpendicular to the sides. To produce the root of the notch, a precision vise was positioned on a drill-press table so that when the sample was flush with one side of the vise, the #47 drill would form the root of the notch in the right place. The vise was then securely fastened to the table and all samples were drilled using this set-up. The slot from the outer surface to the hole was formed by milling with a one thirty-second inch milling saw. In Figure 12, a completed sample is shown.

The samples were tested on a Tinius Olson Impact tester. The sample was positioned in the vise using a jig to insure that the notch was located in the same position each time. In Figure 13, an overall view of the testing

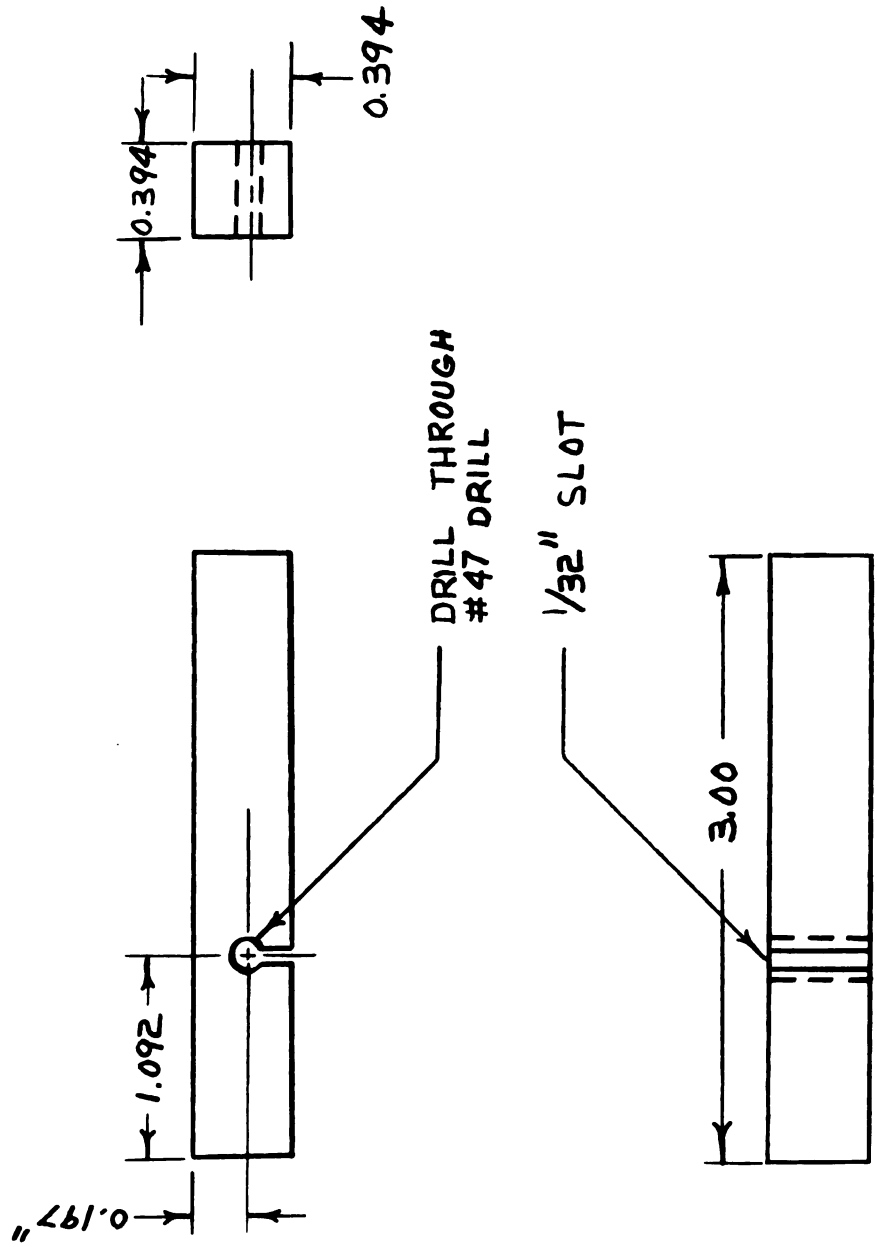

FIGURE 11

IMPACT SAMPLE

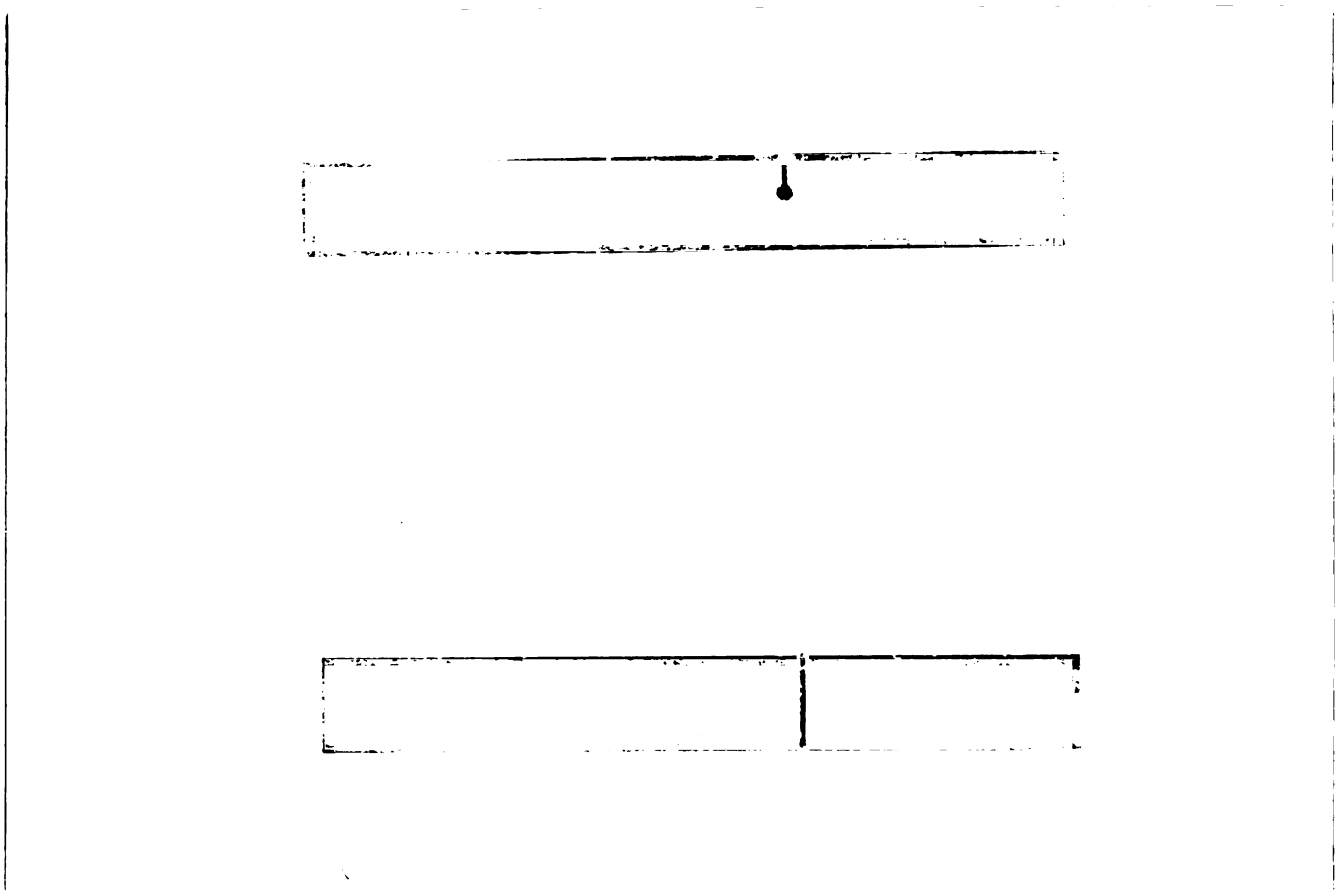

FIGURE 12

COMPLETED IMPACT SAMPLES

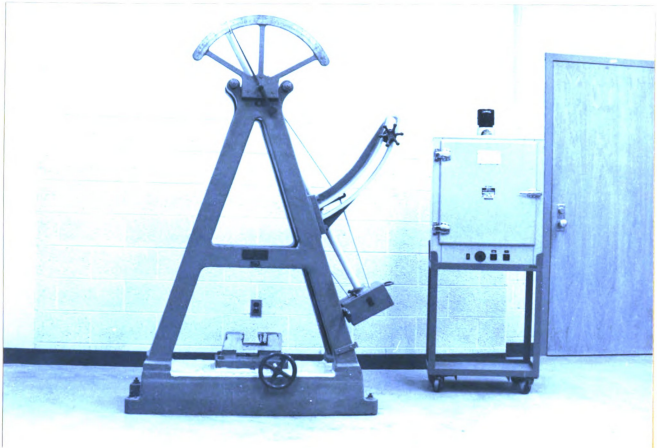

FIGURE 13

IMPACT TESTING FACILITY

facility is shown. A close-up of a sample ready for testing is shown in Figure 14.

Four different sets of samples were tested. They were as-received, annealed, solution treated, and solution treated and then aged for six hours at 158° F. The annealing was accomplished by heating the bar stock up to 1350° F, holding for one and one half hours and then shutting off the furnace. About three hours were required for the samples to cool to 500° F. No special atmosphere was used during annealing since almost two tenths of an inch had to be machined away while making the samples. The solution treated and the solution treated-aged samples were solution treated in the finished condition as outlined in section 3.4. From each set of samples, three impact bars were tested at 14, 70, 158, and 300° F. These temperatures were obtained using the oven and refrigerator discussed in section 3.5. At all temperatures, the jaws of the impact tester were held at the test temperature for one hour before the sample was brought to the test temperature in the same oven or refrigerator and held fifteen minutes. The jaws and samples were transferred from the oven or refrigerator as a unit. Using this procedure, temperature loses in the sample were kept to a minimum.

3.7 Static Compression Tests

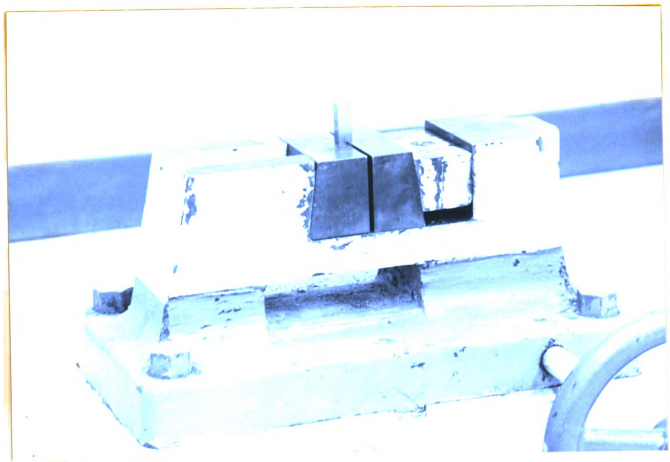

FIGURE 14

CLOSE-UP OF SAMPLE READY FOR TESTING

Compression tests were performed on cylindrical specimen 0.505 inches diameter by 1.000 inches long. An Instron model TTCMLM1-6 testing machine was used to apply the load. The displacement rate was 0.05 centimeters per minute. Since this instrument gives a constant displacement rate regardless of the load, it was possible to record the strain by running the recorder chart at a constant speed. The time axis on the chart may thus be converted to strain.

Sheet teflon disks 0.003 inches thick by three fourths inch diameter were placed on both ends of the specimen to lubricate the ends and eliminate any barreling effects. With the teflon sheets on the ends, samples were deformed plastically 25 percent and showed no barreling.

Samples in the annealed, solution-treated, and solution-treated-aged six hours at 158° F condition were tested at 14, 70, 158, and 300° F. The annealing, solution treating, and solution treating-aging were carried out in the same manner as described for the impact samples in section 3.6.

To ensure that the temperature did not change appreciably during the test, two large steel heat sinks were made. The sinks were three and one half inches in diameter and two inches thick. Before each test the sinks were brought to the test temperature and held one hour before running the test. The specimen to be tested was brought to the test temperature and held fifteen minutes

before being transferred with the heat sinks to the Instron for testing. Each test required about one to one and one half minutes to complete. In Figure 15, an overall view of the test facility is shown. A close-up of the heat sinks with a specimen in place is shown in Figure 16.

3.8 Pressure-Bar System for Delay Time Measurements

A split pressure bar was used to produce flat top loading pulses approximately two milliseconds long. The magnitude of the stress generated is determined by the velocity at which the striker bar strikes the pressure bar. The relationship is given by:

$$\epsilon_2 = \frac{v}{c_2}^2$$

where ϵ_2 is the strain in the pressure bar.

V_2 is the velocity of the pressure bar after being struck.
(equals $\frac{1}{2}$ V, if the striker bar and pressure bar are the same diameter and length.

C_2 is the speed of propagation in the pressure bar.

The speed of propagation is in turn given by the expression:

$$C = (E/\rho)^{\frac{1}{2}}$$

where E is the modulus of elasticity, ρ is the density of the medium in which the pulse is traveling.

FIGURE 15

OVERALL VIEW OF STATIC STRESS-STRAIN TESTING

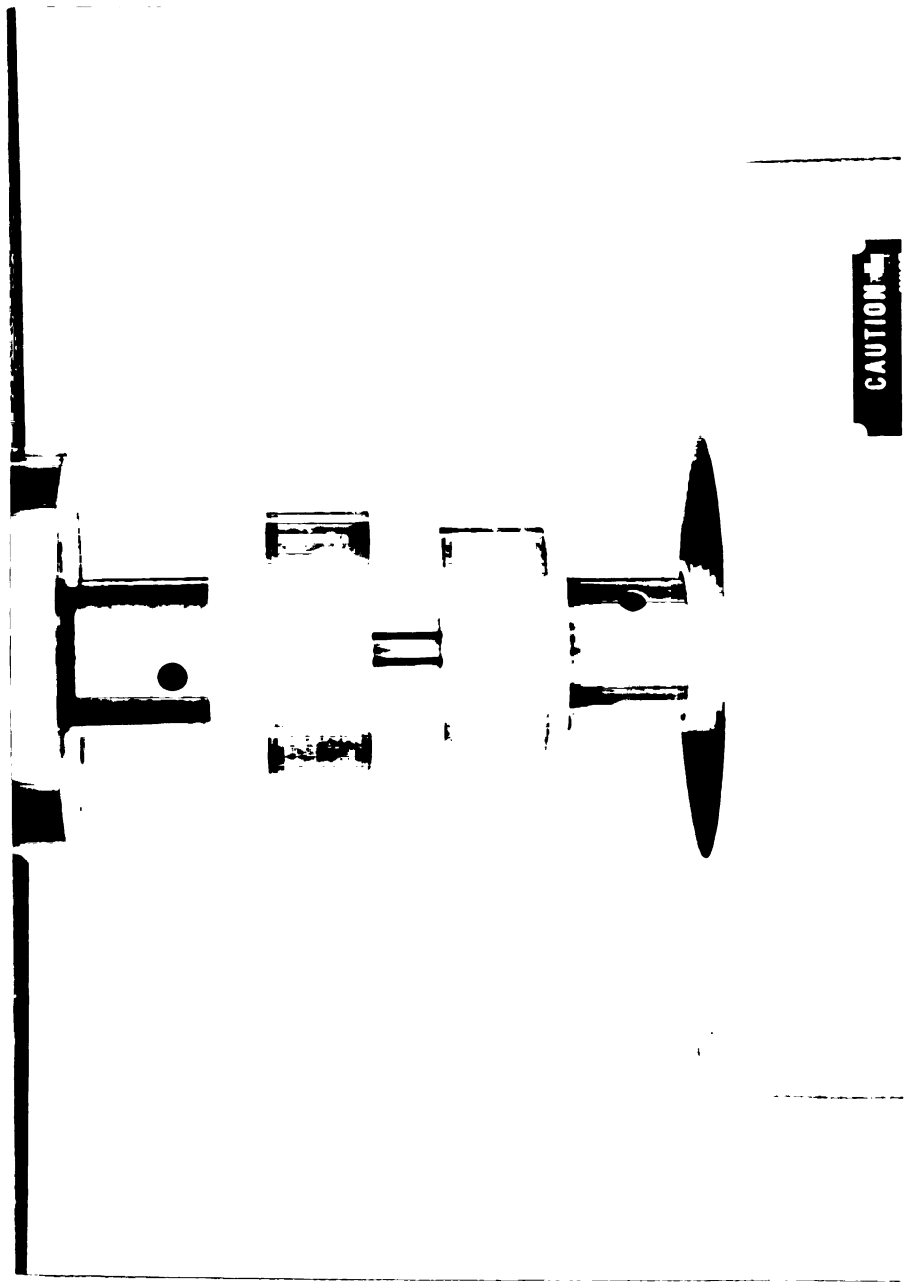

FIGURE 16

CLOSE-UP OF SAMPLE AND HEAT SINKS

The duration of the pulse is determined by the time required for the pulse to go down the bar, reflect off the end, and travel back. Thus, the longer the bar, the longer the stress will be held.

In this experiment, the striker bar was one bar sixteen feet nine inches long and the pressure bar was made up of two separate bars; one sixteen inches (spreader bar) and one fifteen-feet-five inches long. In use the sample was placed between the spreader bar and the fifteen foot-five-inch bar and struck with the striker bar. It was necessary to place the spreader bar in front of the sample to eliminate end effects. The bars are shown in Figure 17.

All the bars were made from prehardened (27-30 R_c) SAE 4140 steel. The steel was purchased in five-eighths inch diameter by twenty foot-long bars and then centerless ground to nine sixteenths inch diameter to ensure straightness and a good surface. After cutting to the desired lengths, one end of the striker and spreader bar and both ends of the fifteen-foot-nine inch bar were carefully turned on a lathe to produce a good flat surface perpendicular to the sides of the bar. The other end of the striker bar was shaped into a hemisphere and the other end of the spreader bar was slightly counter-bored to help keep the bars together during impact.

To contain the bars and hold them in line during impact, a large bed was made. The base of the bed consisted of two eight-inch heavy-web-I-beams forty-seven feet long

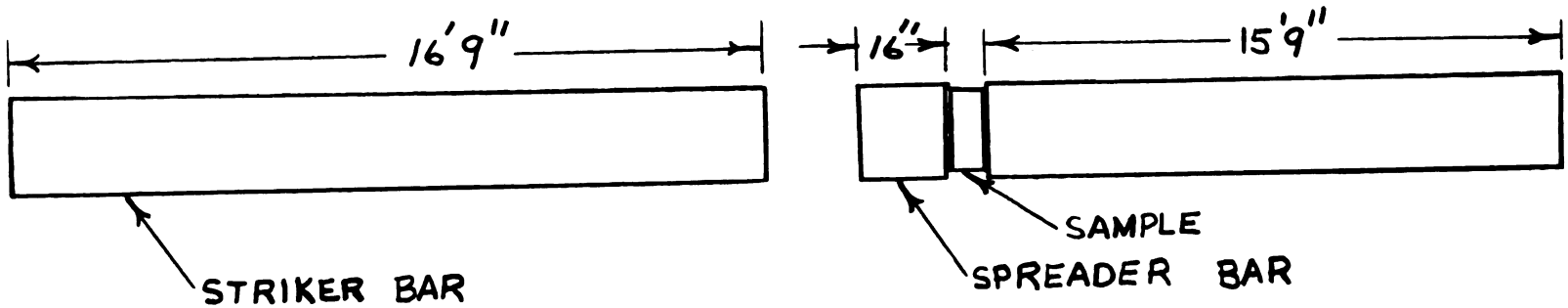

FIGURE 17

STRIKER AND PRESSURE BAR

each. The beams were welded together with six-inch pieces of the same eight inch heavy-web I-beam at about every twenty-four inches. L-brackets made of two-inch angle-iron were bolted to the eight-inch-I-beams every twenty-four inches. Two-inch light-weight angle-iron was bolted to the L-brackets and specially designed pillow blocks were bolted to the angle-iron every twenty-four inches to carry the striker and pressure bars in rubber "O" rings inserted in grooves machined in the pillow blocks to prevent radial constraint and lubricated with molybdenum disulfide. Special care was taken to align the whole system so that the bars were in good alignment. The whole bed was securely fastened to the floor. The massiveness of the system was necessary to keep the system aligned during testing and to dissipate the energy generated. In Figure 18, the bed is shown with the bais in place. The pillow blocks used to carry the bars are shown in Figure 19.

To generate stresses high enough to cause the samples to yield required that the striker bar strike the pressure bar at velocities sometimes above fifty feet per second. To dissipate the energy generated, two-inch lead cubes were bolted to a large cast iron L-bracket fastened to the rear of the bed. The bars were caught in the lead blocks and their energy dissipated in the deforming of the lead. The lead blocks had to be replaced after each run.

Another problem arising from the large forces generated was the tendency for the striker bar to slip off the end of the spreader bar thus bending both bars. This problem

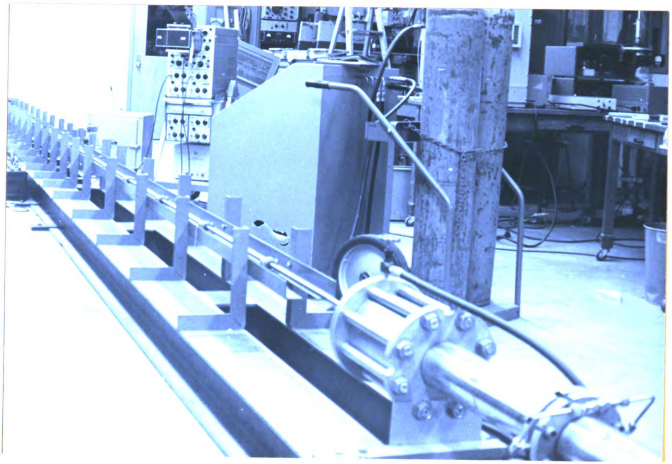

FIGURE 18

HYGE BED

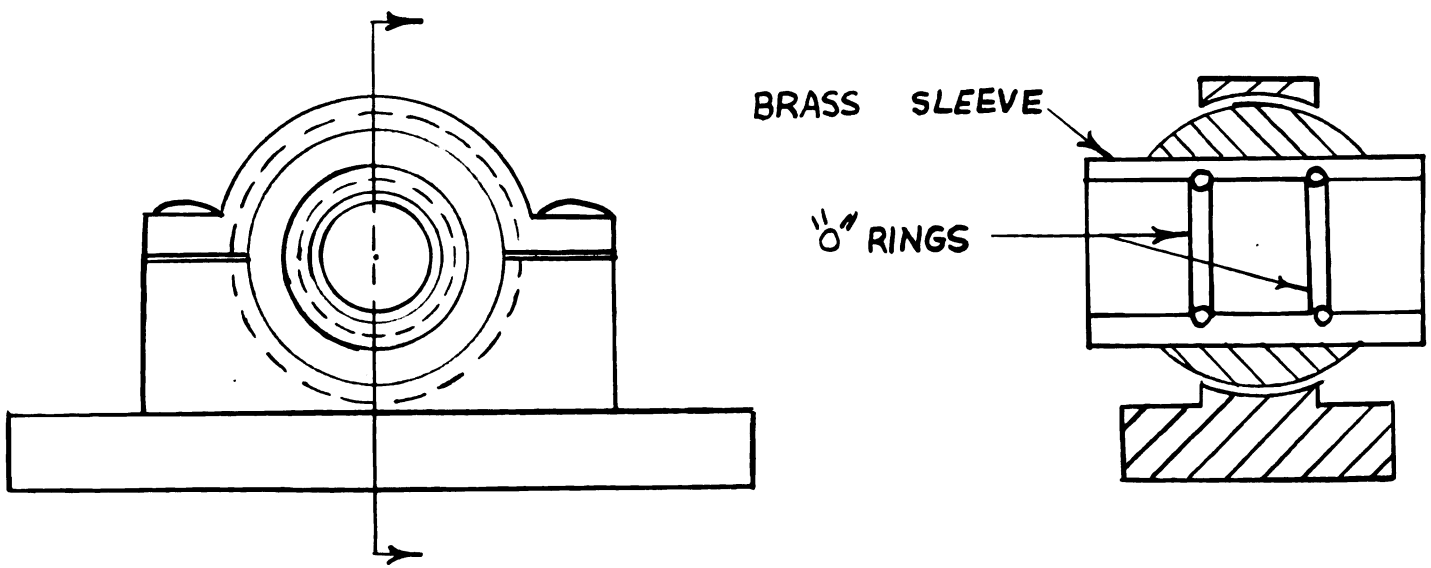

FIGURE 19

PILLOW BLOCKS

was solved by designing an aluminum funnel which constrained the lateral movement of the bars after striking. The small end of the funnel was a slip fit on the spreader bar and was two-inches long. The large opening was seven-eighths inch diameter and it gradually tapered to the small diameter in one-and one-half inches. In Figure 20, a cross section of the funnel is shown.

3.9 Loading Device For Delay Time Measurements

A Hyge Shock Tester, type HY-3422, was used to accelerate the striker bar. The tester was used as received from the Consolidated Electrodynamics Corporation except that it was mounted horizontally on the bed holding the bar assembly rather than in a vertical position on a three-foot cube of concrete as suggested by the maker. In Figure 21, the mounted tester is shown. A schematic sketch of the tester is shown in Figure 22.

The acceleration of the piston is achieved by applying a set pressure to chamber B with dry compressed nitrogen. This pressure acts over the full area of the piston and seals it against a ring seal at C. A pressure is then applied to chamber A, which is restricted to only about one-fourth the area of the piston by the seal at C. When the pressure in chamber A is approximately four times greater than that in B, the piston moves away from the seal at C and the pressure in chamber A is suddenly applied over the entire piston, causing a forward acceleration. The acceleration

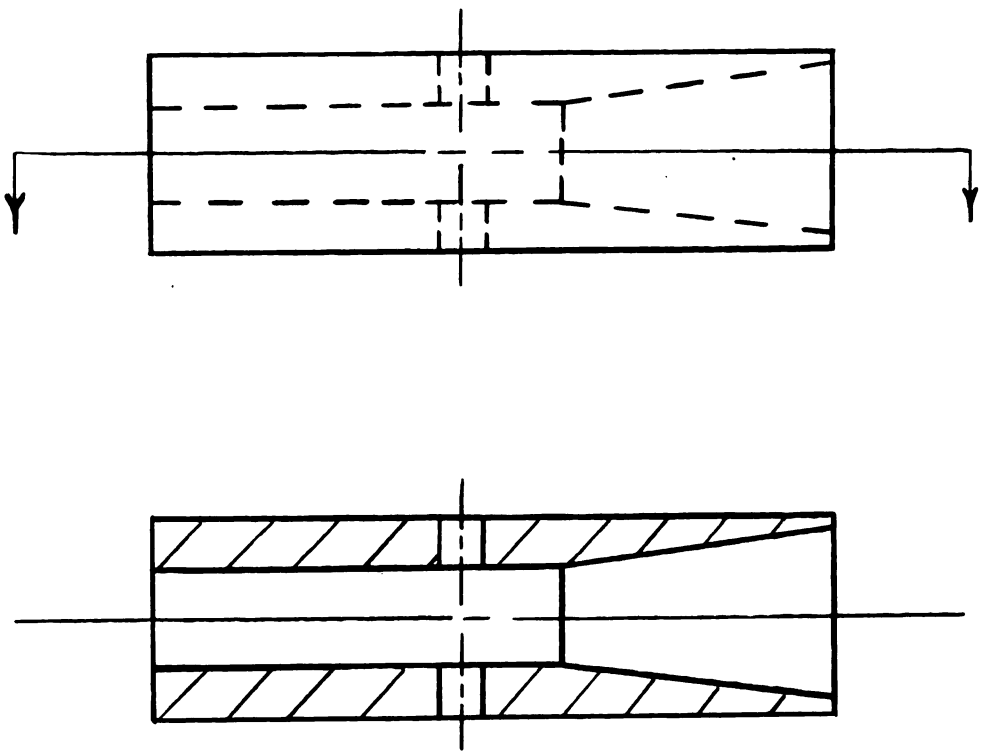

FIGURE 20

ALUMINUM FUNNEL USED TO

KEEP STRIKER AND SPREADER BARS

ALIGNED DURING IMPACT.

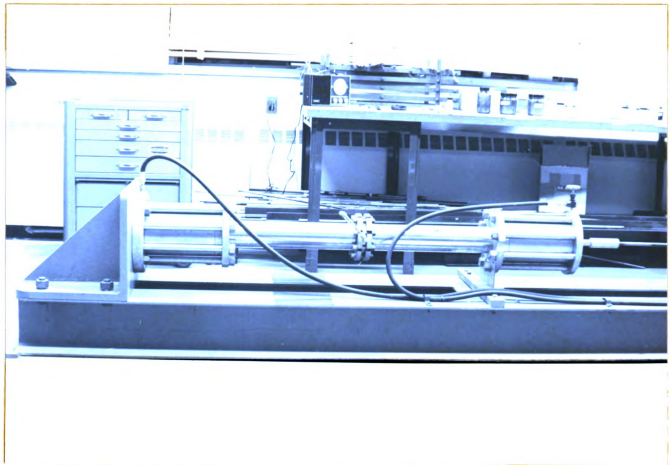

FIGURE 21

SIDE VIEW OF MOUNTED HYGE TESTER

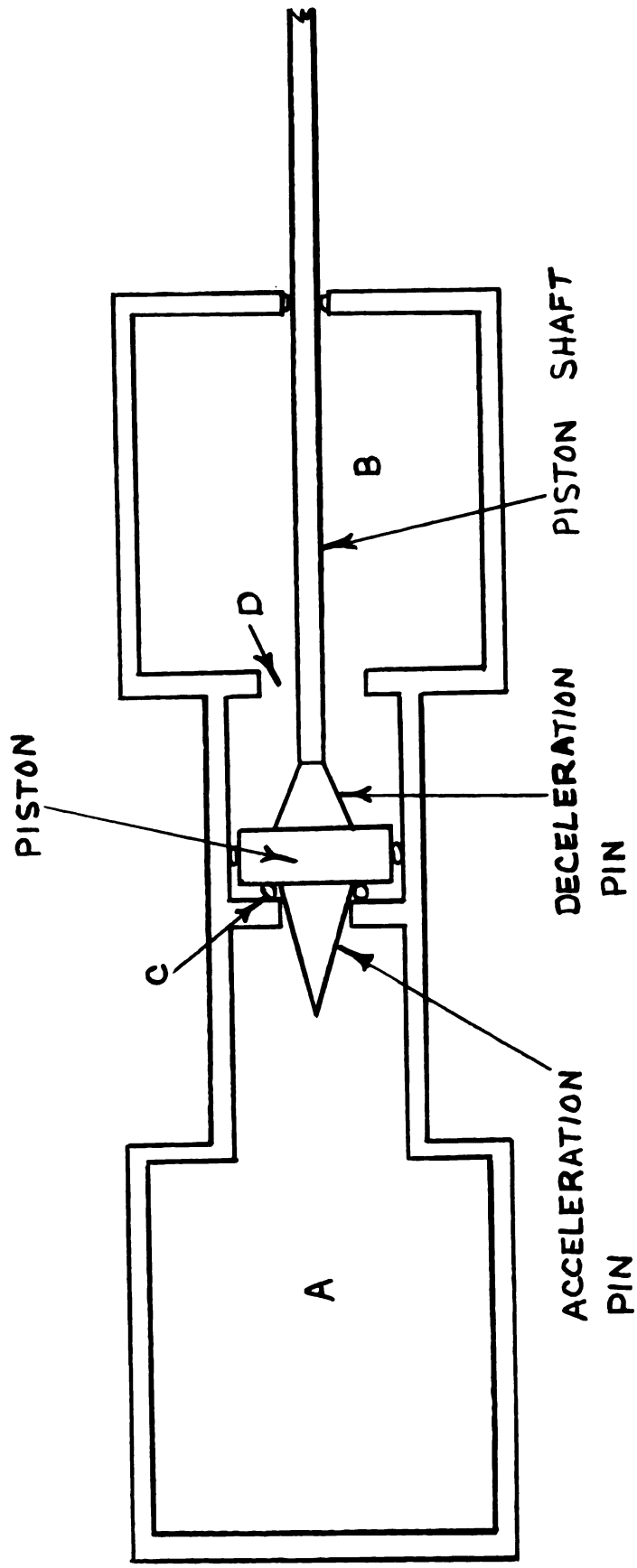

FIGURE 22

SCHEMATIC SKETCH OF HYGE TESTER

pin determines the wave form of the acceleration pulse by regulating how fast the gas pressure acts on the piston. The deceleration is accomplished by hydraulic fluid which occupies about one half the volume of chamber B. The fluid at the end of the stroke is forced through the orifice D, which is gradually being closed by the deceleration pin. A series of valves mounted on a control panel is used to control the gas pressures.

An aluminum sleeve was designed for the connection between the piston and the striker bar. A brass plug was screwed into the sleeve and the sleeve screwed to the piston. Two rubber "O" rings were used to align the striker bar in the sleeve. Molybdenum disulfide was used as a lubricant on the "O" rings.

The stroke of the piston was sixteen and one half inches. The striker bar was separated from the spreader bar by eighteen inches before firing. As a result, when the striker bar struck the spreader bar; the striker bar was free from the sleeve and essentially in free flight.

3.10 Instrumentation for Delay Time Measurements

Two type MA-06-125AD-120 foil strain gages cemented seven inches from the sample end of the spreader bar were used to measure the magnitude of the pulse. BAP-1 cement purchased from William T. Bean was used as the adhesive. After the gages were in place Gage Kote #4 was applied to the gage area to provide abrasion resistance to the installation.

Gage Kote #1 was then applied over the same areas to provide moisture resistance.

The gages were connected in opposite arms of a Wheatstone bridge. Since the gages were on opposite sides of the bar, any bending stresses introduced were cancelled. The temperature error is doubled using this hook-up, but since the tests were dynamic and the gages self temperature compensated, no appreciable error was introduced; the zero point was determined before each run and at the location of these gages no actual temperature change could be detected.

A new twelve-volt heavy duty wet-cell provided the driving power for the bridge. The battery was charged each evening to keep it at full power. To provide a calibration independent of the driving voltage, two precision calibration resistors were hooked in parallel with the two strain gages through two switches. A schematic diagram of the bridge is shown in Figure 23.

The output from the bridge was fed into a Tektronix Type D Plug-In Unit, set for a DC signal with vertical sensitivity of five millivolts per centimeter. This output was fed into the upper beam of a Tektronix Type 555 Dual Beam Oscilloscope, which swept only once for each pulse, triggered internally.

To calibrate the system, two strain gages of the same type and from the same lot were cemented to a three-inch section cut from the diffuser bar. The sample was placed in

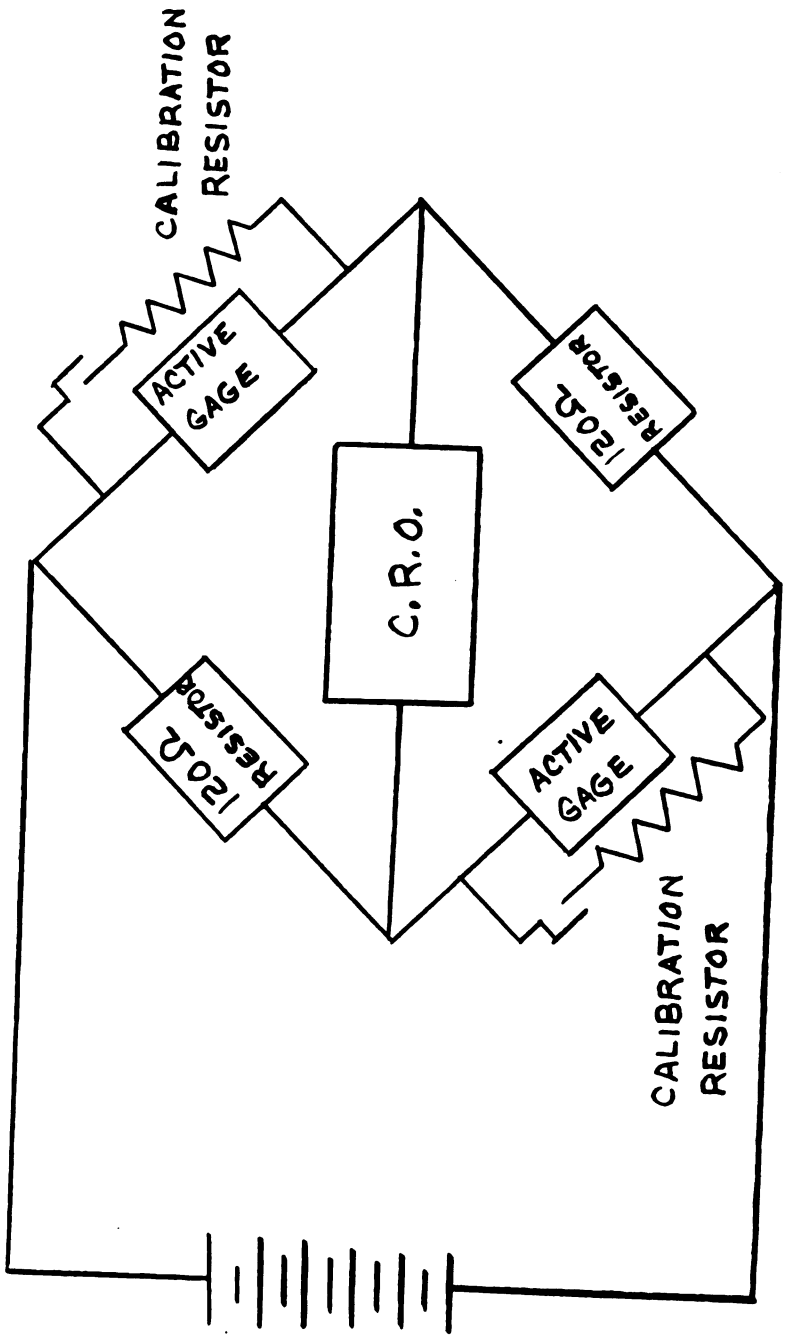

FIGURE 23

STRAIN GAGE BRIDGE

the Instron machine, and the switches to the precision resistor were closed. The vertical displacement of the trace was carefully noted. The switches were opened and stress was applied until the trace came to the same position. 27,960 pounds per square inch was required. To further check the system, a stress of 20 thousand pounds per square was applied and the vertical position of the trace carefully noted. After removing the load, the scope was allowed to sweep once with the resistors in the circuit and the vertical position of the trace was noted. Using the vertical displacement caused by the load and the resistors, the stress was calculated to be 20,120 psi. The same procedure was carried out at 30, 40, and 50 thousand pounds per square inch.

The length of time the specimen supported the load (delay time) was measured with a separate circuit. A type MA-06-125AD-120 self-temperature-compensated foil strain gage was cemented with Eastman 910 adhesive to each specimen. The gage was connected in a Wheatstone bridge using a quick disconnect plug. A twelve volt heavy duty wet cell was used to power the bridge. The output from this bridge was put through a Tektronix Type D Plug in Unit and then into the lower beam of a Tektronix Type 555 Dual Beam Oscilloscope. Since this circuit was used to measure the delay time only, no calibration of the vertical displacement was necessary. Triggering was accomplished internally. The sweep speed for both the upper and lower beam was two

tenths milli-seconds per centimeter. An overall view of the instrumentation is shown in Figure 24.

3.11 Samples and Procedure for Delay Time Measurements

Cylindrical specimens 0.505 inches diameter by one inch long were turned from the three quarter inch ingot iron using a collet lathe.

Six to eight samples each of the three conditions (annealed, solution-treated, and solution-treated aged for six hours at 158°F) were tested. The annealed specimens were turned from ingot iron that was annealed as described in section 3.6. The solution-treated and solution-treated-aged specimens were first turned from the cold drawn ingot iron then solution treated, or solution-treated and aged, as described in section 3.4.

After heat-treating the samples, a type EA-06-125-AC-120 foil gage was cemented in place with Eastman 910 adhesive after properly cleaning the sample. Lead wires with a quick disconnect plug were installed and a coat of Gage Kote #1 applied. After measuring the specimen with micrometers, the specimen ends were coated with molybdenum disulfide and inserted into a special holder before being placed in the oven or refrigerator previously described, to be brought to the test temperature. In Figure 25 a cross-section of the sample holder is shown. The sample ready for testing is shown in Figure 26. Fifteen minutes were allowed for the heating to ensure uniform temperature.

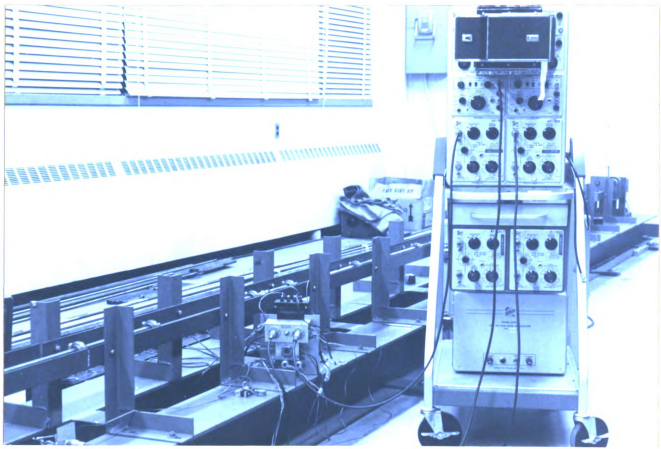

FIGURE 24

OVERALL VIEW OF INSTRUMENTATION

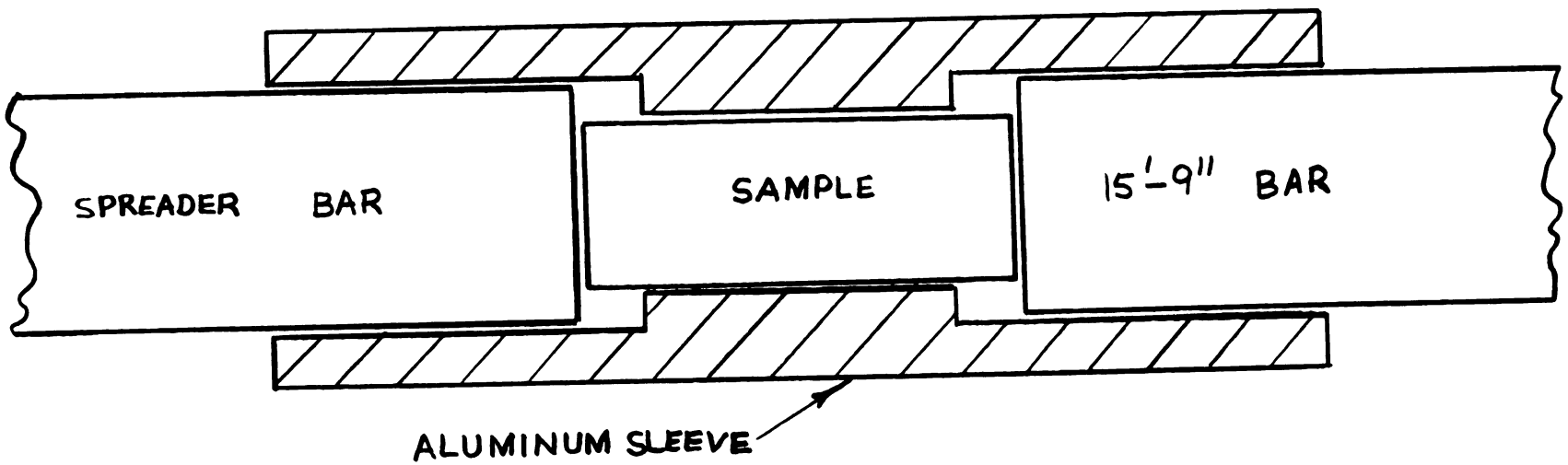

FIGURE 25

CROSS SECTION OF SAMPLE HOLDER

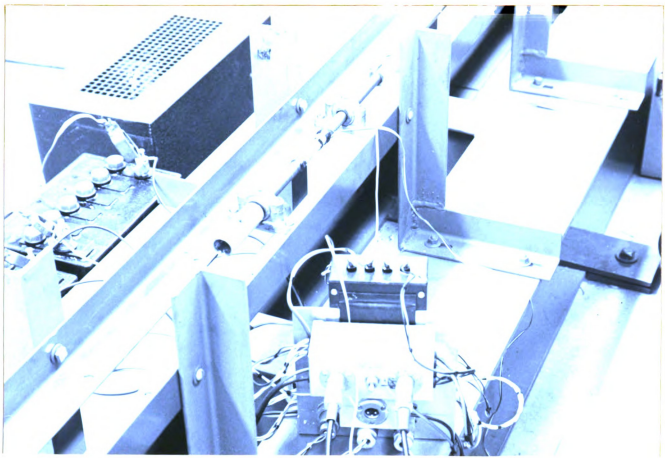

FIGURE 26

SAMPLE AND SAMPLE HOLDER IN POSITION

While the sample was being brought to the test temperature, the Hyge was preloaded, the oscilloscope was brought to zero, the zero point photographed, the single-sweep set, and approximately three fourths of the firing pressure was introduced in the rear cyclinder of the Hyge. When fifteen minutes had elapsed, the sample was quickly transferred to the pressure bar and the rest of the firing pressure introduced. After firing, the calibration trace and the grid were photographed using a Tektronix Series 125 camera, with Type 47 Polaroid film. The size of the sample after testing was measured and recorded.

3.12 Optical and Electron Microscope Investigation

All samples were mounted in bakelite. After wet grinding on a coarse and medium wet-grinding wheel, the samples were ground on a 180 and 140 grit wet belt sander. Hand sanding was accomplished on 240, 320, 400, and 600 grit silicon carbide paper flushed continuously with water. The sample was then polished on a wax lap charged with levigated aluminia mixed with tincture of green soap before polishing on a lap charged with 1.0 and 0.3 micron aluminia. AB Metpolish #3 was used for the final polishing. Etching was done with 4 percent nitric acid in amyl alcohol for approximately ten seconds. All optical examination was performed on a Bausch and Lomb Research Metallograph. A Hitachi HU-11A electron microscope was used for higher magnification examinations.

CHAPTER IV

EXPERIMENTAL RESULTS

4.1 Aging Experiments

All samples showed an increase in hardness with time. The first two hours accounted for the greatest hardness change. At times in excess of eight hours, softening was noted in most cases.

Samples aged at 158° F gave very consistent aging curves. The increase in hardness was easily followed and no appreciable over-aging occurred. Samples aged below 158° F did not give as smooth aging curves and tended to be sporadic. The hardness changes in samples aged above 158° F occurred so fast, that the changes were difficult to follow. The samples also showed appreciable over-aging. In Table 2, the six hardnesses taken at each time interval are shown for a typical sample. A plot of the average hardness versus aging time is shown in Figure 27 for a typical sample aged at 158° F.

Because the aging reaction was most dependable at 158° F, all aged samples used for impact testing, compression testing, and delay time specimens were aged at 158° F for six hours after solution treating. An aging time of six hours was used because the maximum effect was observed at six hours. Also, in this region, the curve was flat and small errors in time made little difference.

TABLE 2

HARDNESS (R_K) DATA FOR A

TYPICAL SPECIMEN AGED AT 158° F

Time (Hrs.)	HARDNESS READINGS, R_K						AVERAGE HARDNESS
0.0	80.0,	78.8.	77.8,	80.7,	81.2,	80.0	79.75
1.0	79.9,	80.2,	79.0,	82.0,	83.5,	81.0	80.93
2.0	83.8,	84.0,	82.5,	85 ,	87.1,	84.4	84.46
3.0	85.1,	84.8,	83.0,	86.4,	88.0,	86.1	85.57
4.0	85.9,	85.8,	87.6,	83.1,	84.6,	87.0	86.50
4.5	85.9,	85.1,	85.1,	87.2,	88.2,	86.2	86.28
6.0	87.1,	86.1,	85.2,	88.2,	88.7,	87.3	87.10
7.0	85.8,	86.1,	85.1,	89.0,	89.0,	88.6	87.27
8.0	85.7,	86.1,	87.1,	88.1,	89.1,	86.1	87.03
9.0	87.2,	87.8,	85.1,	85.9,	88.8,	84.9	86.62
9.5	83.9,	85.8,	86.7,	85.1,	90.0,	89.7	86.87
11.0	82.5,	86.0,	87.1,	87.2,	91.0,	90.3	87.35
12.0	82.1,	86.3,	85.7,	95.0,	90.4,	90.5	86.67

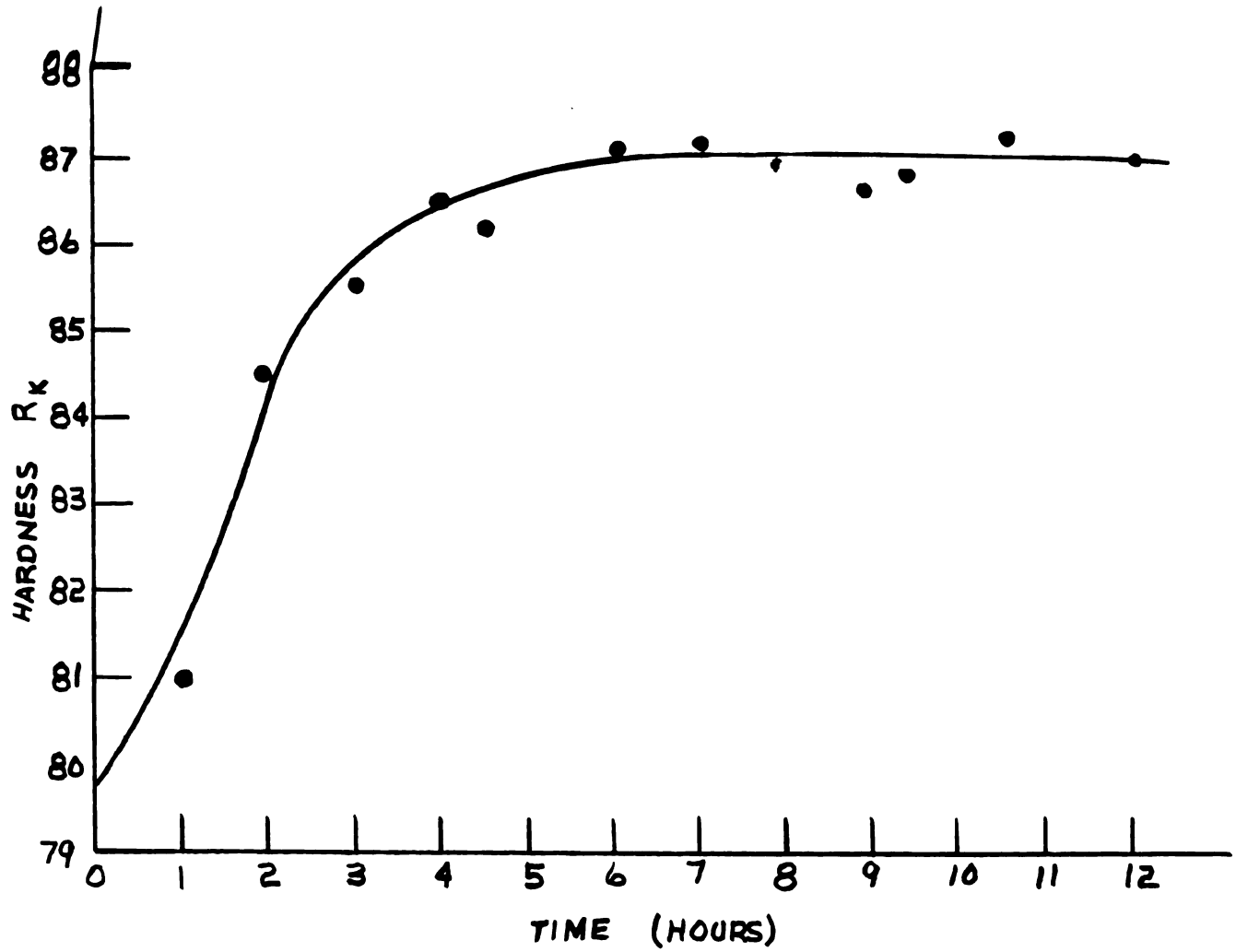

FIGURE 27

TYPICAL HARDNESS VERSUS TIME FOR A SOLUTION TREATED SAMPLE AGED AT 153° F

4.2 Impact Tests

The impact strength of the as received, annealed, solution treated, and solution treated, and solution treated-aged samples varied greatly. The as-received samples showed a transition at about 158° F. The impact strength versus temperature is shown in Figure 28. The impact strength values plotted are averages of three samples tested at each temperature. The precision of the test was good except at 158° F. This was probably due to the fact that the testing was carried out near the transition temperature where the impact strength changes very rapidly with a small change in temperature. The impact data are given in Table 3.

The annealed samples showed a transition also at about 153° F. A plot of the average impact strength versus temperature is shown in Figure 29. The impact data are shown in Table 4. The precision of the tests was good except at the transition temperature.

The solution treated samples did not show a transition in the temperature range of the tested. A slight decrease in the impact strength was observed at higher temperatures. The decrease was most likely due to aging. The higher testing temperatures caused the greatest drop. In Figure 30, the average impact strength versus the test temperature is shown. The data for these samples are shown in Table 5.

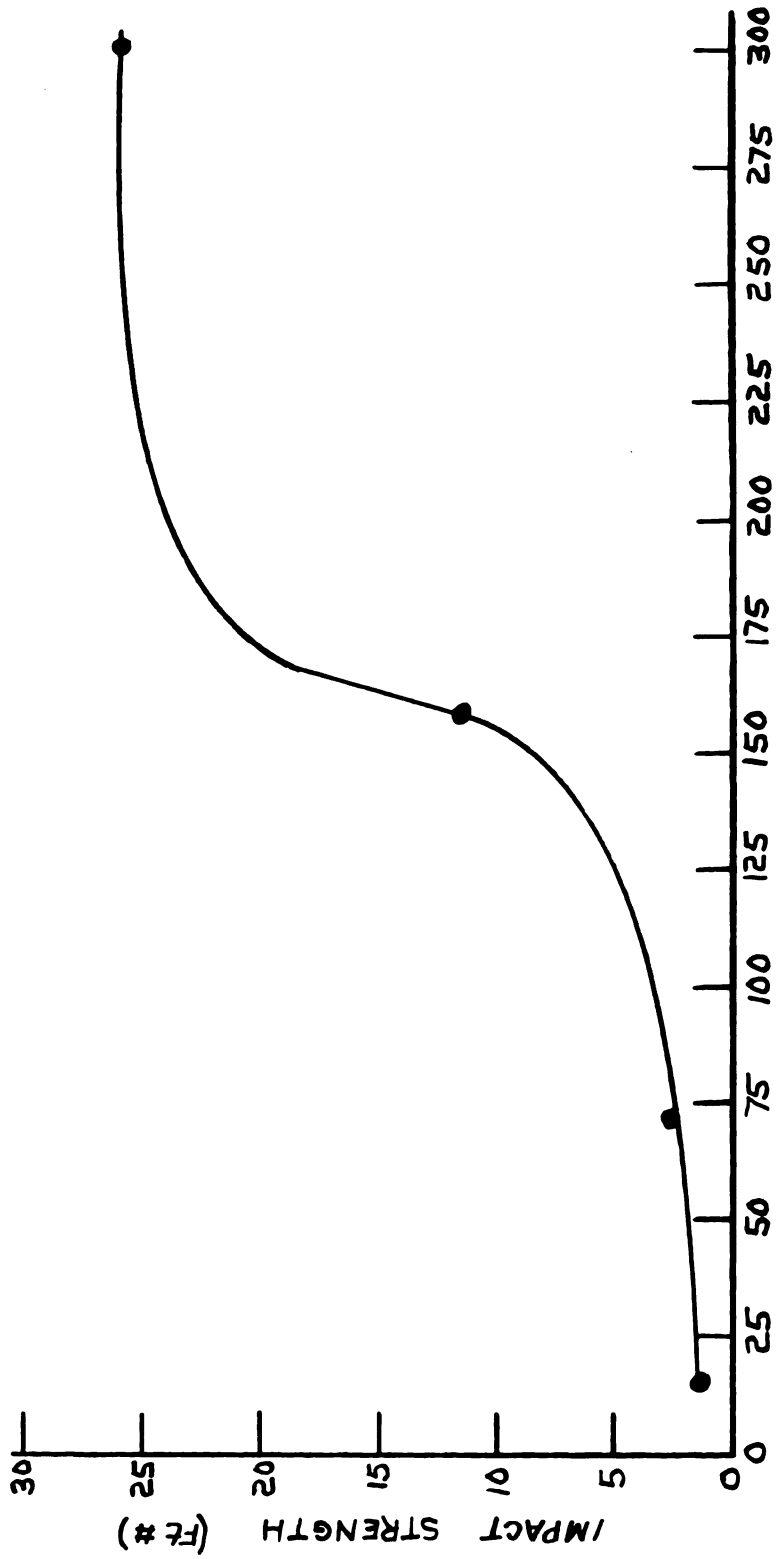

FIGURE 28

IMPACT STRENGTH VERSUS TEMPERATURE FOR AS-RECEIVED SAMPLES

TABLE 3

IMPACT DATA FOR AS-RECEIVED SAMPLES

Test Temperature (°F)	Sample Number	Impact Strength
14	169	2.0
14	170	1.0
14	171	1.0
Average Impact Strength		1.3
72	166	3.0
72	167	2.0
72	168	3.0
Average Impact Strength		2.67
158	163	4.0
158	164	5.0
158	165	28.0
Average Impact Strength		12.3
300	160	26.0
300	161	25.0
300	162	27.0
Average Impact Strength		26.0

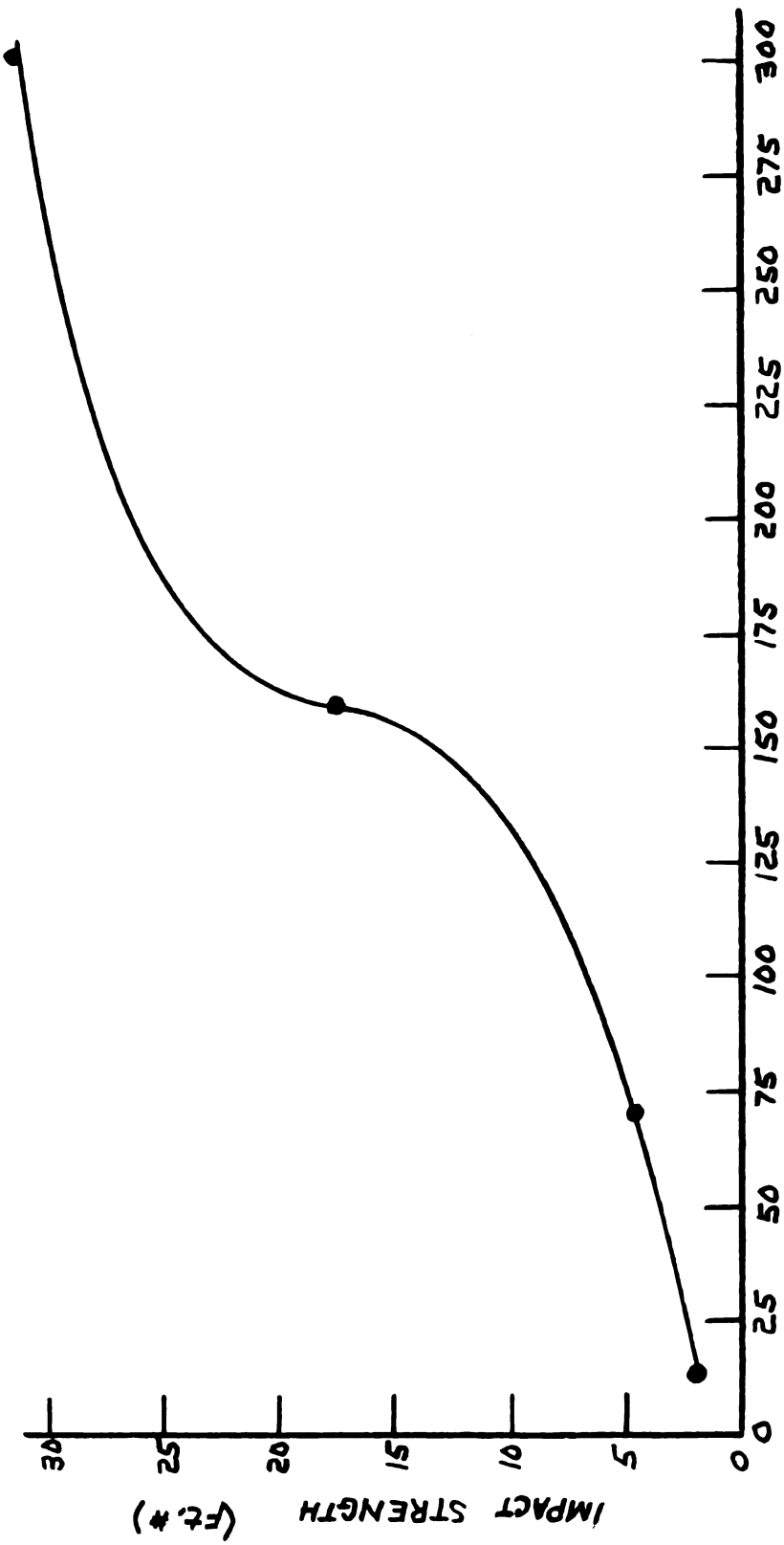

FIGURE 29

IMPACT STRENGTH VERSUS TEMPERATURE FOR ANNEALED SAMPLES

TABLE 4

IMPACT DATA FOR ANNEALED SAMPLES

Test Temperature (°F)	Sample Number	Impact Strength
14	245	2.0
14	246	2.0
14	247	2.0
Average Impact Strength		2.0
70	242	4.0
70	243	3.0
70	244	5.0
Average Impact Strength		4.0
158	239	20.5
158	240	16.0
158	241	17.0
Average Impact Strength		17.8
300	236	30.5
300	237	30.0
300	238	30.5
Average Impact Strength		30.3

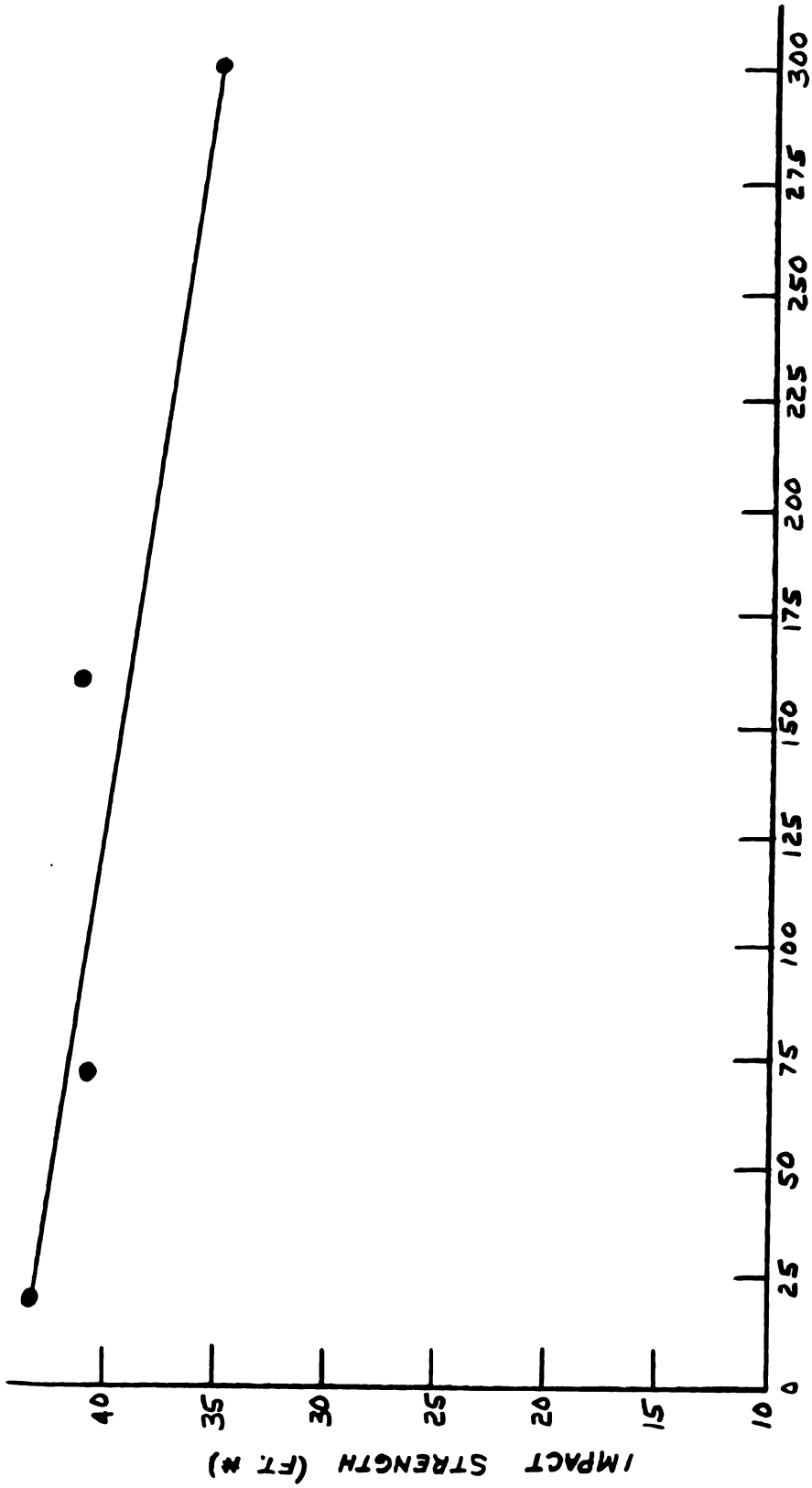

FIGURE 30

IMPACT STRENGTH VERSUS TEMPERATURE FOR SOLUTION-TREATED SAMPLES

TABLE 5

IMPACT DATA FOR SOLUTION TREATED SAMPLES

Test Temperature (°F)	Sample Number	Impact Strength
14	193	44.0
14	194	42.0
14	201	44.0
Average Impact Strength		43.3
70	202	40.0
70	203	42.0
70	204	40.0
Average Impact Strength		40.7
158	210	40.0
158	211	42.0
158	214	42.0
Average Impact Strength		41.3
300	198	36.0
300	199	36.0
300	200	36.0
Average Impact Strength		36.0

The solution-treated samples aged six hours at 158° F did not show a transition in the temperatures used in the test. The impact strength remained essentially constant for these samples at all test temperatures. At 300° F, the impact strength of the solution-treated and the solution-treated and aged samples was nearly the same. At all temperatures except 300° F, the impact strength of the solution-treated and aged samples was less than that of the solution-treated samples. The average impact strength versus test temperature for the solution-treated and aged samples is shown in Figure 31. The impact data are shown in Table 6.

4.3 Static Compression Tests

The stress-strain curves for tests at 14, 70, 158, and 300° F are shown in Figures 32, 33, 34, and 35 for the annealed samples, in Figures 36, 37, 38, and 39 for solution-treated samples, and in Figure 40, 41, 42, and 43 for the samples solution-treated and aged six hours at 158° F. Each curve was averaged from at least three specimens.

The annealed samples showed a yield point below the transition temperature. Above the transition temperature, the yield point disappeared. Neither the solution-treated nor the solution-treated and aged samples showed a yield point. The proportional limit was highest for the solution-

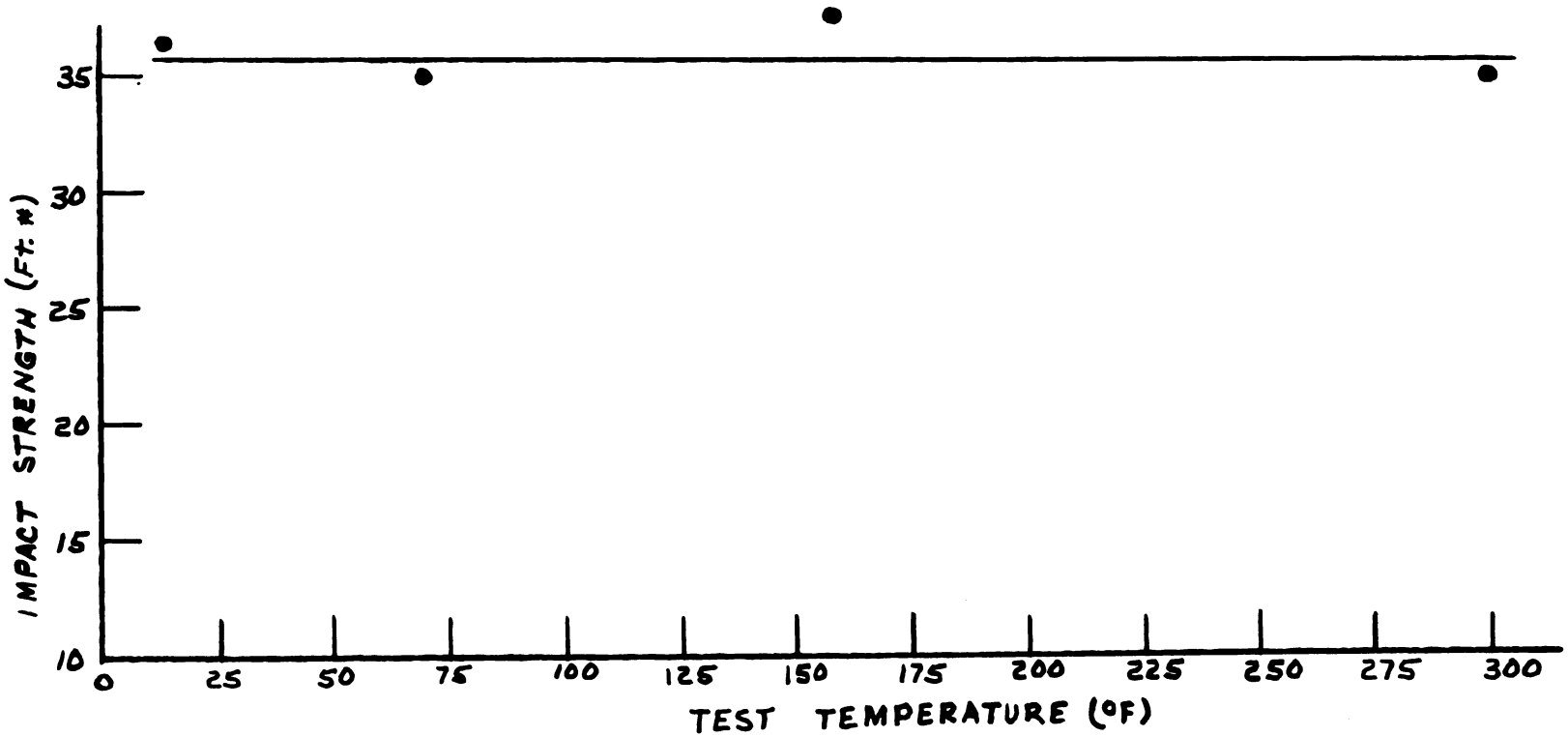

FIGURE 31

IMPACT STRENGTH VERSUS TEMPERATURE FOR SOLUTION TREATED AGED SAMPLES

TABLE 6

IMPACT DATA FOR SOLUTION TREATED-AGED SAMPLES

Test Temperature (°F)	Sample Number	Impact Strength (Ft.#)
14	190	36.0
14	191	37.0
14	192	36.0
Average Impact Strength		36.3
70	205	36.0
70	215	34.0
70	216	35.0
Average Impact Strength		35.0
158	207	37.0
158	217	37.0
158	218	36.0
Average Impact Strength		36.7
300	195	34.0
300	196	35.0
300	197	36.0
Average Impact Strength		35.0

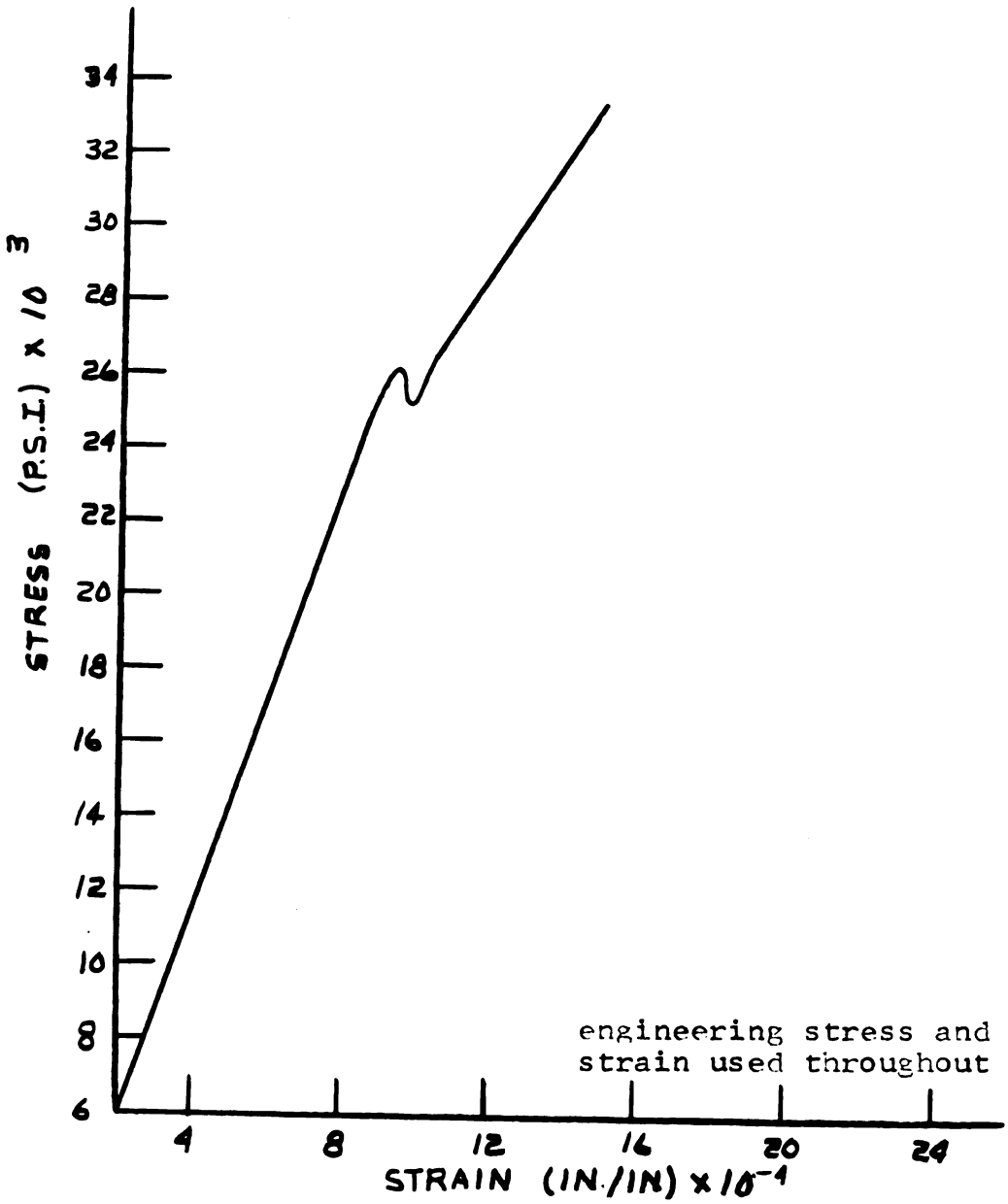

FIGURE 32

STRESS STRAIN CURVE FOR

ANNEALED SAMPLES TESTED AT 14^{o} F

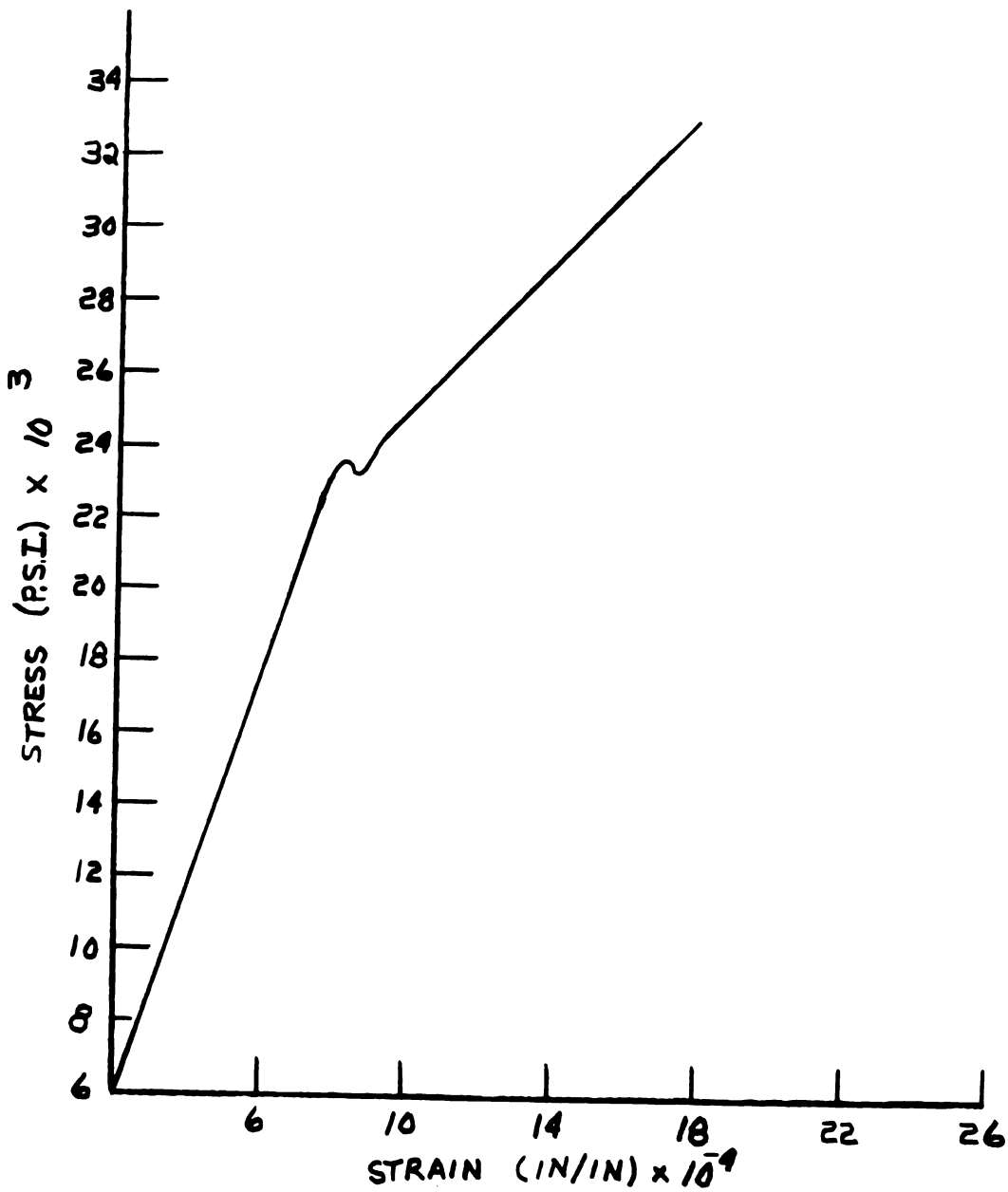

FIGURE 33

STRESS STRAIN CURVE FOR

ANNEALED SAMPLES TESTED AT 70° F

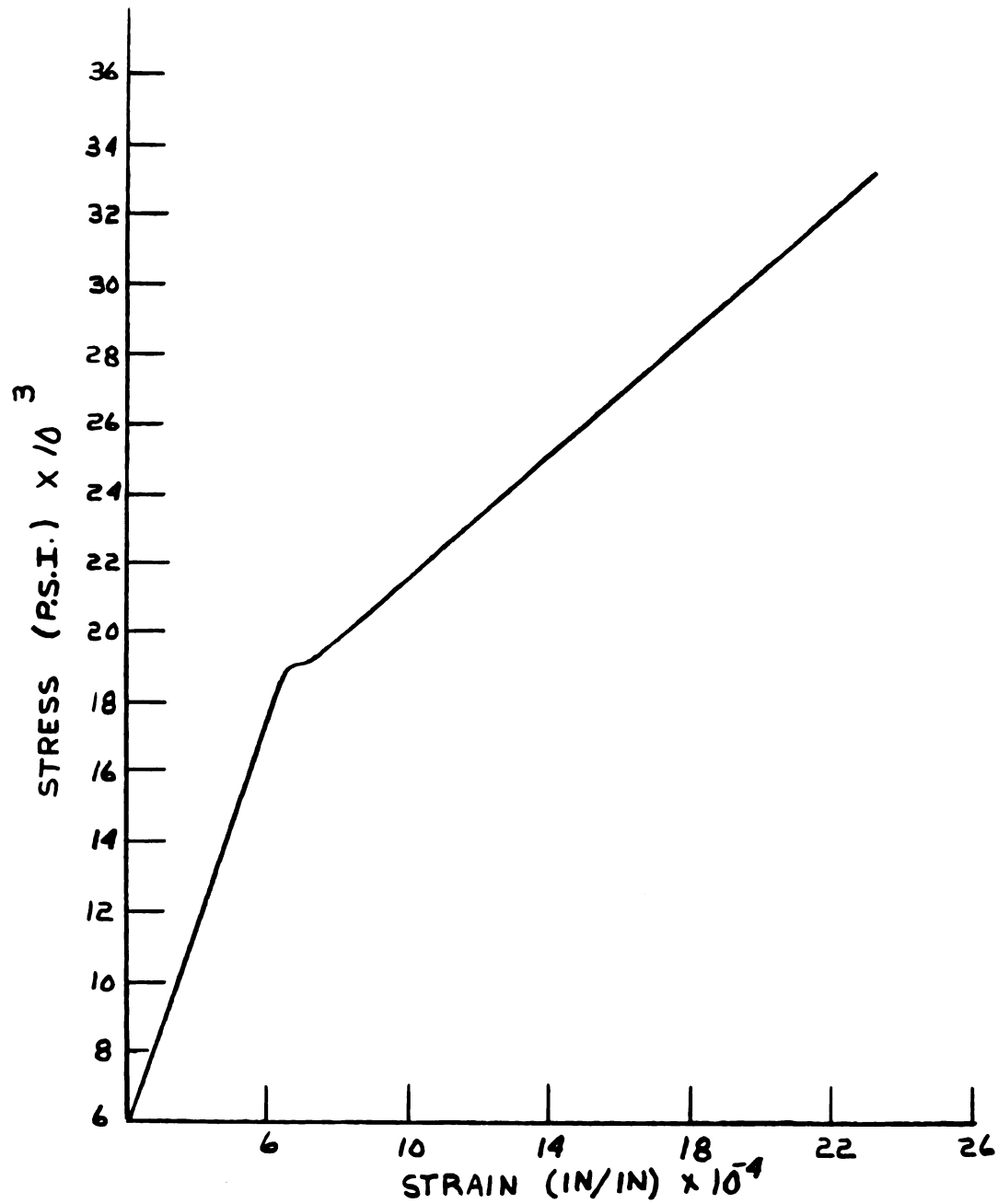

FIGURE 34

STRESS STRAIN CURVE FOR

ANNEALED SAMPLES TESTED AT 158° F

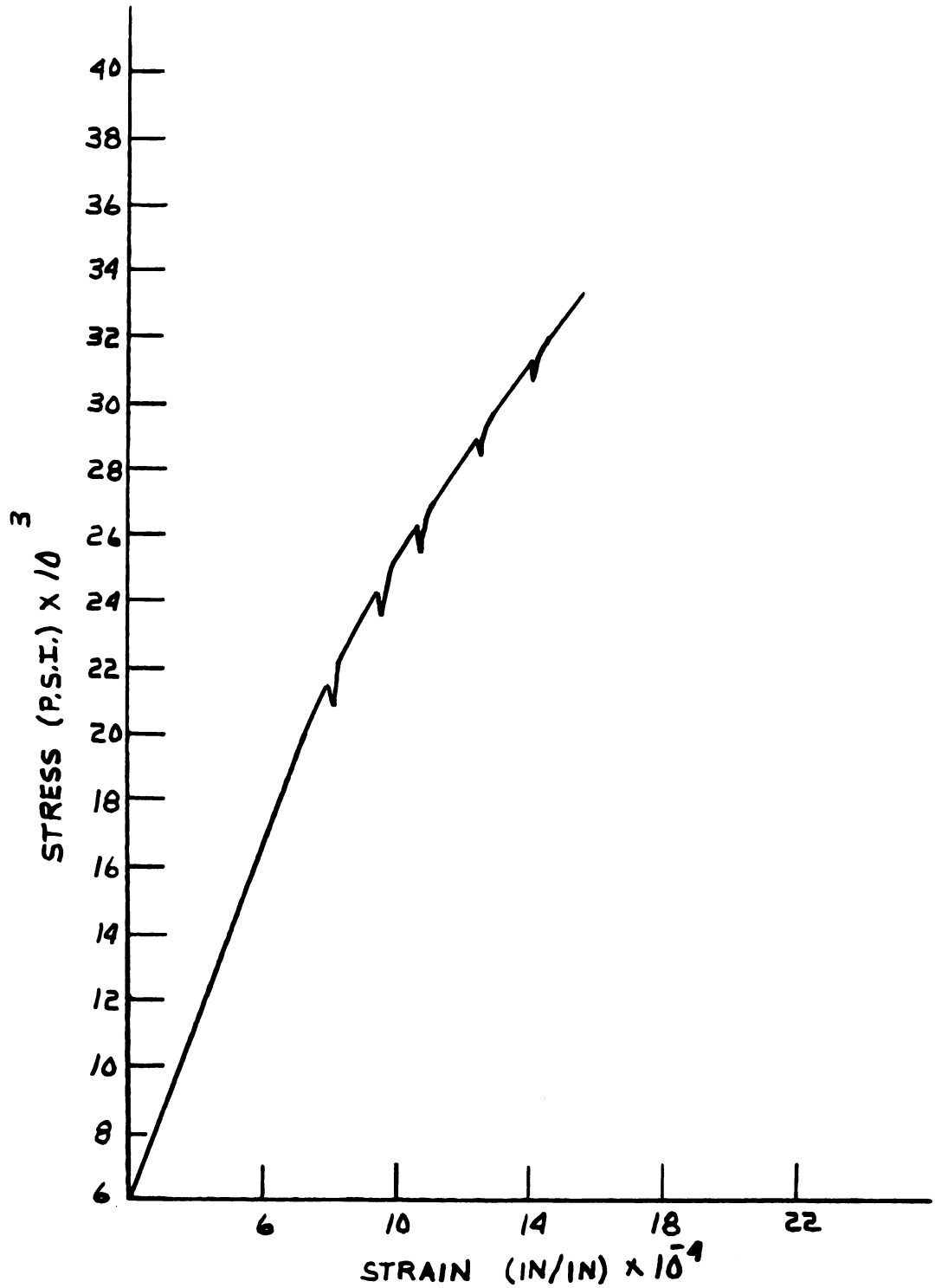

FIGURE 35

STRESS STRAIN CURVE FOR

ANNEALED SAMPLES TESTED AT 300° F

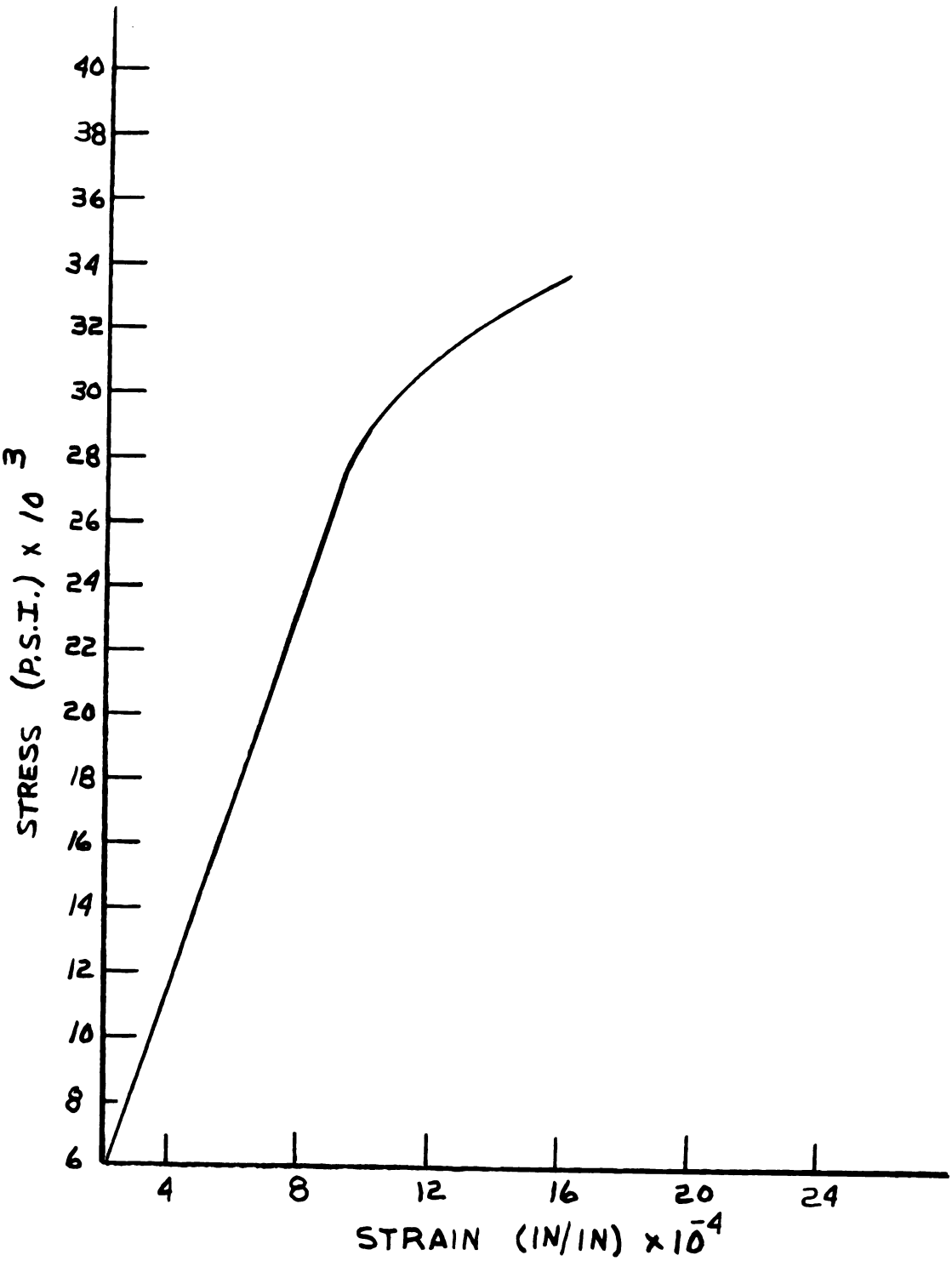

FIGURE 36

STRESS STRAIN CURVE FOR SOLUTION

TREATED SAMPLES TESTED AT 14° F

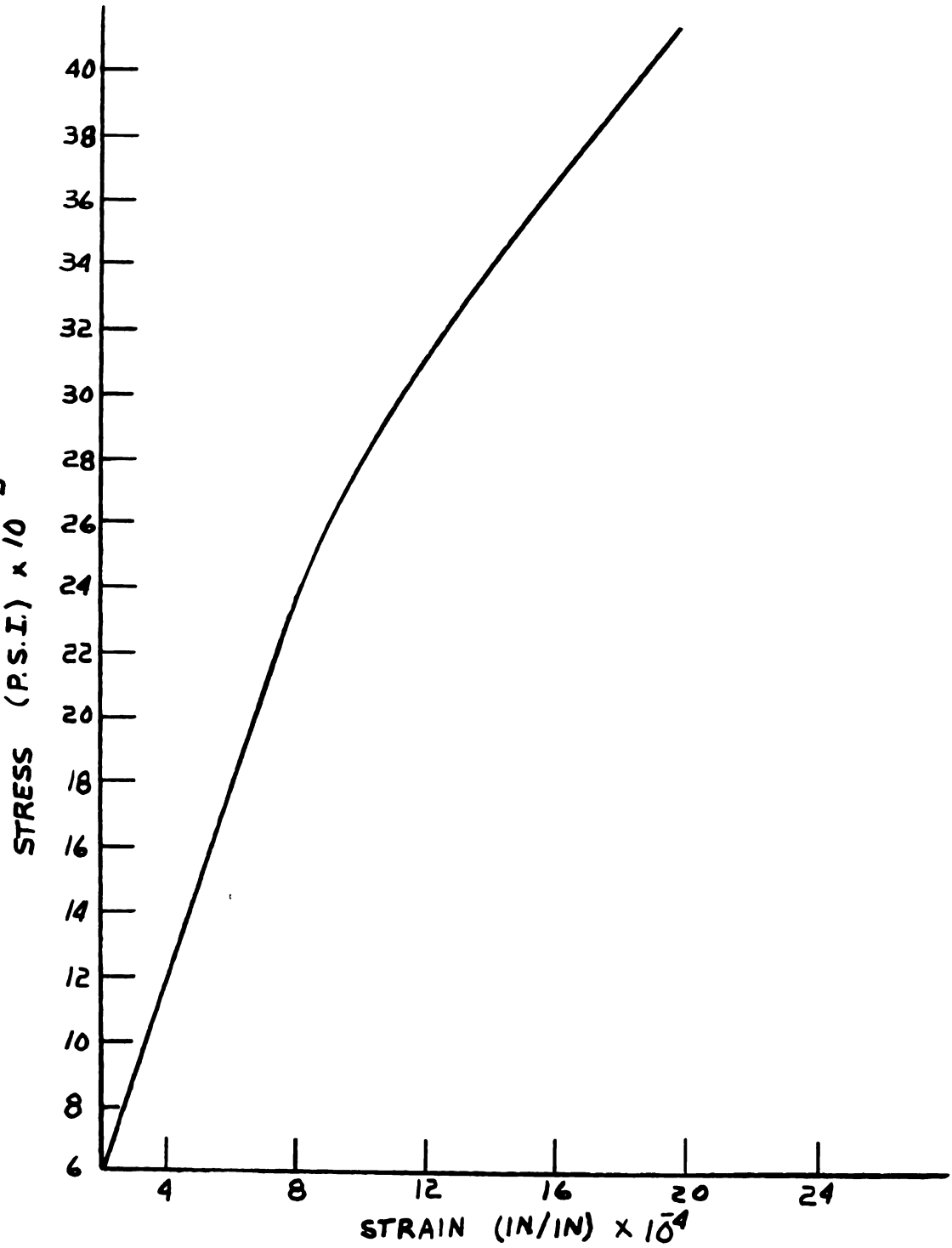

FIGURE 37

STRESS STRAIN CURVE FOR SOLUTION

TREATED SAMPLES TESTED AT 70° F

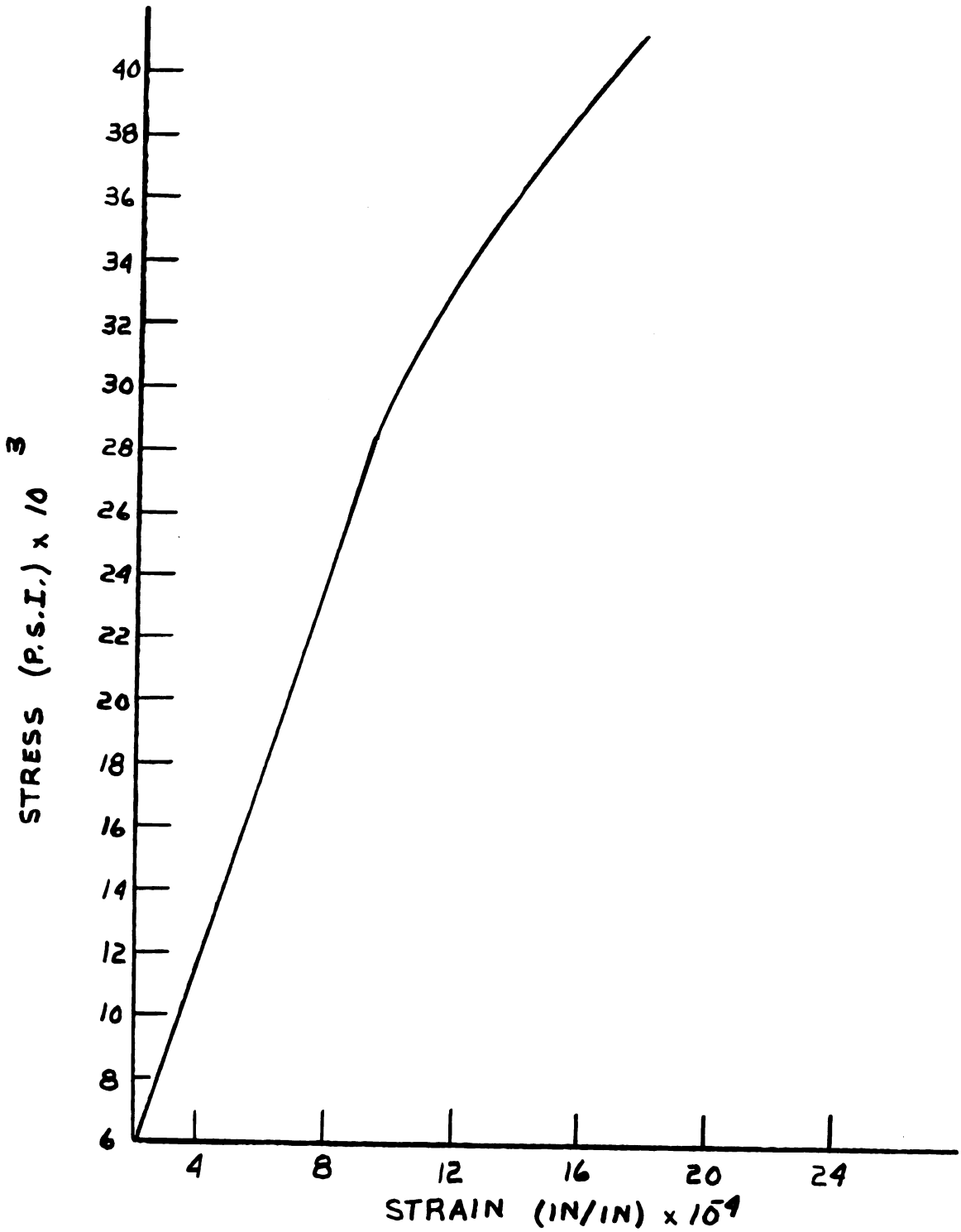

FIGURE 38

STRESS STRAIN CURVE FOR SOLUTION

TREATED SAMPLES TESTED AT 158° F

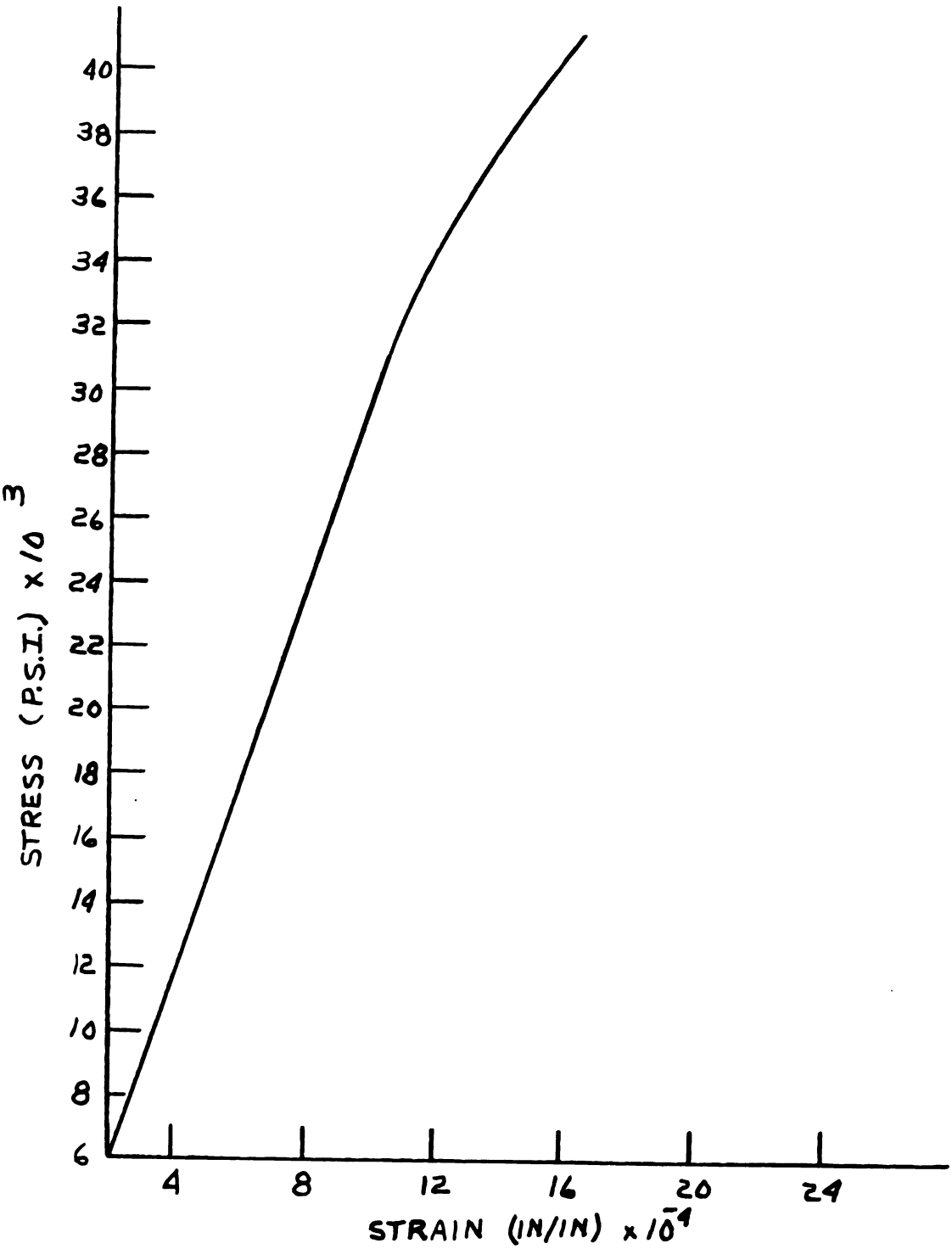

FIGURE 39

STRESS STRAIN CURVE FOR SOLUTION

TREATED SAMPLES TESTED AT 300° F

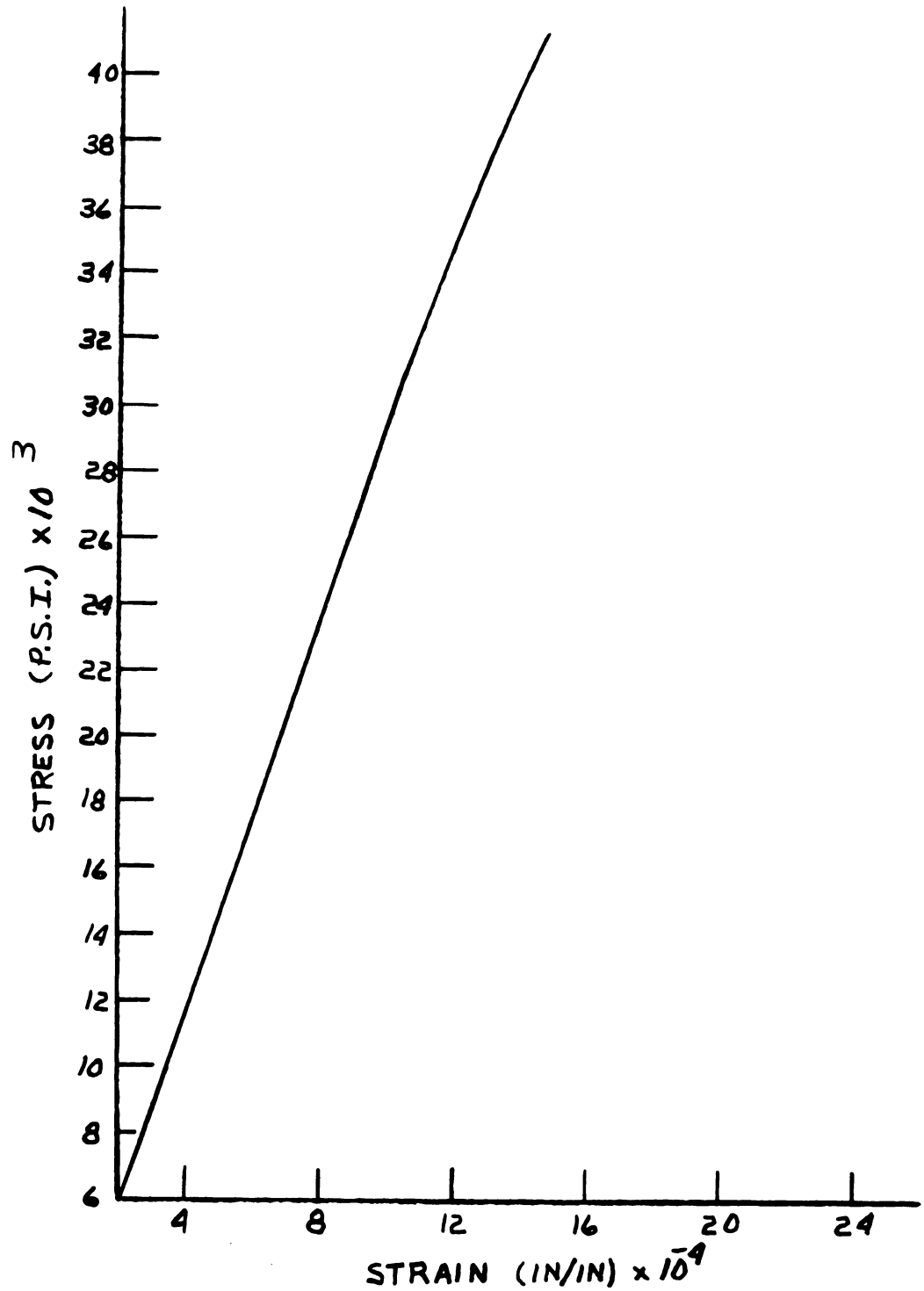

FIGURE 40

STRESS STRAIN CURVE FOR SOLUTION

TREATED AGED SAMPLES TESTED AT 14° F

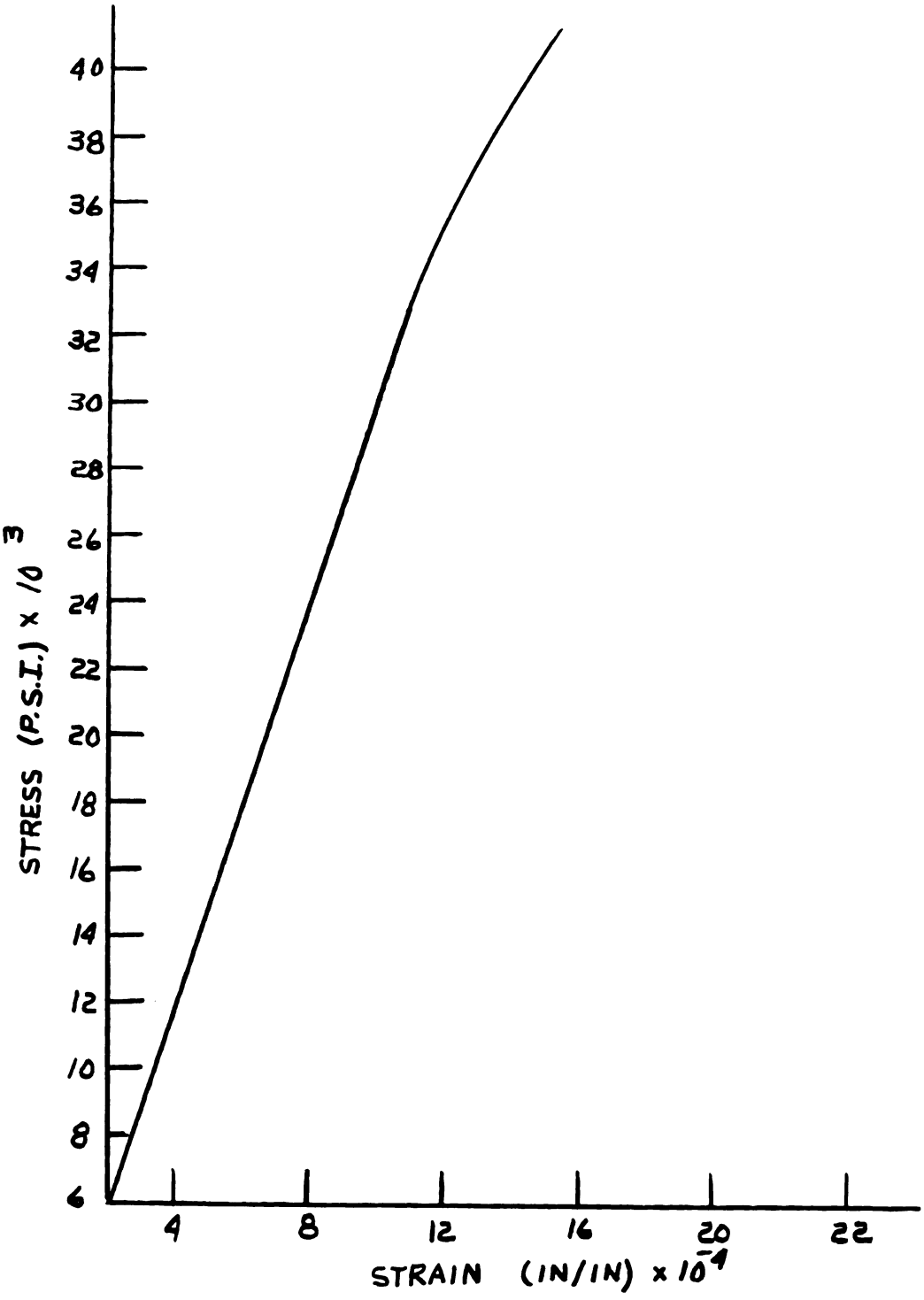

FIGURE 41

STRESS STRAIN CURVE FOR SOLUTION

TREATED AGED SAMPLES TESTED AT 70° F

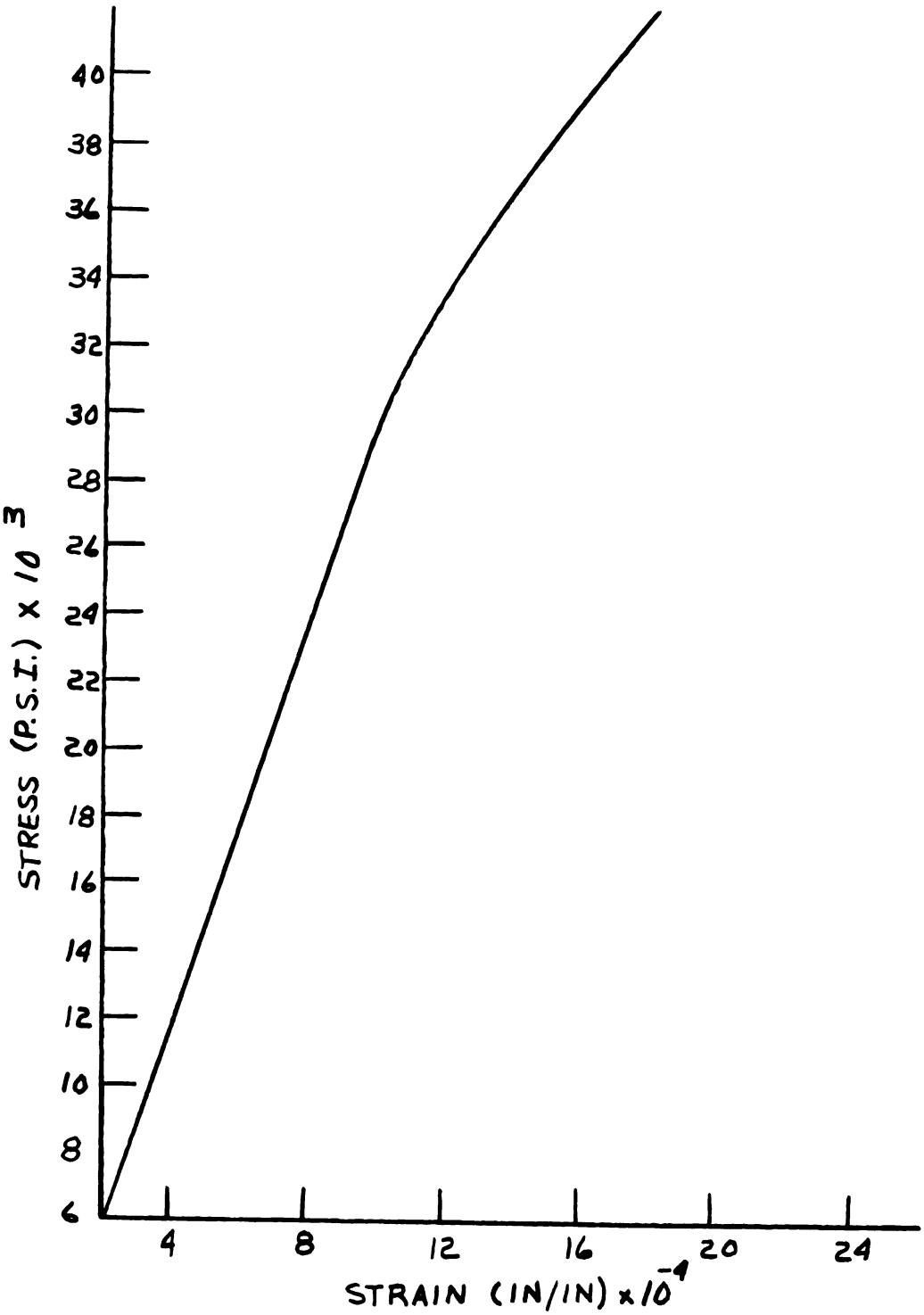

FIGURE 42

STRESS STRAIN CURVE FOR SOLUTION

TREATED AGED SAMPLES TESTED AT 158° F

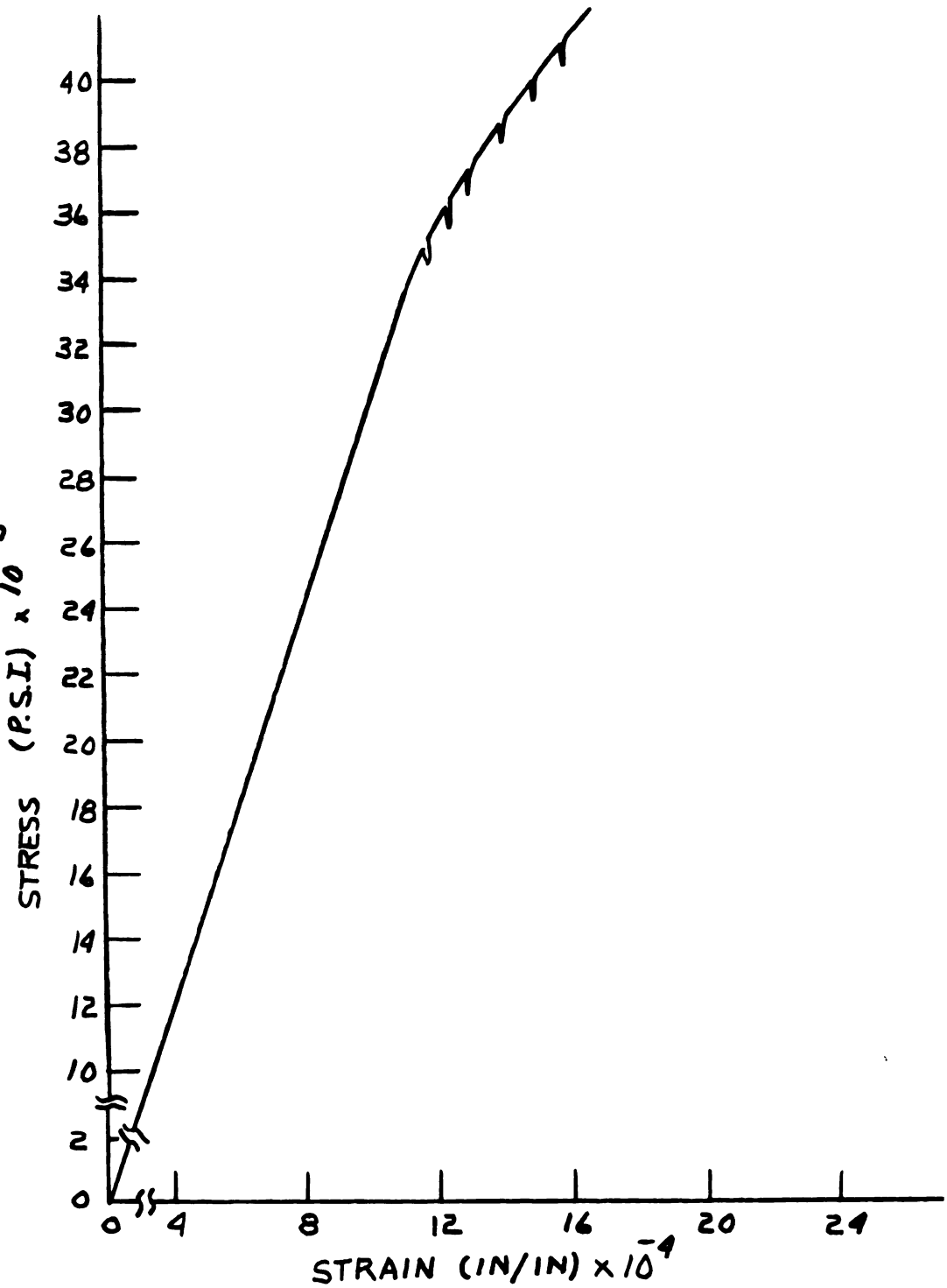

FIGURE 43

STRESS STRAIN CURVE FOR SOLUTION

TREATED AGED SAMPLES TESTED AT 300° F

treated and aged samples and lowest for the annealed samples. In Table 7, the proportional limit and the yield point drops are listed for the annealed samples. In Table 8, the proportional limit and yield point drop are listed for the solution treated samples. In Table 9, the proportional limit and yield point drops are listed for the solution-treated-aged samples. In Figure 44, the proportional limit versus test temperature for all three types of specimens is plotted. The sharp drops observed in the stress-strain curves for the annealed samples at 300° F, Figure 35, and for the solution-treated-aged samples at 300° F, Figure 43, are not fully understood. They may be associated with Lüder band formation. More work is planned on this subject at a later date.

4.4 Delay Time Measurements

The sample number, history, static elastic limit, applied dynamic stress, the difference between the applied dynamic stress and the static elastic limit, and the delay time are given in Table 10. An attempt was made during these tests to keep the dynamic stress applied with the Hyge at approximately 8,000 psi. above the static elastic limit. In these experiments delay time appears on the lower oscilloscope trace as a horizontal plateau (except for high-frequency components) after the intiial elastic rise and before the steadily-increasing plastic strain.

The annealed samples tested below and at 158° F showed

TABLE 7

PROPORTIONAL LIMIT AND YIELD DROP

FOR ANNEALED SAMPLES

Test Temperature (°F)	Sample Number	Proportional Limit (PSI)	Yield Point Drop (PSI)
14	1006	24,214	1100
14	1007	24,765	1375
14	1008	24,214	550
Average		24,397	1,008
70	1003	22,013	687
70	1004	22,013	825
70	1005	22,563	550
Average		22,196	687
158	1012	16,510	small arrest
158	1013	18,710	small arrest
158	1014	18,711	small arrest
Average		17,977	small arrest
300	1009	19,261	very small arrest
300	1010	18,711	no arrest
300	1011	18,160	no arrest
Average		18,710	

TABLE 8

PROPORTIONAL LIMIT AND YIELD DROP

FOR SOLUTION TREATED SAMPLES

Test Temperature (°F)	Sample Number	Proportional Limit (PSI)	Yield Point Drop (PSI)
14	1027	28,066	none
14	1028	27,516	none
14	1029	24,214	none
Average		26,599	
70	1030	24,701	none
70	1031	23,070	none
70	1032	26,386	none
Average		26,386	
158	1033	29,117	none
158	1034	25,315	none
158	1035	27,516	none
Average		27,316	
300	1036	33,684	none
300	1037	29,718	none
300	1038	33,019	none
Average		32,140	

TABLE 9

PROPORTIONAL LIMIT AND YIELD DROP

FOR SOLUTION TREATED-AGED SAMPLES

Test Temperature (°F)	Sample Number	Proportional Limit (PSI)	Yield Point Drop (PSI)
14	1015	30,268	none
14	1016	33,020	none
14	1017	31,368	none
Average		31,548	
70	1018	33,020	none
70	1019	33,020	none
70	1020	33,020	none
Average		33,020	
158	1021	30,877	none
158	1022	32,000	none
158	1023	29,244	none
Average		30,707	
300	1024	33,020	none
300	1025	32,459	none
300	1026	33,020	none
Average		32,833	

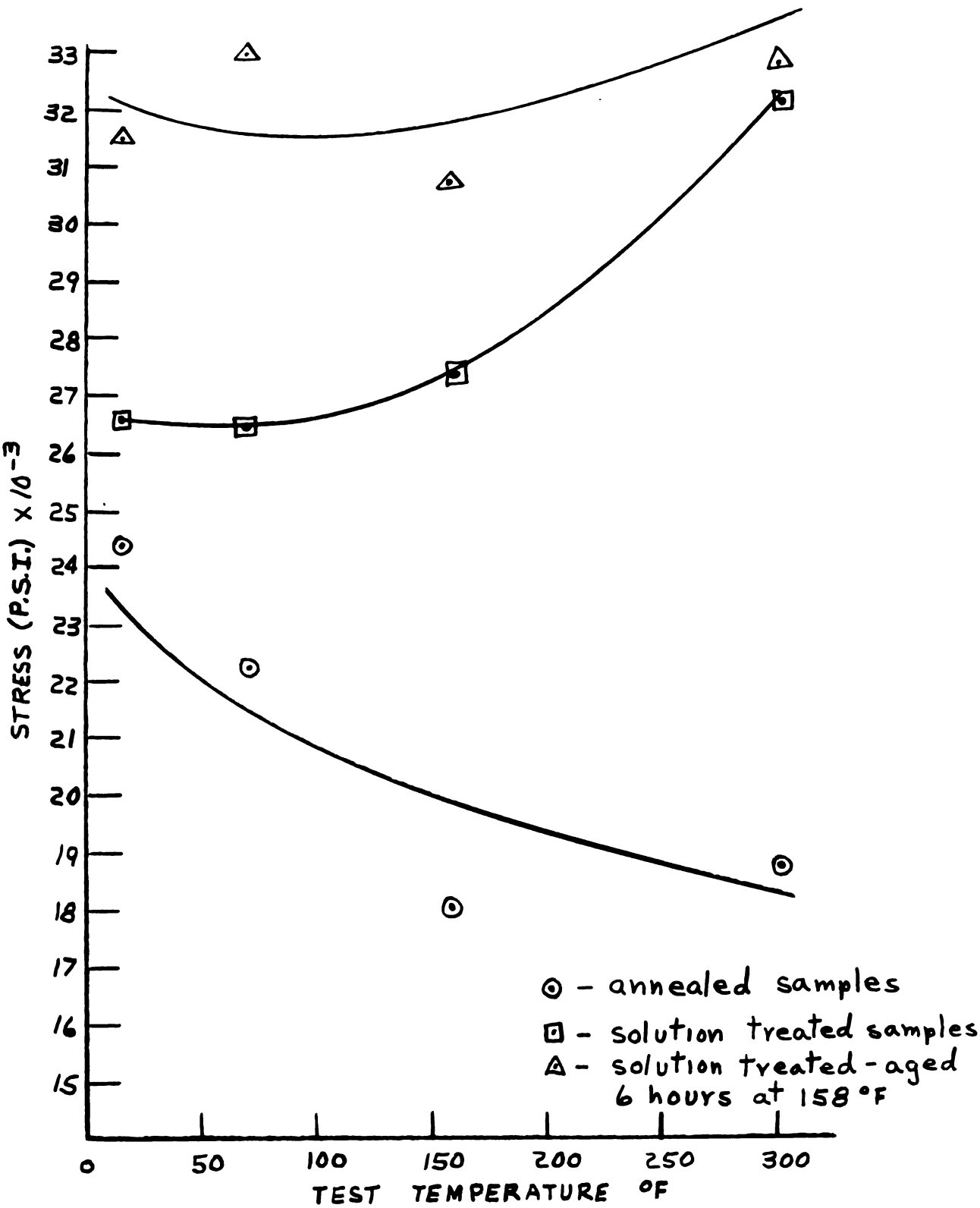

FIGURE 44

PROPORTIONAL LIMIT VERSUS TEST TEMPERATURE FOR ANNEALED, SOLUTION-TREATED, AND SOLUTION-TREATED-AGED SAMPLES.

TABLE 10

HISTORY AND DATA FOR DELAY TIME SPECIMENS

Specimen Number	History	Test Temperature ^{o}F	Static Elastic Limit O_E, (PSI)	Dynamic Stress O_D, (PSI)	O_D-O_E	Delay Time (Millisec.)
2019	Annealed	14	24,000	31,900	7,900	0.68
2018	Annealed	14	24,000	35,397	11,397	0.01
2009	Annealed	70	21,500	31,441	9,941	0.42
2010	Annealed	70	21,500	31,595	10,095	0.44
2015	Annealed	158	19,500	27,130	7,630	0.68
2016	Annealed	158	19,500	27,960	8,460	0.64
2020	Annealed	300	18,000	26,758	8,758	0.0
2021	Annealed	300	18,000	25,986	7,986	0.0
2037	Quenched & Aged	14	31,500	39,787	8,287	0.0
2033	Quenched & Aged	14	31,500	39,563	8,063	0.0
2024	Quenched & Aged	70	31,500	35,448	3,943	0.0
2025	Quenched & Aged	70	31,500	38,526	7,026	0.0

TABLE 10 continued

HISTORY AND DATA FOR DELAY TIME SPECIMENS

Specimen Number	History	Test Temperature ^{o}F	Static Elastic Limit σ_E, (PSI)	Dynamic Stress σ_D, (PSI)	$\sigma_D-\sigma_E$	Delay Time (Millisec.)
2041	Quenched & Aged	158	31,500	38,713	7,213	0.0
2042	Quenched & Aged	158	31,500	38,772	7,272	0.0
2029	As-quenched	14	26,500	35,504	9,004	0.0
2036	As-quenched	14	26,500	37,508	11,008	0.0
2022	As-quenched	70	27,500	32,159	4,659	0.0
2023	As-quenched	70	27,500	33,353	5,853	0.0
2043	As-quenched	158	27,500	35,814	8,314	0.0
2044	As-quenched	158	27,500	34,849	7,349	0.0

appreciable delay times. In Figures 45, 46, 47, and 48 representative traces for annealed samples tested at 14, 70, and 158° F are shown. The annealed samples tested at 300° F did not show any delay time as shown in Figure 48.

The solution-treated samples showed no delay time at any test temperature. In Figures 49, 50, and 51 representative traces for solution treated samples tested at 14, 70, and 158° F are shown. Because no quick-setting adhesive was available that would withstand temperatures of 300° F, no solution-treated or solution-treated and aged samples were tested at 300° F.

The solution-treated and aged samples also showed no delay time at any test temperature. In Figures 52, 53, and 54 representative traces for solution-treated and aged samples tested at 14, 70, and 158° F are shown. The aging was carried out by heating the sample to 158° F and then holding for six hours.

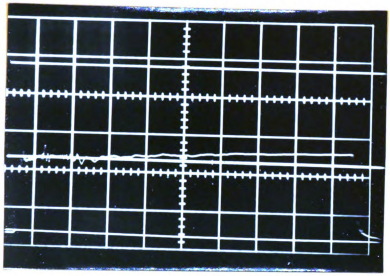

FIGURE 45

OSCILLOSCOPE TRACE FOR ANNEALED SAMPLES TESTED AT 14° F

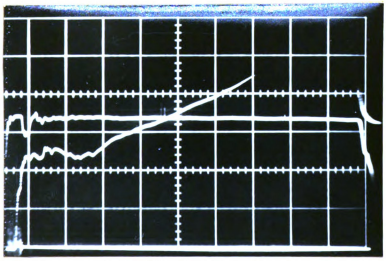

FIGURE 46

OSCILLOSCOPE TRACE FOR ANNEALED SAMPLES TESTED AT 70° F

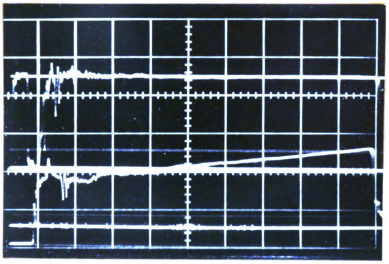

FIGURE 47

OSCILLOSCOPE TRACE FOR ANNEALED SAMPLES TESTED AT 158° F

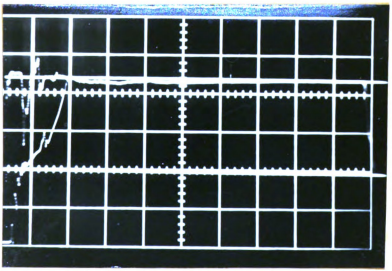

FIGURE 48

OSCILLOSCOPE TRACE FOR ANNEALED SAMPLES TESTED AT 300° F

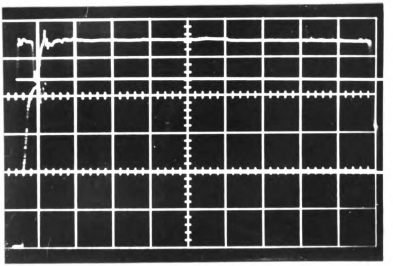

FIGURE 49

OSCILLOSCOPE TRACE FOR SOLUTION TREATED SAMPLES TESTED AT 14° F

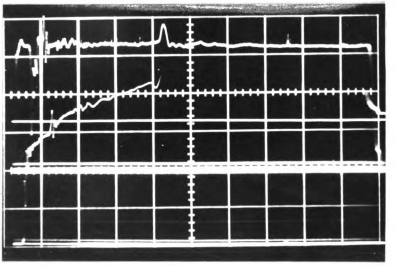

FIGURE 50

OSCILLOSCOPE TRACE FOR SOLUTION TREATED SAMPLES TESTED AT 70° F

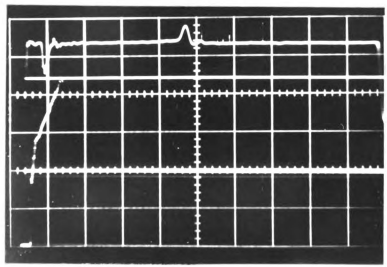

FIGURE 51

OCILLOSCOPE TRACE FOR SOLUTION TREATED SAMPLES TESTED AT 158° F

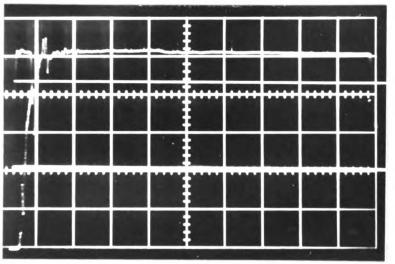

FIGURE 52

OSCILLOSCOPE TRACE FOR SOLUTION TREATED-AGED SAMPLES TESTED AT 14° F

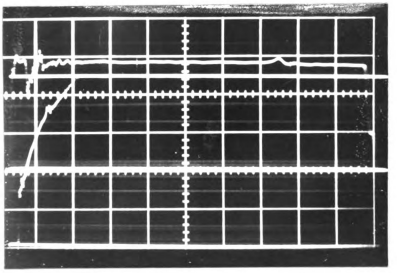

FIGURE 53

OSCILLOSCOPE TRACE FOR SOLUTION TREATED-AGED SAMPLES TESTED AT 70° F

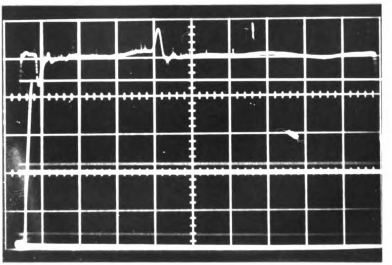

FIGURE 54

OSCILLOSCOPE TRACE FOR SOLUTION TREATED-AGED SAMPLES TESTED AT 158° F

CHAPTER V

DISCUSSION

5.1 Observed Differences in the Brittle to Ductile Transition, Yield Point, and Delay Time in the Annealed, Solution Treated, and Solution Treated- and Aged Samples.

The annealed samples showed a brittle to ductile transition at approximately 160° F. All annealed samples tested in compression below 160° F showed a sharp yield point. Samples tested above 160° F showed no yield point. The annealed samples also showed a delay time when tested below 160° F. Above 160° F, these samples showed no delay time. The yield point and delay time disappeared above the brittle to ductile transition. The solution-treated and the solution-treated and aged samples showed no brittle to ductile transition, yield point, or delay time in the temperature range used for these experiments.

5.2 Observed Chemical and Structural Differences Between the Different Types of Samples

A complete chemical analysis was carried out at the United States Steel Corporation. The chemical composition of the as-received material is given in Table 11. To determine the quality of the atmosphere, a second group of samples was prepared. As-received ingot iron was rolled to a thickness of twenty thousandths of an inch and then etched in thirty percent nitric acid solution

TABLE 11

Chemical Composition of the Ingot Iron Before Heat-Treatment. All percentages are based on weight.

Carbon	0.015 %
Manganese	0.063 %
Phosphorous	0.004 %
Sulphur	0.021 %
Silicon	0.004 %
Nitrogen	0.004 %
Oxygen	0.0962%

until one thousandth of an inch was removed from each side. The etching was designed to remove any impurities introduced during rolling. The samples were then placed in the solution treating furnace and held at 1480° F for twenty-four hours before being furnace cooled. The samples were etched again in the 30 percent nitric acid to remove any surface irregularities and were then analyzed. The resulting composition of the samples is shown in Table 12. As can be seen from these two tables some carbon was lost and some oxygen was gained in the twenty-four hours. However, all the samples used for testing were heated to 1350° F for only one and one half hours. In this short period of time no gross compositional changes could occur. Any changes occurring would be limited to the immediate surface and certainly would be no greater than those experienced in the twenty thousandths thick strips. In addition, the samples which failed in a brittle fashion showed intracrystalline failure across the entire sample and not just at the surface. In Figure 55, the fracture of a sample that failed in a brittle fashion is shown. It appears, therefore, that a change in the average chemical composition from heatreating cannot be responsible for the differences observed between the solution-treated, or solution-treated and aged samples and the annealed samples.

Careful examination of all three types of samples under the optical and electron microscopes revealed that

TABLE 12

Chemical Composition of the Ingot Iron After Heating for Twenty-four Hours at 1480° F. Twenty thousandths of an inch thick strips were used to insure that equilbrium was attained. All percentages are based on weight.

Carbon	0.007 %
Manganese	0.058 %
Phosphorous	0.004 %
Sulphur	0.019 %
Silicon	0.005 %
Nitrogen	0.006 %
Oxygen	0.1026%

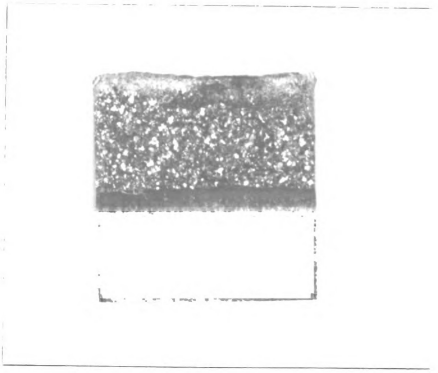

FIGURE 55

Fracture Surface of a Sample That Failed in a Brittle Fashion. Notice that the failure is intracrystalline across the entire sample.

there were definite differences between the samples. The annealed samples showed wide grain boundaries with definite precipitates present. In figure 56, a typical microstructure is shown. Notice the precipitates present. In figures 57 and 58 enlargements of the precipitates are shown. The as-quenched samples showed very little grain boundary precipitates and narrow well defined grain boundaries. In figure 59, a typical microstructure is shown. The solution treated-aged samples like the as-quenched samples did not show much grain boundary precipitate. In figure 60, a typical microstructure is shown. Notice the lack of precipitates.

Examination of replicas of the samples under the electron microscope confirmed the observations made with the optical microscope. In general, however, the detail was better under the optical microscope. The magnification of the electron microscope appeared to be too high. Transmission examination of thin films and replicas made with improved techniques might, however, yield some interesting results.

The grain size of all the annealed, solution treated, and solution treated-aged samples was the same. See figures 56, 59, and 60. Since all three types of samples were made from the same starting material and heated to the same homogenizing temperature, 1350^{o} F, and held for the same length of time, the grain size should be the same.[46]

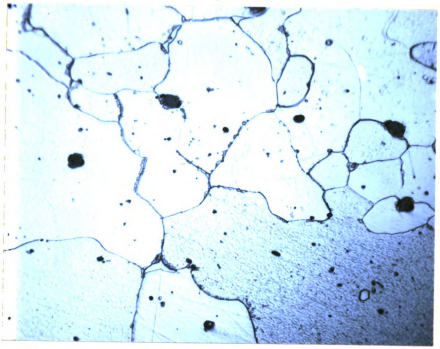

Etch: 4% Nitric Acid in Amyl Alcohol

500 X Mount #65-132

FIGURE 56

Microstructure of the Annealed Ingot Iron. Notice the grain boundary precipitates present.

Etch: 4% Nitric Acid in Amyl Alcohol

1000 X Mount #65-132

FIGURE 57

Enlargement of a Typical Precipitate Found in the Annealed Ingot Iron. These precipitates were not found in the as-quenched or solution treated aged samples.

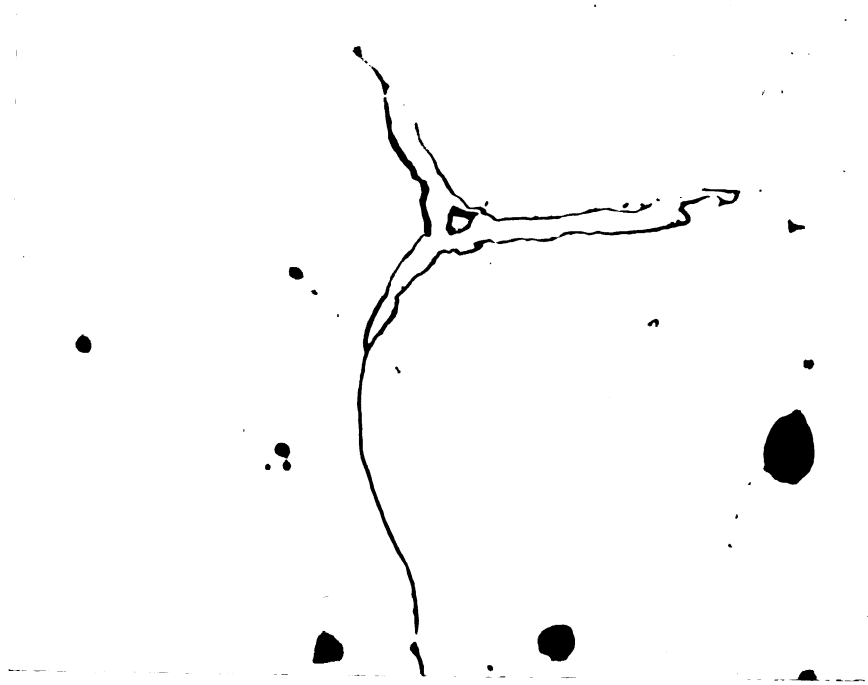

Etch: 4% Nitric Acid in Amyl Alcohol

1000 X Mount #65-132

FIGURE 58

Enlargement of a Typical Precipitate Found in the Annealed Ingot Iron.

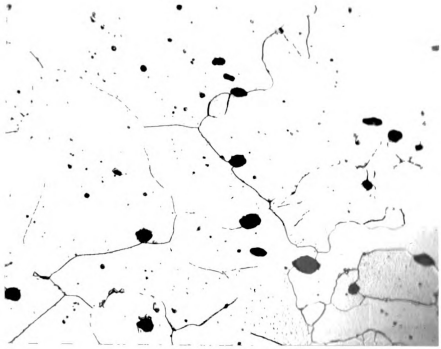

Etch: 4% Nitric Acid in Amyl Alcohol

500 X Mount #65-135

FIGURE 59

Typical Microstructure of the As-quenched Samples. Notice the absence of grain boundary precipitates.

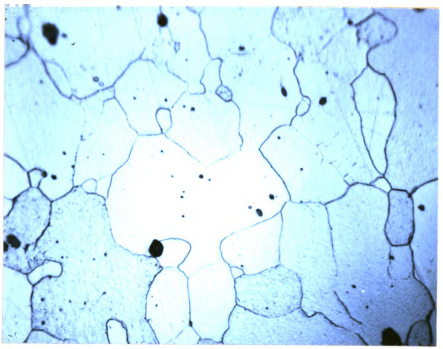

Etch: 4% Nitric Acid in Amyl Alcohol

500 X Mount #65-134

FIGURE 60

Typical Microstructure of the Solution - Treated Aged Samples. Notice the absence of grain boundary precipitates.

5.3 Origin of the Precipitates Observed in the Annealed Samples.

Seybolt[47] has determined the solubility of oxygen in iron. In Figure 61, a partial phase diagram from his work is reproduced.* The material used for this investigation contained about 0.10 percent oxygen. As can be seen from looking at Figure 61, this alloy would be expected to precipitate some iron oxide particles.

Seybolt[48] has also studied the precipitation of oxygen from alpha ferrite. Oxygen dissolves in a general manner and precipitates nearly in a general manner. Metallographic examination reveals no gross movements to the grain boundaries but, as expected, the boundaries are favorable sites for nucleation. The presence of actual iron oxide films in the grain boundaries has never been proved by experiment.

Iron oxide precipitates would be expected to form in the case of the annealed samples. This, no doubt, contributed to the precipitates observed in the grain boundaries. The as-quenched and the solution treated and aged samples would not be expected to have iron oxide precipitates present in the grain boundaries because quenching serves to keep them in solution.[47] The 158° F

* FeO is not the recognized equilibrium phase at room temperature. Wüstite is the equilibrium phase. In this paper, the oxide will be referred to as FeO, iron oxide, just as Seybolt does in his numerous works including references 47 and 48.

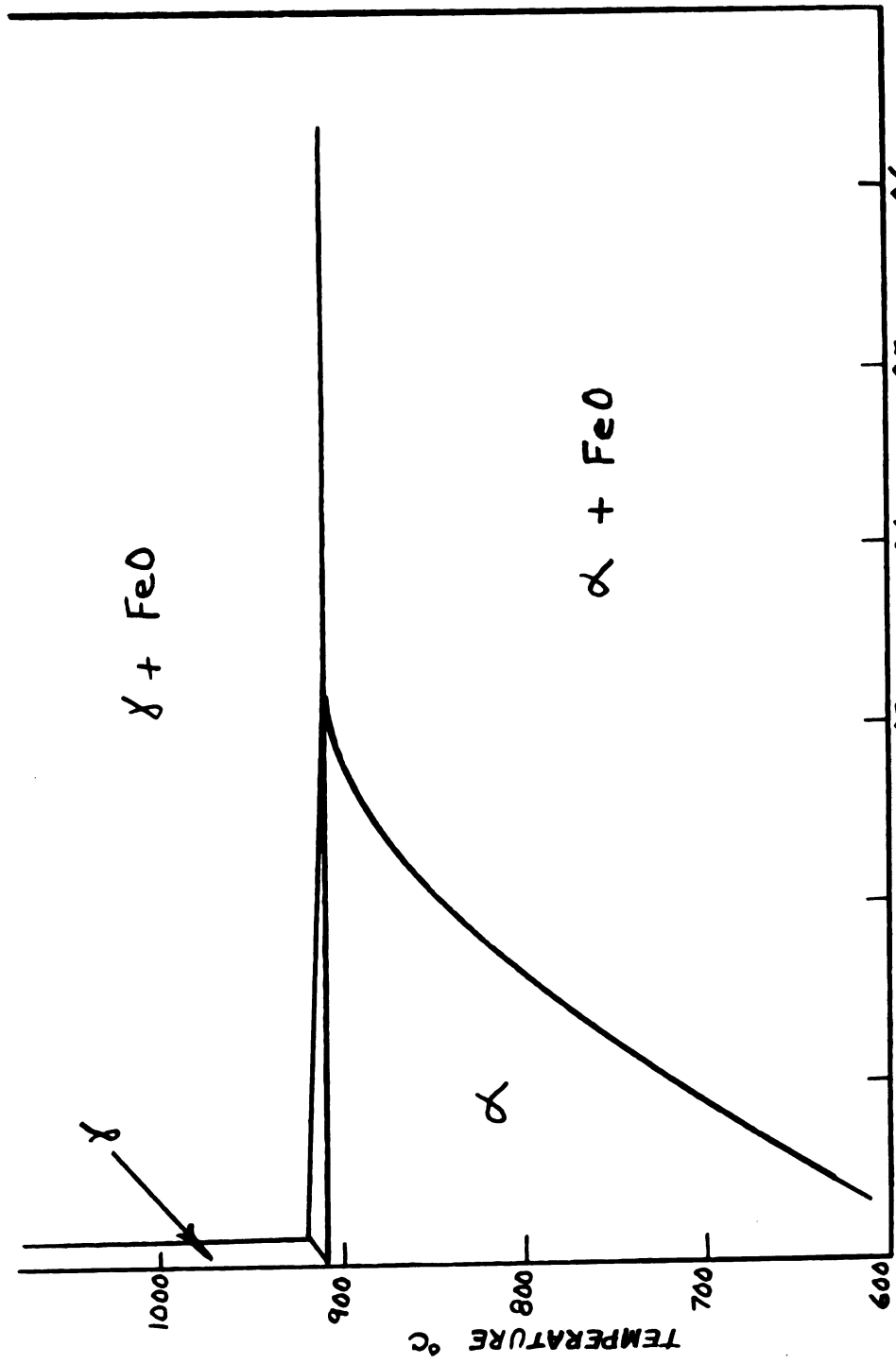

FIGURE 61

PHASE DIAGRAM FOR IRON-OXYGEN

aging treatment does not provide enough activation energy to precipitate any appreciable amounts of iron oxide.[48]

Both carbon and nitrogen also become less soluble in alpha iron as the temperature is lowered. At 1320° F, about 0.018 percent carbon is soluble. At 72° F, only about 1×10^{-7} weight percent of carbon is soluble.[49, 50] The solubility of nitrogen at room temperature is approximately 10^{-4} weight percent.[51] As can be seen from Table 1, precipitates containing carbon and nitrogen should be present in the annealed sample.[52] In the annealed samples the precipitates of carbon and nitrogen should be associated mainly with the grain boundaries.[53, 54]

The as-quenched samples should not have many precipitates present,[55] since quenching effectively prevents the precipitation. The solution treated-aged samples will have some small precipitates present. Tsou, Nutting, and Menter[52] have shown that aging temperatures below 400° F on solution treated ingot iron cause precipitates that are uniformly distributed throughout the grain and not concentrated in the grain boundary. Since the solution-treated and aged samples were aged at 153° F, the precipitates should be uniformly distributed in the grain and not primarily associated with the grain boundaries.

The annealed samples did show precipitates at the grain boundaries; see Figures 56, 57, and 58. The solution treated samples did not show any marked precipitation

in the grain boundaries as expected; see Figure 59. The solution treated-aged samples also showed grain boundaries free from precipitates; see Figure 60. However, the solution-treated samples probably have very fine precipitates uniformly distributed throughout grains[52] since their yield and tensile strengths were markedly higher than the solution treated samples. See Tables 7, 8, and 9.

5.4 Relationship Between the Brittle to Ductile Transition, Yield Point, and Delay Time

As pointed out in section 5.1, the annealed samples showed a brittle to ductile transition at approximately 160° F. All annealed samples tested in compression below 160° F showed a yield point. Samples tested above 160° F showed no yield point. The annealed samples also showed a delay time when tested below 160° F. Above 160° F, these samples showed no delay time. The yield point and delay time disappeared above the brittle to ductile transition. The solution treated and solution treated-aged samples showed no brittle to ductile transition, yield point, or delay time in the temperature range used for these tests. The fact that all these phenomena appear and disappear at the same temperature in the annealed samples and do not appear in either the solution treated or solution treated and aged samples shows that they are all controlled by a very similar or the same mechanism.

It is well established that the yield point depends

upon some type of precipitation. Cottrell visualized an atmosphere of carbon and or nitrogen precipitated around dislocations as the responsible agent.[32, 34] Adair, Hook, and McGaughey[36] have shown that the extent of segregation of the interstitials to the grain boundaries determines whether a yield point occurs or not. They conclude that there must be considerable grain boundary segregation leading to actual precipitates in order to cause a yield point. Delay time studies, especially by Clark and Wood,[43] have shown that the greater the amount of precipitated carbon, the longer the delay time for a given stress above the static yield strength. Thus, to observe a yield point or appreciable delay time, precipitates must be present.

In the present experiments only the annealed samples showed a brittle-to-ductile transition in the temperature range of testing. The annealed samples were also the only samples to show a yield point and appreciable delay time. Since precipitates are required for both the yield point and delay time and the brittle to ductile transition occurred only in the samples having a yield point and delay time, precipitates must contribute to the transition behavior of the material.

As pointed out in sections 5.2 and 5.3, the annealed samples showed grain boundary precipitates and the solution treated and aged samples have a fine general precipitate. Since the annealed samples showed a brittle-to-ductile transition and the solution treated and aged samples

did not in the temperature range used in these experiments, grain boundary precipitates must be more effective in causing a brittle-to-ductile transition.

5.5 A Proposed Mechanism for the Brittle to Ductile Transition in Ingot Iron

In the annealed samples tested below the brittle to ductile transition, dislocations can move relatively easily in the interior of the grains. The precipitates present are large due to the slow cooling. When the dislocations reach the grain boundary, a pile-up occurs at precipitates which causes a stress concentration. At low temperatures with oxides, nitrides, and carbides in the grain boundaries, the dislocations cannot propagate the slip into the next grain before the grain boundary actually fractures. The presence of the precipitates especially oxygen, reduces the strength of the grain boundary. This leads to a brittle fracture as shown in figure 62. Above 160^{o} F, the dislocations have enough mobility to move around the precipitates and thus reduce the stress concentration. The precipitates do not dissolve or change above 160^{o} F, but rather the mode of deformation changes. In the solution treated, solution-treated and aged, and the annealed samples tested at temperatures above the brittle to ductile transition, the dislocations can propagate the slip more easily into the next grain. As a result, the stress from piled up

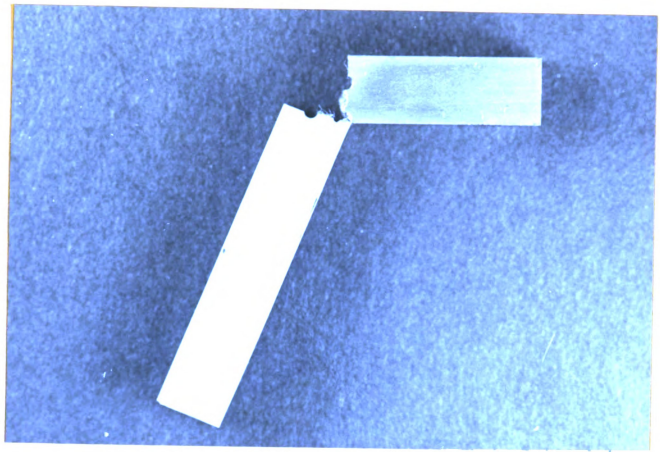

FIGURE 62

SIDE VIEW OF BRITTLE FRACTURE

Notice the lack of plastic deformation.

dislocations is not as great as in the annealed samples below the transition temperature. The lower stress concentrated at the grain boundary makes ductile fracture more favorable. A typical fracture of both the solution treated and solution-treated and aged samples is shown in Figure 63. A side view of the same type of fracture is shown in Figure 64.

5.6 Additional Observations

Impact samples made from as-received ingot iron and impact tested at the same temperatures as annealed impact specimens showed essentially the same transition temperature and impact strength versus testing temperature curve as the annealed samples. When both types of samples were heated to 1350° F for one and one-half hours and quenched in iced brine, their impact strength versus testing temperature curves showed no brittle to ductile transition in the temperature range used for these tests. Their impact strength versus testing temperature curves were identical to those for solution treated samples.

In industry, it is common practice to heat ingot iron in a low dew point hydrogen atmosphere to lower the transition temperature of the as-received material. From observations made during this work, it appears that a less costly method would be to simply quench the material rather than slowly cool it. This could be done right after rolling to save reheating. A dry hydrogen atmosphere is not necessary.

FIGURE 63

CROSS SECTION OF A TYPICAL

TOUGH FRACTURE.

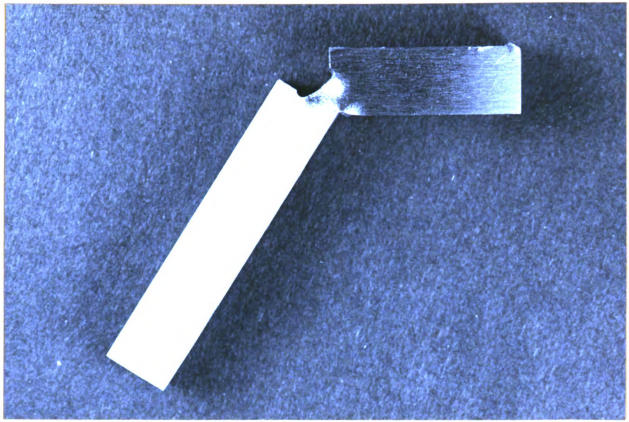

FIGURE 64

SIDE VIEW OF A TYPICAL DUCTILE SAMPLE

Notice the extensive plastic deformation.

CHAPTER VI

CONCLUSIONS

1. The annealed ingot iron used for these tests showed a brittle to ductile transition at approximately 160° F. The solution treated and the solution treated and aged samples showed no brittle to ductile transition down to 14° F.

2. The annealed samples showed a marked yield point below the brittle to ductile transition. Above the transition, no yield point existed in the annealed samples. The solution-treated and the solution-treated and aged samples showed no yield point in these tests.

3. The annealed samples showed a marked delay time below the brittle to ductile transition. Above the transition, no delay time existed for the annealed samples. The solution-treated and the solution-treated and aged samples showed no delay time.

4. Low temperature aging, 160° F for six hours, of solution treated samples did not markedly alter the samples as did annealing. For the test conditions used in these tests, no brittle to ductile transition, yield point, or delay time was

detected. The yield strength was considerably higher, however.

5. Grain boundary precipitates appear to be important in determining whether a strong yield point, delay time, and thus a high brittle to ductile transition will be present.

6. The transition temperature of as-received ingot iron can be markedly lowered by quenching from 1350° F rather than slow cooling.

BIBLIOGRAPHY

1. Engineering News Record, Vol. 87, no. 9, Sept. 1, 1921, pp. 372.

2. Shank, M. E., "Brittle Failure of Steel Structures- a Brief History," Metal Progress, Vol. 66, no. 3, September, 1954, pp. 83-88.

3. Tipper, C. F., The Brittle Fracture Story, Cambridge University Press, Cambridge, 1962, pp. 1-20.

4. Shank, M. E., "Brittle Failure of Nonship Steel-Plate," Mechanical Engineering, Vol. 76, No. 1, 1954, pp. 23-28.

5. Lorig, C. H., "Influence of Metallurgical Factors," Behavior of Metals at Low Temperatures, American Society for Metals, Cleveland, Ohio, 1954, pp. 71-105.

6. Cottrell, A. H., Dislocations and Plastic Flow in Crystals, Clarendon Press, Oxford, 1958, pp. 2-4.

7. Barrett, C. S., Structure of Metals, McGraw Hill Book Company, New York, 1952, pp. 385-387.

8. Tipper, C. F., The Brittle Fracture Story, University Press, Cambridge, 1962, pp. 21-24.

9. Tipper, C. F., The Brittle Fracture Story, University Press, Cambridge, 1962, pp. 25-28.

10. Jaffe, L. D., Reed, E. L., Man, H. C., "Discontinuous Crack Propagation-Further Studies," Transactions of the American Institute of Mining and Metallurgical Engineers, Vol. 185, 1949, pp. 683-687.

11. Smallman, R. E., Modern Physical Metallurgy, Butterworths, Washington, 1963, pp. 72-73.

12. Mesnager, A., "Rapport Non-officiele," No. Abf, International Association for Testing Materials, Brussels Congress, 1906, pp. 1-16.

13. Ludwik, P., "Ueber Kerbwirkungen bei Flusseisen," Stahl and Eisen, Vol. 43, 1923, p. 999.

14. Orowan, E., Nye, J. F., Cairns, W. J., Theoretical Research Report No. 16/45, Armament Research Dept. MOS, London, 1945.

15. Orowan, E., "Classical and Dislocation Theories of Brittle Fracture," Fracture, John Wiley, New York, 1959, p. 148.

16. Eldin, A. S., Collins, S. C., "Fracture and Yield Stress of 1020 Steel at Low Temperature," Journal of Applied Physics, Vol. 22, 1951, pp. 1296-1297.

17. Low, J. R., "The Influence of Mechanical Variables," Behavior of Metals at Low Temperatures, American Society for Metals, Cleveland, Ohio, 1953, pp. 48-56.

18. Robertson, T. S., "Propagation of Brittle Fracture in Steel," Journal of the Iron and Steel Institute, Vol. 175, 1953, pp. 361-374.

19. Robertson, T. S., "Brittle Fracture of Mild Steel," Engineering, 1951, pp. 445-448.

20. Wessel, E. T., "Abrupt Yielding and the Ductile-to-Brittle Transition in Body-Centered-Cubic Metals," Journal of Metals, Vol. 9, 1957, pp. 930-935.

21. Stroh, A. N., "Brittle Fracture and Yielding," Philosophical Magazine, Vol. 46, pp. 968-972.

22. Mott, N. F., "Fracture in Metals," Journal of the Iron and Steel Institute, Vol. 183, 1956, pp. 233-243.

23. Koehler, J. S., "Nature of Work Hardening," Physical Review, Vol. 86, 1952, pp. 52-59.

24. Cottrell, A. H., "Theory of Brittle Fracture in Steel and Similar Metals," Transactions of the American Institute of Mining and Metallurgical Engineers, Vol. 212, 1958, pp. 192-203.

25. Low, J. R., Symposium on the Relation of Properties to Microstructure, A.S.M., 1954, p. 163.

26. Owen, W. S., Averbach, B. L., and Cohen, M., "Brittle Fracture of Mild Steel at -196° C," Transactions of the American Society for Metals, Vol. 50, 1958, pp. 634-655.

27. Petch, N. J., "The Ductile-Cleavage Transition in Alpha Iron," Fracture, John Wiley and Sons, Inc., New York, 1959, pp. 54-64.

28. Griffith, A. A., "The Phenomena of Rupture and Flow in Solids," Philosophical Transaction of the Royal Society, Vol. A221, 1920, pp. 163-198.

29. Hall, E. O., "The Deformation and Aging of Mild Steel: II Characteristics of Luders Deformation," Physical Society of London, Proceedings, Section B, Vol. 64, pp. 742-752.

30. Cracknell, A., and Petch, N. J., "Frictional Forces, on Dislocation Arrays at the Lower Yield Point in Iron," Acta Metallurgica, Vol. 3, 1955, pp. 186-189.

31. Heslop, J., and Petch, N. J., The Stress to Move a Free Dislocation in Alpha Iron," Philosophical Magazine, Vol. 1, Ser. B, 1956, pp. 866-873.

32. Cottrell, A. H., Dislocations and Plastic Flow in Crystals, Clarendon Press, Oxford, 1953, pp. 139-145.

33. Edwards, C. A., Phillips, D. L., Liu, Y. H., "The Yield Point in Steel," Journal of the Iron and Steel Institute, Vol. 147, pp. 145-172.

34. Cottrell, A. H., and Bilby, B. A., "Dislocation Theory of Yielding and Strain Aging in Iron," Proceedings Royal Physical Society, London, 1949, Vol. A62, pp. 49-62.

35. Ardley, G. W., Cottrell, A. H., "Yield Points in Brass Crystals," Proceedings of the Royal Society of London, Vol. 219, pp. 328-341.

36. Adair, A. M., Hook, R. E., and McGaughey, R. L., "The Effect of Thermal History on the Yield Behavior of the American Institute of Mining and Metallurgical Engineers, Vol. 236, No. 2, February, 1966, pp. 174-178.

37. Stein, D. F., Low, J. R., Seybolt, A. U., "The Mechanical Properties of Iron Single Crystals Containing Less Than 5 x 10^{-3} ppm Carbon," Acta Metallurgica, Vol. 11, No. 11, November, 1963, pp. 1253-1262.

38. Johnson, W. S., and Gilman, J. J., Dislocation Velocities, Dislocation Densities, and Plastic Flow in Lithium Fluoride Crystals," Journal of Applied Physics, Vol. 30, No. 2, 1959, pp. 129-144.

39. Hahn, G. T., "A Model for Yielding With Special Reference to the Yield-Point Phenomena of Iron and Related BCC Metals," Acta Metallurgica, Vol. 10, No. 8, August, 1962, pp. 727-738.

40. Lur, T., Kramer, I. R., and Steinberg, M. A., "The Delay-Time Phenomenon in Metal Single Crystals," Acta Metallurgica, Vol. 4, No. 4, July, 1956, pp. 364-370.

41. Clark, D. S., Wood, D. S., "The Time Delay for the Initiation of Plastic Deformation at Rapidly Applied Constant Stress," Proceedings of the American Society for Testing Materials, Vol. 49, 1949, pp. 717-721.

42. Kramer, I. R., and Maddin, R., "Delay Time for the Initiation of Slip in Metal Single Crystals," Journal of Metals, Vol. 4, No. 4, February, 1952, pp. 197-203.

43. Wood, D. S., Clark, D. S., "Delayed Yield in Annealed Steels of Very Low Carbon and Nitrogen Content," Transactions of the American Society for Metals, Vol. 44, 1952, pp. 726-745.

44. Ureeland, T., Wood, D. S., Clark, D. S., "A Study of the Mechanism of the Delayed Yield Phenomena," Transactions of the American Society for Metals, Vol. 45, 1953, pp. 620-631.

45. Fisher, J. C., "Application of Cottrell's Theory of Yielding to Delayed Yield in Steel," Transactions of the American Society for Metals, Vol. 47, 1955, pp. 451-462.

46. Smith, M. C., Alloy Series in Physical Metallurgy, Harpers and Brothers Publishers, New York, 1956, pp. 200-208.

47. Seybolt, A. U., "Solubility of Oxygen in Alpha Iron," American Institute of Mining and Metallurgical Engineers, Vol. 200, 1954, pp. 641-644.

48. Seybolt, A. U., "Precipitation of Iron Oxide from Alpha Fe-O Solid Solutions," Transactions of the American Institute of Mining and Metallurgical Engineers, Vol. 200, 1954, pp. 979-982.

49. Wert, C. A., "Solid Solubility of Cementite in Alpha Iron," Journal of Metals, Vol. 2, 1950, pp. 1242-1244.

50. Allen, N. P., "The Mechanical Properties of the Ferrite Crystals," Journal of the Iron and Steel Institute, Vol. 191, 1959, pp. 1-18.

51. Kamber, K., Keefer, D., and Wert, C., "Interactions of Interstitials with Dislocations in Iron," Acta Metallurgica, Vol. 9, 1961, pp. 403-414.

52. Tsow, A. L., Nutting, J., Menter, J. W., "The Quench-Aging of Iron," Journal of the Iron and Steel Institute, Vol. 172, 1952, pp. 163-171.

53. Leslie, W. C., and Keh, A. S., "An Electron Transmission Study Of The Strain Aging Of Iron," Journal of the Iron and Steel Institute, Vol. 200, 1962, pp. 722-728.

54. Russell, T. L., Wood, D. S., Clark, D. S., "The Influence of Grain Size On The Yield Phenomenon In Steel, Acta Metallurgica, Vol. 9, 1961, pp. 1054-1063.

55. Phillips, V. A., "New Evidence For Segregation At Grain Boundaries, Subgrain Boundaries, And Dislocations In Dilute Iron-Carbon-Nitrogen Alloys," Acta Metallurgica, Vol. 11, 1963, pp. 1139-1150.